Rishikesh Kumar Gupta

Role of Stim2a protein in the neuroprotection in *Danio rerio*

Dissertation on Doctorate in Medical and Health Sciences

in the discipline of Medical Science

Supervisor: Prof. dr hab. Jacek Kuźnicki

Laboratory of Neurodegeneration

International Institute of Molecular and Cell Biology in Warsaw

Defending the doctoral dissertation before the Medical Science Discipline Council

Warsaw Medical University

Warsaw 2020

Keywords (in English): Store-operated calcium entry, Stim2, zebrafish, brain, neurons, behavior, *in vivo* imaging, GCaMP5G, Calcium homeostasis

Keywords (in Polish): Napływ wapnia zależny od siateczki endoplazmatycznej, Stim2, danio pręgowany, mózg, zachowanie, obrazowanie *in vivo*, GCaMP5G, homeostaza wapniowa

Name and number of the research project: OPUS12 No 2016/23/B/NZ3/03142

ACKNOWLEDGEMENTS

I sincerely thank the Almighty for granting me his strength to go through this journey and accomplish my goal. It was divine help that kept me going despite all difficulties I passed through.

It is my pride privilege to express my sincere thanks and a deep sense of gratitude towards Prof. Jacek Kuznicki for his valuable advice, fantastic supervision, and constant patience through which this work was able to take the shape in which it has been presented. He is a fantastic scientist and human being who cared deeply about my success and happiness. I do not know how any word I write here will ever convey how grateful and blessed I am to receive this much support from him. Without his support, it would not have been possible for me to come this far. He helped me develop a practical approach to study neuroscience, without taking my head out of the clouds. He is always a great source of inspiration, and I am proud that I had the opportunity to work with a stalwart in neuroscience. His inspiring words in a few vulnerable moments of life helped me breathe once again and overcome the obstacles during my PhD journey. I thank Prof. Kuznicki for his valuable suggestions and support during bench work and writing the manuscript and thesis with a deep sense of gratitude.

My senior, Dr. Iga Wasilewska, inspired me to be patient and kind. She was always there for me for fruitful discussion and assistance during experiments. She always has a smile on her face, and it is so motivating to work in the same lab/office together as she does. Thank you so much, Iga, for introducing me to working with zebrafish and learning many methods that I could use.

I sincerely owe my deepest gratitude to Dr. Łukasz Majewski for the kind support and valuable advice during my research.

A special word of thanks to the staff of the Zebrafish Core Facility (ZCF) at IIMCB. This work could not have been possible without their efficient cooperation.

I am also thankful to Dr. Tomasz Węgierski for his time he spent to make me learn how to use the Lightsheet microscope and other microscopes. I also thank Dr. Katarzyna Misztal, who helped me with the FACS sorting. I would also like to thank Dr. Oksana Palchevska, Prof. Vladimir Korzh, and Dr. Malgorzata Korzeniowska for their valuable comments and suggestions, which were invaluable in creating this work. I am also grateful to Prof. Bożena Kamińska and her graduate students, who were extremely cooperative while I was doing single-cell RNA seq experiments at the Nencki Institute of Experimental Biology. I cannot name everyone for the sake of space, but thank you to everyone who has shared whatever care and kindness you have shown. Thank you to all employees of the Neurodegeneration Laboratory for their help and kindness.

I express my sincere gratitude to the Postgraduate School of Molecular Medicine, Medical University of Warsaw, for offering me the valuable opportunity to pursue my PhD studies.

On a more personal note, the whole credit of my achievements goes to my parents, who were always there for me in my difficulties. It was their unshakable faith in me that has always helped me to proceed further. The life lessons and values they taught me starting from childhood will always stay with me; the work ethics and sense of responsibility that they imparted to me truly helped me through these last few years. Finally, I would like to pay my deepest gratitude to my beloved friend Sarita who had been encouraging me, prayed for me in every step of difficulties. She has been instrumental in this achievement, and I dedicate my thesis to my family and her.

Rishikesh Kumar Gupta

Table of contents

List of the Figures

List of the Tables

List of the abbreviations

Abbreviations	Full Form
Ca^{2+}	Calcium ions
IP3Rs	IP_3 receptors
RNA	Ribonucleic acid
PCA	Principle Components analysis
ER	Endoplasmic reticulum
RyRs	ryanodine receptors
SOCE	store-operated calcium entry
CCE	capacitative calcium entry
WT	Wild type
PTZ	pentylenetetrazole
CaTK	Calcium toolkit
VMR	visual-motor response
GO	gene ontology
VGCC	voltage-gated calcium channels
CICR	calcium-induced calcium release
STIM	Stromal interaction molecule
DMEM	Dulbecco's modified Eagle's medium
SERCA	sarco/endoplasmic reticulum Ca^{2+}-ATPase
FBS	Fetal bovine serum
mM	Millimolar
µM	Micromolar
SOAR	STIM-Orai Activating Region
TRPC	Transient Receptor Potential Canonical ion channel
bp	Base pair
DESeq2	Differential Expression analysis for Sequence count data version 2
edgeR	Empirical analysis of digital gene expression in R
FDR	False Discovery Rate
AMPAR	α-amino-3-hydroxy-5-methyl-4-isoxazole propionic acid receptor
NMDAR	N-methyl-D-aspartate receptor
nSOCE	neuronal SOCE

Abstract (in English)

Calcium ions (Ca^{2+}) play a vital role in the signaling of any eukaryotic cell. An influx of Ca^{2+} into the cytoplasm originates either from the endoplasmic reticulum (ER), the main store of these ions, or the external environment. Refilling of these stores is possible by store-operated calcium entry (SOCE or CCE, capacitative calcium entry); (Putney 1986). The SOCE relies on the detection of a reduced level of Ca^{2+} in the ER by STIM sensory proteins and subsequent activation of Orai/TRP channels located in the plasma membrane (Hartmann et al., 2014, Shin et al., 2016), by which these ions can enter the cytoplasm and then transferred to the ER by the ATP-dependent calcium pump (SERCA). STIM proteins have been established in neuronal Ca^{2+} signaling in mammalian primary neuronal cell cultures (reviewed in (Majewski et al., 2015, Wegierski et al., 2018)). However, *in vivo* data supporting neuronal Ca^{2+} homeostasis and complex behavior analysis were not available because of the early lethality of S*tim2* knockout in mice (Berna-Erro et al., 2009, Garcia-Alvarez et al., 2015).

Zebrafish possess two isoforms of STIM2 – Stim2a and Stim2b encoded by *stim2a* and *stim2b*. Using the CRISPR/Cas9 technique, *stim2a* mutant zebrafish line was created, which was viable. In this present study, it was shown that *stim2a* deletion caused distinct behavioral changes in zebrafish larvae. Hyperactivity was observed in *stim2a*$^{-/-}$ zebrafish larvae. An increase in thigmotaxis (i.e., a preference for remaining close to the well) was also observed compared to the WT. Moreover, reduction of phototaxis in *stim2a*$^{-/-}$ zebrafish larvae was also found compared with WT. Furthermore, *stim2a*$^{-/-}$ zebrafish larvae reacted to the changes in light and showed higher activity in the low activity phase in the visual-motor response (VMR) test. To establish the link between the behavior with cellular events, *in vivo* changes in the Ca^{2+} fluorescence (due to GCaMP5G activity) in neurons were measured. An increase in Ca^{2+} oscillation frequency was observed in neurons in the optic tectum in *stim2a*$^{-/-}$ zebrafish larvae compared to the WT. Furthermore, *in vivo* Ca^{2+} activity in neurons were measured after larvae were treated with glutamate, which showed a further increase in the neuronal Ca^{2+} oscillation frequency. Next-generation RNA sequencing was performed, and differential gene expression analysis was done to further establish the molecular level link. Total 392 genes were found, which showed ≥ 2-fold change in *stim2a*$^{-/-}$ zebrafish. Out of these 392 genes, 86% of genes were upregulated, and 14% were downregulated. Among the differentially expressed genes, encoding proteins of CaTK: *anxa3a, grinab, hp, hpca, mast2,*

pkn3, pvalb7, and *slc25a25b* showed significant change in expression in *stim2a*$^{-/-}$ zebrafish. This indicates that a number of genes that encode proteins involved in Ca^{2+} homeostasis are affected in *stim2a*$^{-/-}$ zebrafish neurons in the absence of Stim2a isoform. For this reason, single-cell RNA sequencing was performed on the pure population of cells of neuronal origin. In cells of neuronal origin in WT zebrafish, 13 different clusters were identified, representing different cell types and early neuronal subtypes based on cellular marker genes. Eleven of them were identified as a specific type of neurons, and two clusters were identified as not known. Further analysis showed 88 unique CaTK genes from all neuronal cell clusters; those could be involved in neuronal Ca^{2+} signaling. However, the number of these genes were varied in each neuronal cell cluster. 15 different clusters were identified based on cellular marker genes representing different cell types in *(stim2a;stim2b)*$^{-/-}$ double mutant. Overall, in all cell clusters, a total of 102 unique CaTK genes from all neuronal cell clusters were identified. Six cell types were identified in both WT and *(stim2a;stim2b)*$^{-/-}$ double mutant. Despite the same cell type, the CaTK genes in these six clusters showed heterogeneity. Four out of eight CaTK genes, which were found to be significantly upregulated in bulk RNA sequencing data of *stim2a*$^{-/-}$ mutant, were also identified in the scRNA seq data (*grinab*, *hpca*, *mast2*, and *pvalb7*) in the cells of neuronal origin. The other four genes (*anxa3a*, *hp*, *pkn3*, and *slc25a25b*), which were found to be upregulated by bulk RNA-Seq in *stim2a*$^{-/-}$ larvae brains, were not identified in GCAMP5G positive cells by scRNA seq, indicating that these genes were expressed in other cells than cells of neuronal origin. It was found recently in our lab that the *anxa3a* gene was upregulated in the GCAMP5G negative cell population separated by FACS in the *(stim2a;stim2b)*$^{-/-}$ double mutant.

Abstrakt

Jony wapnia (Ca^{2+}) odgrywają istotną rolę w sygnalizacji każdej komórki eukariotycznej. Napływ Ca^{2+} do cytoplazmy pochodzi albo z retikulum endoplazmatycznego (ER), głównego magazynu tych jonów, albo ze środowiska zewnętrznego. Ponowne napełnianie tych magazynów jest możliwe dzięki napływowi wapnia w procesie (SOCE, ang. *Store operated calcium entry*, dawniej zwanym CCE, pojemnościowym napływem wapnia; ang. *Capacitative calcium entry*); (Putney 1986). SOCE polega na wykrywaniu obniżonego poziomu Ca^{2+} w ER przez białka sensoryczne STIM i aktywacji przez nie kanałów Orai/TRP zlokalizowanych w błonie komórkowej (Hartmann i wsp. 2014, Shin i wsp. 2016), przez co te jony dostają się do cytoplazmy, a następnie są przenoszone do ER przez pompę wapniową zależną od ATP (SERCA). Białka STIM zostały zidentyfikowane w naszym laboratorium w hodowlach pierwotnych komórek nerwowych ssaków i pokazaliśmy ich udział w sygnalizacji Ca^{2+} (przegląd w (Majewski i wsp. 2015, Wegierski i wsp. 2018)). Ze względu na wczesną śmiertelność nokautu Stim2 u myszy (Berna-Erro i wsp. 2009, Garcia-Alvarez i wsp. 2015) obserwacje potwierdzające udział SOCE w homeostazie neuronalnego Ca^{2+} i jego wpływ na behawior nie mogły być potwierdzone *in vivo* (Berna-Erro i wsp. 2009, Garcia-Alvarez i wsp. 2015).

Danio pręgowany posiada dwie izoformy STIM2 – Stim2a i Stim2b kodowane przez *stim2a* i *stim2b*. Stosując technikę CRISPR/Cas9, stworzono zmutowaną linię danio pręgowanego *stim2a*, która była żywotna. W niniejszym badaniu wykazano, że delecja *stim2a* powodowała wyraźne zmiany behawioralne u larw *stim2a*$^{-/-}$ danio pręgowanego, np. zaobserwowano nadpobudliwość, wzrost tigmotaksji (tj. preferencję do pozostawania blisko krawędzi naczynia) w porównaniu z WT. Ponadto, w larwach *stim2a*$^{-/-}$ stwierdzono zmniejszenie fototaksji w porównaniu z WT. Jednocześnie, larwy *stim2a*$^{-/-}$ danio pręgowanego reagowały na zmiany światła i wykazywały wyższą aktywność w fazie niskiej aktywności w teście odpowiedzi wzrokowo-ruchowej (VMR). Aby ustalić związek między zachowaniem a zmianami w komórce mierzono *in vivo* poziom fluorescencji sondy wapniowej - GCaMP5G. Zaobserwowano wzrost częstotliwości oscylacji Ca^{2+} w neuronach w osłonie wzrokowej larw danio pręgowanego *stim2a*$^{-/-}$ w porównaniu z WT. Po potraktowaniu larw glutaminianem aktywność Ca^{2+} w neuronach mierzona *in vivo* wykazywała wzrost częstotliwości oscylacji Ca^{2+}. Przeprowadzono sekwencjonowanie RNA nowej generacji i analizę różnicowej ekspresji genów. Znaleziono łącznie 392 geny, które

wykazywały ≥ 2-krotną zmianę w *stim2a*$^{-/-}$ danio pręgowanego. Spośród tych 392 genów 86% genów było regulowanych w górę, a 14% w dół. Wśród genów o zróżnicowanej ekspresji, były też geny kodujące białka zaangażowane w CaTK: *anxa3a, grinab, hp, hpca, mast2, pkn3, pvalb7* i *slc25a25b*. Wskazuje to, że ekspresja genów kodujących białka zaangażowane w homeostazę Ca^{2+} jest zaburzona w neuronach *stim2a*$^{-/-}$ danio pręgowanego. Następnie przeprowadzono analizę ekspresji genów w populacji pojedynczych komórek pochodzenia neuronalnego izolowanych z mózgu larw (scRNASeq). W komórkach z larw WT zidentyfikowano w oparciu o geny markerów komórkowych 13 klastrów, reprezentujących różne typy komórek. Jedenaście z nich zidentyfikowano jako określony typ neuronów, a dwa jako nieznane. Dalsza analiza wykazała 88 unikalnych genów CaTK ze wszystkich skupisk komórek neuronalnych; mogą one być zaangażowane w sygnalizację neuronalną Ca^{2+}. W każdym skupisku komórek neuronalnych liczba i rodzaj tych genów były różne. W podwójnym mutancie *(stim2a;stim2b)*$^{-/-}$ w oparciu o komórkowe geny markerowe zidentyfikowano 15 klastrów reprezentujące różne typy komórek pochodzenia neuronalnego. We wszystkich skupiskach komórek zidentyfikowano łącznie 102 unikalne CaTK geny. Sześć typów komórek zidentyfikowano zarówno w WT, jak i podwójnym mutancie *(stim2a;stim2b)*$^{-/-}$. Pomimo tego samego typu geny CaTK w tych sześciu klastrach wykazywały niejednorodność. Cztery z ośmiu genów CaTK (*grinab, hpca, mast2* i *pvalb7*), których ekspresja oznaczona przy pomocy sekwencjonowania RNA była znacząco podwyższona w próbach mózgów mutanta *stim2a*$^{-/-}$, zidentyfikowano metodą scRNA w kilku klastrach komórek neuronalnych. Pozostałe cztery geny (*anxa3a, hp, pkn3* i *slc25a25b*) z podwyższoną ekspresją w mózgach larw *stim2a*$^{-/-}$, nie zostały zidentyfikowane w komórkach ekspresjonujących GCAMP5G. To sugeruje, że geny te wykazują ekspresję przede wszystkim w komórkach innych, niż komórki pochodzenia neuronalnego. Ta interpretacja wydaje się uzasadniona, ponieważ niedawno w naszym laboratorium odkryto, że gen *anxa3a* był podwyższony w populacji komórek nieekspresjonujących GCAMP5G, oddzielonych przez FACS z podwójnego mutanta *(stim2a;stim2b)*$^{-/-}$.

Chapter 1: Introduction

1.1 Calcium signaling

Calcium (Ca^{2+}) signaling is a process in which cells convert external information and transfer it inside the cell via changing the intracellular calcium dynamics. Many physiological processes take place as a result of such changes in intracellular calcium levels. That is why Ca^{2+} is known as universal secondary messengers (intracellular), as it conveys the information within the cell to control its action. Ca^{2+} signaling is involved in the regulation of many cellular physiologies like cell migration (Kim et al., 2016), differentiation (Poloz et al., 2012), contraction (Halaidych et al., 2019) as well as metabolism (Shanmughapriya et al., 2015). Furthermore, many important processes in neurons such as neurogenesis (Brustein et al., 2013), neurotransmission (Chanaday et al., 2021, Ramirez et al., 2021), synaptic plasticity (McDaid et al., 2021), and gene transcription (Muller et al., 2012) depend on Ca^{2+} signaling.

The cytosolic Ca^{2+} stays at a very low concentration under resting conditions. It is around 100 nM, which is 20,000 to 100,000-fold lower than typical extracellular Ca^{2+} concentration (Demaurex et al., 2016). Changes in the Ca^{2+} flux are precisely regulated in the cells, allowing Ca^{2+} influx into the cytosol and then into the endoplasmic reticulum (ER) (largest store of Ca^{2+}), mitochondria, and other organelles. During physiological cell activation, Ca^{2+} enter the cell via specific channels and/or get released into the cytosol from the endoplasmic reticulum (ER) via ryanodine receptors (RyRs) and/or Inositol 1,4,5-Triphosphate-3 receptors (IP3Rs) (Hunt et al., 2020). These ions initiate many Ca^{2+}-dependent signaling pathways. However, if an excessive increase of Ca^{2+} in cytosol occurs, it activates the cascades of the biological reactions, which eventually lead to cell death (Guzel et al., 2021).

1.2 Modes of Ca^{2+} signaling in neuronal cells

Ca^{2+} signaling in neurons is regulated by various pathways (Wojda et al., 2008). One of them are voltage-gated calcium channels (VGCCs, also known as voltage-dependent calcium channels (VDCCs)) (Yamakage et al., 2002). The other are ligand-gated calcium channels (also known as receptor-operated calcium channels) (Striggow et al., 1996). VGCCs are a group of voltage-gated ion channels present in the membrane of neurons and allow the permeability to the Ca^{2+} (Yamakage et al., 2002). VGCCs are mainly involved in rapid action and consist of two components: voltage-gated (VGI) and calcium-gated (CGI) (Cens et

al., 2006). In resting-state, these VGCCs are normally closed but get activated and open when membrane potentials develop. Opening of these VGCCs allows a Ca^{2+} influx into the cell (Wilson et al., 2005), which ultimately leads to excitation of neurons, regulation of gene expression, or release of neurotransmitters. VGCCs are broadly divided into five sub-types: L-type calcium channel, P/Q-type calcium channel, N-type calcium channel, R-type calcium channel, and T-type calcium channel. L-type calcium channels (e.g., $Ca_v1.1$, $Ca_v1.2$, $Ca_v1.3$, $Ca_v1.4$) get activated on high voltage, mainly present on dendrites and dendritic spines of cortical neurons (Felizola et al., 2014). P/Q-type calcium channels (e.g., $Ca_v2.1$) are mainly present on Purkinje neurons in the cerebellum/cerebellar granule cells (Nimmrich et al., 2012). N-type calcium channels (e.g., $Ca_v2.2$) are present on neurons throughout the brain and peripheral nervous system (Heyes et al., 2015). R-type calcium channels (e.g., $Ca_v2.3$) are mainly found on cerebellar granule cells (Soong et al., 1993). T-type calcium channels (e.g., $Ca_v3.1$, $Ca_v3.2$, $Ca_v3.3$) are mainly present on neurons, cells that have pacemaker activity and in thalamus (Rossier 2016).

Ligand-gated calcium channels, also referred to as ionotropic receptors, are a group of transmembrane proteins which open to allow Ca^{2+} to pass through the membrane in response to the binding with a ligand (e.g., a neurotransmitter). Upon excitation, a presynaptic neuron releases neurotransmitters into the synaptic cleft at the neuronal junctions, binding to receptors on the postsynaptic neuron. This leads to a conformational change in the ligand-gated ion channels, resulting in their opening and a flow of ions across the plasma membrane. This creates depolarization and hyperpolarization in excitatory response or inhibitory response, respectively. IP3Rs and RyRs are ligand-gated calcium channels located in ER and are responsible for releasing Ca^{2+} from this store in response to IP_3 or calcium-induced calcium release (CICR) (Secondo 2009, Taylor et al., 2010, Santulli et al., 2017). Other ionotropic receptors are nicotinic acetylcholine receptors (nAChRs), serotonin receptors (5-HT receptors), γ-aminobutyric acid receptors ($GABA_AR$), glycine receptor (GlyR or GLR), α-amino-3-hydroxy-5-methyl-4-isoxazolepropionic acid receptor (AMPA receptor), N-methyl-D-aspartate receptor (NMDA receptor). They are well characterized and are involved in the Ca^{2+} regulation of neuronal excitability, synaptic plasticity (Li et al., 2009), and neurotransmitter release. One of the regulatory mechanisms of Ca^{2+} homeostasis in neurons is the process of capacitive calcium entry, recently called store-operated Ca^{2+} entry (SOCE) (Wegierski et al., 2018) (Skopin et al., 2021). SOCE allows restoring Ca^{2+} levels in the ER, but it is also involved in signaling.

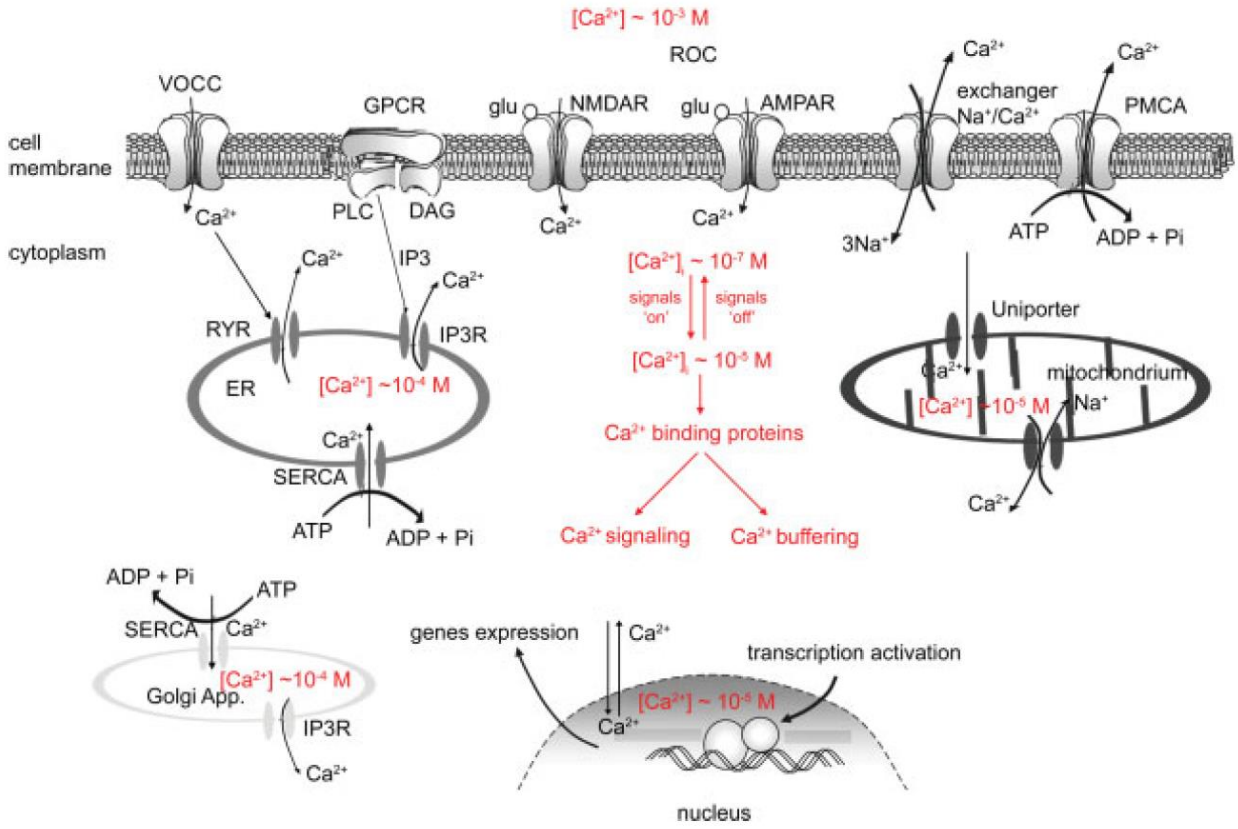

Figure 1.1: Ca^{2+} homeostasis in healthy neuronal cells. Different entry modes of the Ca^{2+} inside the cell from the extracellular environment. (Figure opted from review by Wojda et al., 2008).

The SOCE gets initiate on the detection of a low level of Ca^{2+} in the ER by STIMs sensory proteins and subsequently activates Ca^{2+} channels in the plasma membrane, through that Ca^{2+} can enter into the cytoplasm. The SOCE channels are mainly mediate the Orai proteins and transient receptor potential (TRP) channels (Salido et al., 2011, Shin et al., 2016). Although neurons have multiple mechanisms of Ca^{2+} entry involved in the regulation of neuronal processes (e.g., via voltage-gated calcium channels and ligand-gated channels), SOCE in neurons also appears to orchestrate a variety of cellular mechanisms, such as gene expression, spine morphology, neuronal excitation, stem and progenitor cell proliferation, and axonal growth (reviews by (Putney 2003, Lefkimmiatis et al., 2009, Majewski et al., 2015, Moccia et al., 2015)).

1.3 Regulation of Ca^{2+} homeostasis inside the cell via SOCE

Stromal interacting molecules (STIMs) were first discovered in 2001 (Williams et al., 2001). They are ER-resident proteins (Ma et al., 2015), have EF-hand Ca^{2+} binding domains,

and sense changes of Ca^{2+} level (Emrich et al., 2021). In 2005, Liou et al. first showed that STIM is essential for Ca^{2+}-store-depletion-triggered Ca^{2+} influx in non-excitable cells (Liou et al., 2005). As a result of ER Ca^{2+} store depletion, STIMs change their conformation, oligomerize and translocate with the ER membrane towards the plasma membrane (Ma et al., 2015). There, they interact with Ca^{2+}-conducting channels like Orai1, Orai2, or Orai3 (He et al., 2021) and/or transient receptor proteins channels (TRPs) (Froghi et al., 2021) to induce Ca^{2+} influx in the cytosol. Ca^{2+} gets pumped into ER lumen from cytosol via Sarco/endoplasmic reticulum Ca^{2+}-adenosine triphosphatase (SERCA) (Shin et al., 2016, Weber et al., 2021). STIMs family includes STIM1 and STIM2 proteins, which have different functions and sensitivity to the level of Ca^{2+} in ER (Gruszczynska-Biegala et al., 2011). It was already established that STIM2 proteins primarily regulate the steady-state ER and cytosolic $Ca2^{+}$ homeostasis (Brandman et al., 2007).

SOCE was investigated mostly in non-excitable cells (Liou et al., 2005, Bergmeier et al., 2013). Nevertheless, neurons also require very precise spatial-temporal control of Ca^{2+}-dependent processes involved in many vital functions (Chanaday et al., 2021). In that direction, in 2009, Klejman et al. reported the presence of STIMs and Orais transcripts in the cortical neuron cultures of rat brain and showed that they interact with each other, forming a puncta at the low Ca^{2+} concentrations (Klejman et al., 2009). They also showed that the small decrease in ER Ca^{2+} levels was sensed and recovered by STIM2 action, but not by STIM1 (Gruszczynska-Biegala et al., 2011). Their subsequent report provided evidence of the interaction of endogenous STIM with endogenous Orai in rat cortical neuronal cultures (Gruszczynska-Biegala et al., 2013). In the subsequent year, it was shown that in mutant presenilin mice, a model of familial Alzheimer's disease, synaptic STIM2 expression was reduced, which impaired SOCE leading to destabilization of mature spines of neurons (Sun et al., 2014).

1.4 Calcium signaling in neurodegenerative diseases

Intracellular Ca^{2+} signaling has been shown to affect cell functioning in diseased conditions of the central nervous system (Wojda et al., 2008). For instance, many complex neurodegenerative diseases, such as Alzheimer's disease (AD) (Khachaturian 1994, Bojarski et al., 2008, Wojda et al., 2013), Huntington's disease (HD) (Tang et al., 2005), Parkinson's disease (PD) (Genovese et al., 2020) and traumatic brain injury (TBI) (Niu et al., 2012) are linked to the dysregulation of the Ca^{2+} homeostasis. Since Ca^{2+} is known to control memory

formation (Zheng et al., 2016) and during the developmental state of neurons (Peng et al., 2007), it was also suggested that drugs designed to normalize Ca^{2+} oscillations have a potential role in delaying the consequences of neurodegeneration (Berridge 2013, Dey et al., 2020, Latoszek et al., 2021).

1.5 Role of STIM2 neurodegenerative diseases

It has been shown that in immortalized human lymphocytes of patients with FAD, the level of STIMs is decreased (Bojarski et al., 2009) and Ca^{2+} homeostasis disturbed (Jaworska et al., 2013). These observations were confirmed and extended by Bezprozvanny's group, which used mice with presenilin FAD mutations and samples of brains of AD patients (Sun et al., 2014, Rao et al., 2015). The STIM2 mediated neuronal SOCE (nSOC) and Ca^{2+}/calmodulin-dependent protein kinase II (CaMKII) (STIM2-nSOC-CaMKII) help in the stabilization of hippocampal neurons' mushroom spines. In the presenilin-1 M146V knock-in (PS1-M146V KI) mouse model, due to downregulation of STIM2 protein, the STIM2-nSOC-CaMKII pathway was significantly compromised and showed a reduction of mushroom spines in hippocampal neurons (Sun et al., 2014). Neurons from this model also showed an abnormal neuronal-firing signature (Zhang et al., 2015). The mushroom spines in postsynaptic hippocampal neurons were less in the amyloid precursor protein knock-in (APPKI) mouse AD model. It was found that there was a deposition of β-amyloid 42 ($A\beta_{42}$), which overactivated the mGluR5 receptor on the neurons and elevated the Ca^{2+} levels in ER (Sun et al., 2014, Zhang et al., 2015, Chanaday et al., 2021).

Another report showed that transient receptor potential canonical 6 (TRPC6) and Orai2 channels form a STIM2-regulated nSOC Ca^{2+} channel complex in hippocampal mushroom spines. It was also demonstrated that the application of pharmacological agents such as hyperforin, a known TRPC6 activator, and NSN21778 (NSN), a novel nSOC positive modulator, could stimulate the activity of the nSOC pathway in the spines and rescue mushroom spine loss in both presenilin and APP knock-in mouse models of AD (Zhang et al., 2016).

1.6 Stim2 in zebrafish

In recent years, zebrafish (*Danio rerio*) have become a popular model organism for neurological research (Stewart et al., 2014). Fish shares about 70% orthologue genes with human genes (Howe et al., 2013), has similar molecular pathways (Panula et al., 2010), and

brain physiology (Stewart et al., 2015) with humans. Furthermore, the larvae of zebrafish are transparent, which allows *in vivo* whole-brain imaging and is used as an animal model to study brain function, neuronal circuits, and behavior (Blaser et al., 2010, Maximino et al., 2010, Schnorr et al., 2012, Oh et al., 2019). Several studies have demonstrated that zebrafish can be used for a high throughput drug screening (Grossman et al., 2010, Richendrfer et al., 2012).

The genome sequences of zebrafish are well known now. It has many human homologous genes in more than one copy due to its genome duplication (Gasanov et al., 2021). For example, the zebrafish possess two isoforms of s*tim2* – s*tim2a* and *stim2b* (Wasilewska et al., 2019). Besides that, zebrafish have other SOCE component genes, i.e., *stim1a*, *stim1b*, *orai1a*, *orai1b*, and *orai2*. Furthermore, the proteins involved in Ca^{2+} signaling and homeostasis are encoded by calcium toolkit (CaTK) genes (Wasilewska et al., 2019). To understand the function of SOCE and Stim proteins in neurons, behavior studies in *Stim2* knockout mouse lines have been made. However, these *Stim2* knockout mouse lines showed developmental delay at 4-5 weeks of the postnatal and did not survive afterward (Oh-Hora et al., 2008, Berna-Erro et al., 2009). Berna-Erro et al. reported that only 10% of *Stim2* mice could reach up to the age of 30 weeks and showed severe cognitive deficits in the Morris water maze test. Furthermore, *Stim1/Stim2* double-knockout showed increased activity in the visual cliff test (Garcia-Alvarez et al., 2015). An increase in long-term potentiation and impairment in spatial memory reported in this study indicates that due to the absence of both STIM1 and STIM2 proteins, synaptic plasticity is severely impaired. Because of such inconclusive results on the mice model, the role of STIM2 in brain activity and behavior needs to be further explored. Also, there are still a need to understand the roles of Stim2 proteins in the neurons *in vivo* because the knockout and overexpression models Stim2 proteins suggested that these proteins clearly play a vital role in neuronal function such as learning and synaptic plasticity (Berna-Erro et al., 2009, Garcia-Alvarez et al., 2015). Recently, using OptoSTIM1 (an optically controlled construct) in *in vivo* system, it was demonstrated that expression and activation of Stim1 in mouse hippocampus was able to induce SOCE-mediated Ca^{2+} influx, which helped in contextual memory formation (Kyung et al., 2015). Considering the fact that Stim2 isoforms in zebrafish might have diverse effects on brain activity, the role of both Stim2a and Stim2b in zebrafish has been investigated in our laboratory. The characterization of *stim2b*$^{-/-}$ lines have already been published (Wasilewska et al., 2020). The main aim of this present study was to establish the role of Stim2a in brain

neurons of zebrafish using its knockout *stim2a*$^{-/-}$ line and to identify the new candidate genes involved in Ca^{2+} signaling in all types of zebrafish neuronal origin cells (*stim2a*;*stim2b)*$^{-/-}$. The objectives of this study are following:

a. Characterization of generated by CRISPR/Cas9 method *stim2a*$^{-/-}$ knockout line.

b. Description of the behavioral phenotype of *stim2a*$^{-/-}$ knockout zebrafish line.

c. *In vivo* Ca^{2+} imaging in brain neurons of *stim2a*$^{-/-}$ knockout zebrafish line.

d. Analysis of gene expression of *stim2a*$^{-/-}$ line.

e. Single-cell RNA-seq in the neuronal origin cell population (based on *Huc* promotor, expressed in early neurons) from Tg(*HuC:GcaMP5G*);*(stim2a;stim2b)*$^{-/-}$ in comparison to the line expressing both forms of *stim2* and GCaMP5.

Chapter 2: Materials and Methods

2.1 Statement of ethics

All the experiments with larvae and adult fish were conducted in accordance with the European Communities Council Directive (63/2010/EEC). All animals were maintained according to internal regulations in the Zebrafish Core Facility that is a licensed breeding and research facility (PL14656251, registry of the District Veterinary Inspectorate in Warsaw; 064 and 051, registry of the Ministry of Science and Higher Education) at the International Institute of Molecular and Cell Biology in Warsaw.

2.2 Animal husbandry

Wildtype (WT; AB line), *stim2a* mutant (*stim2a*$^{-/-}$), and double mutant for *stim2a* and *stim2b (stim2a;stim2b)*$^{-/-}$ and Tg(*HuC:GCaMP5G*) (Ahrens et al., 2013) zebrafish lines were used in the study. According to standard protocols, the experimental animals were maintained in the Zebrafish Core Facility (Matthews et al., 2002), except before behavior analyses. For the WT, the AB zebrafish line was used as the WT control. Maximum 24 adult fish were kept per tank (Volume: 3.5L), with a zebrafish recirculating system and regular photoperiod (14 h/10 h light/dark cycle) at 28.5°C. For the experiments, zebrafish embryos were obtained by random mating. The collected embryos were sorted in E3 water (2.48 mM NaCl, 0.164 mM $CaCl_2$·2H2O, 0.09 mM KCl, and 0.428 mM MgCl2·6H_2O) at a density of ~50 embryos/Petri dish (10 cm) and kept in an incubator under standard conditions (28.5°C and normal 14 h/10 h light/dark cycle) until the stage of development was reached for specific experiments.

2.3 Creation of *stim2a*$^{-/-}$ mutant line and genotyping

PCR combined with enzyme restriction digestion (RD) was used to determine the WT and *stim2a*$^{-/-}$ fish. The *stim2a*$^{-/-}$ zebrafish line was created, CRISPR/Cas9 system, by introducing a five bp deletion in the 7th exon (Ensembl ID: ENSDART00000114097.4), which give an early stop codon. Tail fin tissue from 2-month-old fish was digested in TE buffer with proteinase K (0.5 mg/ml final concentration) overnight at 50°C. Polymerase chain reaction (PCR) was done on the DNA obtained from the overnight digested fins with the following primer sets: forward (5'-AACTCAGCCGTCTGTGGTATGCG-3'); reverse (5'-TGACGTTGTAGTACTGAACCTCCACCTC-3'). The PCR product was digested with the Mbo II restriction enzyme. The WT fish has the restriction site for this restriction enzyme,

but the mutant does not. After RD, in the gel electrophoresis, WT fish showed two bands, heterozygous (*stim2a*$^{+/-}$) showed three bands, but homozygous mutant fish (*stim2a*$^{-/-}$) showed a strong single band. This generation crossed with the AB line to have the AB background, and then heterozygous fish were in-crossed to obtain homozygous mutants.

2.4 Generation and genotyping of *(stim2a;stim2b)*$^{-/-}$ mutant zebrafish line

To create the double mutant *(stim2a;stim2b)*$^{-/-}$ mutant zebrafish line, *stim2a*$^{-/-}$ fish were outcrossed with *stim2b*$^{-/-}$ line (available in our facility and well-characterized (Wasilewska et al., 2020)). Heterozygous fish of this F1 generation were in-crossed. To identify the homozygous *(stim2a;stim2b)*$^{-/-}$, in the F2 generation, first *stim2b*$^{-/-}$ genotyping was done according to previously set-up protocol, using high-resolution melting (HRM) analysis. From this HRM analysis, WT and *stim2b*$^{-/-}$ fish were screened for the *stim2a*$^{-/-}$, as described above. WT and *(stim2a;stim2b)*$^{-/-}$ fish were identified from this screening.

2.5 GCaMP5G zebrafish lines

For the *in vivo* Ca^{2+} imaging experiments, Tg(*HuC:GcaMP5G*);*stim2a*$^{-/-}$ and Tg(*HuC:GcaMP5G*);*(stim2a;stim2b)*$^{-/-}$ fish on the casper background were created. To create Tg(*HuC:GcaMP5G*);*stim2a*$^{-/-}$ line, Tg(*HuC: GcaMP5G*) line (Ahrens et al., 2013) fish were outcrossed with *stim2a*$^{-/-}$ line, and the 3 dpf embryos were screened for the green fluorescent signal. Embryos with positive GCaMP signal (Tg(*HuC:GcaMP5G*$^{+/-}$);*stim2a*$^{+/-}$) were allowed to grow. At three months of maturity, these Tg(*HuC:GcaMP5G*$^{+/-}$);*stim2a*$^{+/-}$ fish were in-crossed to generate Tg(*HuC:GcaMP5G*);*stim2a*$^{+/+}$ line (used as a control) and Tg(*HuC:GcaMP5G*);*stim2a*$^{-/-}$ line, and the 3 dpf embryos were screened for the GFP signal. To identify the Tg(*HuC:GcaMP5G*);*stim2a*$^{+/+}$ and Tg(*HuC:GcaMP5G*);*stim2a*$^{-/-}$ fish, at ~50 dpf, tail fin tissue was obtained, and genotyping was performed as it was described above in case of *stim2a*$^{-/-}$ line. Similarly, to create Tg(*HuC:GcaMP5G*);*(stim2a;stim2b)*$^{-/-}$ line, Tg(*HuC:GcaMP5G*) line fish were outcrossed with *(stim2a;stim2b)*$^{-/-}$ line, and the 3 dpf embryos were screened for the GCaMP signal. Embryos with positive GCaMP signal (Tg(*HuC:GcaMP5G*$^{+/-}$);*(stim2a;stim2b)*$^{+/-}$ were allowed to grow. At three months of maturity, these Tg(*HuC:GcaMP5G*$^{+/-}$);*(stim2a;stim2b)*$^{+/-}$ fish were in-crossed to generate Tg(*HuC:GcaMP5G*);*(stim2a;stim2b)*$^{+/+}$ line (used as a control) and Tg(*HuC:GcaMP5G*);*(stim2a;stim2b)*$^{-/-}$ line, and the 3 dpf embryos were screened for the GFP signal. To identify the Tg(*HuC:GcaMP5G*$^{+/-}$);*(stim2a;stim2b)*$^{+/-}$ and

Tg(*HuC:GcaMP5G*);*(stim2a;stim2b)*$^{+/+}$ fish, at ~50 dpf, tail fin tissue was obtained and genotyping was performed as it was described above in case of *(stim2a;stim2b)*$^{-/-}$ line.

2.6 Behavioral experiments

According to previously published protocols, the behavioral experiments were performed (Champagne et al., 2010, Colwill et al., 2011, Schnorr et al., 2012, Wasilewska et al., 2020) (in cooperation with Dr. Iga Wasilewska) on 4 dpf larvae. Embryos were collected in a Petri dish (~50 larvae/dish) and kept under a 14h/10h light/dark cycle in an incubator. For the experiments, embryos were randomly selected, and just before starting the actual behavioral experiments, for at least 30 min, larvae were habituated to the behavioral testing room. For the glutamate treatment, the first 30 mM of glutamate stock solution was prepared in E3 water. For the PTZ treatment, 0.5 M stock solution was prepared in the E3 water. Further, 2X concentrated solutions (i.e., 1.2 mM glutamate and 30 mM PTZ) were prepared in E3 water to give the drug treatments during the behavioral tests. These solutions were mixed in a 1:1 proportion in E3 water for the final experiments to obtain final working doses of 600 µM glutamate and 15 mM PTZ. Using the ZebraBox high-throughput monitoring system (ViewPoint), the larvae's locomotor activity was recorded in each experimental condition. The video recordings of these activities were further analyzed using EthoVision XT software (Noldus), and data were exported to MS Excel files for further analysis. There were larvae that were not active during the entire recording period (total distance < 10 mm), their data were excluded from the analyses. The analysis output from EthoVision was exported and analyzed using R software (v.3.6.0). The data were presented as medians with Q1 and Q3 quartiles using boxplots, and dots represent data outliers unless otherwise stated. Following behavioral experiments were performed:

2.6.1 Open field test: As previously described, zebrafish larvae were transferred to a 12-well plate (1 embryo/well) just 2 min before start the recording in the test (Wasilewska et al., 2020). Each well contained 2 ml of E3 medium, and the light intensity was set to 70%. The test duration was 15 min, and the total distance traveled in either the border or central zones of the wells (Schnorr et al., 2012), the duration of movements in each area, and the duration of not-movement in each area. During the data analysis, 15 min recording period was divided into three 5 min periods. As described previously, thigmotaxis was presented as the percent time spent in both borders or center zones (relative to the total time duration of movement plus duration without movement) (Schnorr et al., 2012).

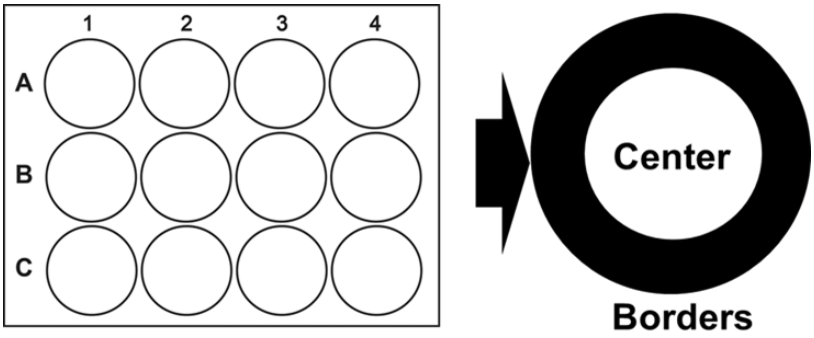

Figure 2.1. Schematic representations of the open field test in a 12-well plate. (schematic was drawn by Dr. Oksana Palchevska and opted from Gupta et al., 2020).

2.6.2 Dark/light preference test: As described previously (Kedra et al., 2020), in this experiment, a 10-cm Petri dish was used, where half of the Petri dish was covered with a photographic filter to divide the area into dark and light parts. The sidewall of the Petri dish was covered with black vinyl tape to avoid light from any other source. In the Petri dish, 20 ml of E3 medium was used, and the light intensity was set to 70% during the experiment, and locomotor activity was recorded for 15 min. To assess phototaxis, the mean total distance traveled (mm) in each part was calculated.

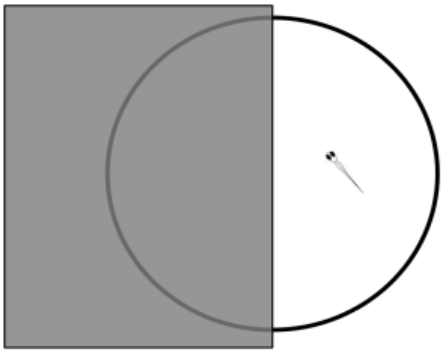

Figure 2.2. Schematic representations of the light/dark preference test in a 10 cm Petri dish. (schematic was drawn by Dr. Oksana Palchevska and opted from Gupta et al., 2020).

2.6.3 Visual-motor response test: as described previously (Liu et al., 2015), before the actual experiment, to acclimatize to the environment, the larvae were placed in 24-well plates containing 1 ml of E3 medium on the day before the experiment. Half an hour before recording the locomotor activity, the plate was placed in the ZebraBox. Just 2 minutes before recording, half of the E3 medium volume was exchanged (based on treatment) with either glutamate solution or PTZ solution. Fish were exposed to E3 water only were considered as a

control. This test was divided into three phases according to the changes in lighting conditions. According to long-lasting changes in activity in zebrafish, that are induced by these changes, phases were named: baseline (0% light intensity, 0-10 min), low activity phase (70% light intensity, 10-20 min), and high activity phase (0% light intensity, 20-30 min). For each of these phases, the mean total distance traveled (mm) was analyzed independently.

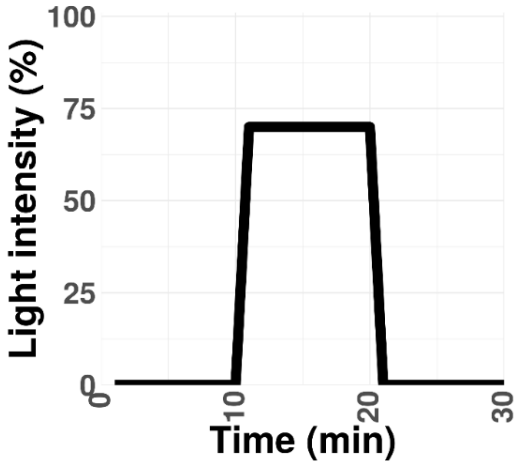

Figure 2.3. Schematic representations of the visual-motor response protocol. (schematic was drawn by Dr. Oksana Palchevska and opted from Gupta et al., 2020).

2.7 *In vivo* Ca^{2+} imaging

The neuronal activity was recorded by *in vivo* calcium imaging in zebrafish larvae brain using a Lightsheet microscope (40X/1.0 objective, Zeiss Z.1). In the case of *stim2a*$^{-/-}$ mutant, Tg(*HuC:GcaMP5G*):*stim2a*$^{-/-}$ zebrafish and their *stim2a*$^{+/+}$ siblings (Tg) were used in *in vivo* calcium imaging experiments. 4 dpf old larvae were used for this experiment. Zebrafish larvae were first immobilized using the cholinergic blocker pancuronium bromide 0.6 µg/µl (Sigma-Aldrich, catalog no. P1918) (Knafo et al., 2017) and then mounted in 1.5% low-melting-point agarose (Sigma-Aldrich, catalog no. A9414). Time-lapse imaging was done for 5 min, with 15 ms exposure and a frequency of 1 frame/s. A plane that contained the cerebellum, habenula, and optic tectum was selected. Changes in GCaMP5G fluorescence were observed, which indicated spontaneous neuronal Ca^{2+} oscillations in the zebrafish larvae brain. As described previously, using MATLAB (Mathworks, Natick, MA), from the cells in the periventricular gray zone of the optic tectum, fluorescence changes were extracted at single-cell resolution (Panier et al., 2013) **(Figure 2.4)**. This change in fluorescence data was exported in the excel file for further analysis. In MATLAB, using a function named

"peakdet" which detects peaks based on changes in slope, peaks of oscillations of Ca^{2+} were selected, and afterword average oscillation frequency and the average amplitude of Ca^{2+} signals were analyzed.

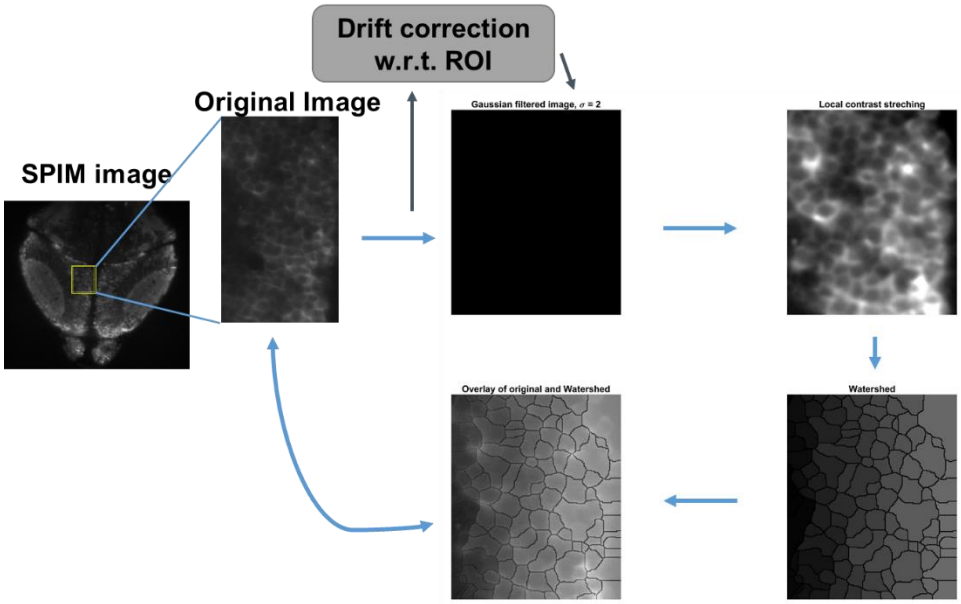

Figure 2.4. Automated image-segmentation prototype to draw the Region of interest (ROI): Automated cell segmentation was performed (Panier et al., 2013). (Figure opted from Gupta et al., 2020).

The Wilcoxon rank-sum test was used to compare average oscillation frequencies between Tg and *stim2a*$^{-/-}$ animals. The data are presented as medians with Q1 and Q3 quartiles using boxplots, and dots represent data outliers. The numbers of cells that were analyzed: 392 cells from seven *stim2a*$^{-/-}$ animals and 168 cells from three Tg animals.

2.8 Quantitative RT-PCR gene expression analysis

Total 30 zebrafish larvae (5dpf) were pooled together to make one sample. Larvae were transferred into Qiazol (Qiagen, Hilden, Germany), and RNA was isolated as described in the previously published protocol (Peterson et al., 2009). Using the iScript cDNA Synthesis Kit (Bio-Rad, Hercules, CA, USA), RNA was converted into cDNA. Using FastStart Essential DNA Green Master (Roche, catalog no. 06402712001), qPCR was performed (in duplicate). The SOCE gene expression was checked as previously described (Wasilewska et al., 2020). For the gene expression level analysis, CFX Connect RT-PCR Detection System (Bio-Rad, Hercules, CA, USA) was used.

2.9 Bulk RNA sequencing

For the RNA sequencing, RNA was isolated exactly the way it was done for the qPCR analysis. Bioanalyzer (Agilent, USA) analysis was done and used for the sequencing (You et al., 2018). The Illumina sequencing platform was us for sequencing at the International Institute of Molecular and Cell Biology in Warsaw with support from the Core Facility.

2.10 Transcriptome analysis

From the raw RNA-seq data, FASTQ format files were formed with bcl2fastq2 (v2.17, Illumina), and then the quality was assessed by FastQC. Using R-software, reads were then aligned to the zebrafish reference genome (GRCz11) with the help of the Rbowtie2 aligner (Langmead et al., 2012).

2.11 Differential gene expression analysis

SeqMonk (Version 1.42.0) () was used for the aligned RNA-seq data for visualization and differential gene expression analyses. Differential gene expression (DEGs) analyses were done using the Bioconductor packages, edgeR (v3.16.0) and DESeq2 (v1.6.378) (Love et al., 2014) across all replicates. In the edgeR analysis, those genes with at least one count per million were used for analysis. Shrinkage of dispersion and fold-change estimates are implemented in DESeq2 to improve stability and interpretability, meaning that logarithmic fold-changes will have more shrinkage when there is little information available gene (i.e., low read count, high dispersion, or few degrees of freedom). *P*-values were corrected for false positives using the Benjamini and Hochberg false discovery rate (FDR) correction for multiple testing within DESeq2 (Love et al., 2014). Genes with an FDR (or *q*-value) < 0.05 were regarded as statistically significantly different. DEGs with a fold change $\geq$ two were subjected to further analysis.

2.12 Gene Ontology and Pathway Analysis

The Protein Analysis Through Evolutionary Relationships (PANTHER) Classification System was used to searching enriched GO terms (Thomas et al., 2003). As a reference gene list (http://pantherdb.org/), *Danio rerio* genome was used, which allowed identifying molecular functions, cellular components, and related pathways from the Gene Ontology (GO) terms (Wasilewska et al., 2020).

2.13 Statistical analysis

Logarithmic (log2) fold changes were analyzed on the RNA sequencing data. The RNA seq data were represented as mean ± SEM if the log2 fold change was > 2 and < -2. The false discovery rate (FDR) was used to estimate the statistical significance of gene expression using RNA sequencing.

2.14 Single-cell RNA sequencing

2.14.1 Isolation of single-cell suspension: 5 dpf larvae were anesthetized by tricaine methanesulfonate (MS222), a neuromuscular blocker (Collymore et al., 2014), and heads were dissected in Dulbecco's Modified Eagle Medium/Nutrient Mixture F-12 (DMEM/F-12; with Ca^{2+}, and L-glutamine, and without HEPES, and Phenol Red; Gibco) with 10% fetal bovine serum (FBS; Gibco). After eyes were removed promptly, tissue dissociation and single-cell suspension were made according to previously described methods (Bresciani et al., 2018) for zebrafish and placed on ice (**Figure 2.5)**.

2.14.2 Isolation of the neuronal origin cells: Immediately after isolation of single-cell suspension, the cells were sorted based on GCaMP5G fluorescence (with 488 nm excitation and 510 nm emission) to obtain the cells of neuronal origin. The GCaMP5 was expressed under the *elav/Huc* promoter, which is an early marker of neuronal cells (Kim et al., 1996, Feng et al., 2019). Cell sorting was performed with a BD FACSAria II (BD Biosciences, Franklin Lakes, NJ) with support from the Core Facility at the International Institute of Molecular and Cell Biology in Warsaw. Cell viability was measured using the trypan blue staining method, and when the viability of cells was ~80%, the cells were immediately loaded on the 10X Chromium system for droplet encapsulation as described previously (Zheng et al., 2016).

2.14.3 Droplet encapsulation, library preparation, and sequencing: Approximately 8000 cells were sorted and suspended in ~40 µl volume. Cells were loaded according to the Chromium single cell 3′ kit's standard protocol (V3 chemistry). To prepare the cells for droplet-based sequencing, GCaMP5G-positive single-cell suspension was carefully mixed with reverse transcription mix before loading the cells on the 10X Genomics Chromium system, the standard manufacturer's protocol. During the encapsulation, the cells were lysed within the droplet, and they released polyadenylated RNA bound to the barcoded bead, which was encapsulated with the cell. Following the 10x Genomics user manual's guidelines, the

droplets were directly subjected to reverse transcription, the emulsion was broken, and cDNA was purified using Silane beads. After the amplification of cDNA with 13 cycles, purification and quantification were performed. The 10X Genomics single-cell RNA-sequencing library preparation – involving fragmentation, dA-tailing, adapter ligation, and 12-cycle indexing PCR – was performed. After quantification, the libraries were sequenced at the Nencki Institute of Experimental Biology on an Illumina NextSeq 550 machine using a HighOutput flowcell in paired-end mode (R1: 26 cycles; I1: 8 cycles; R2: 57 cycles), thus generating 80-125 million fragments.

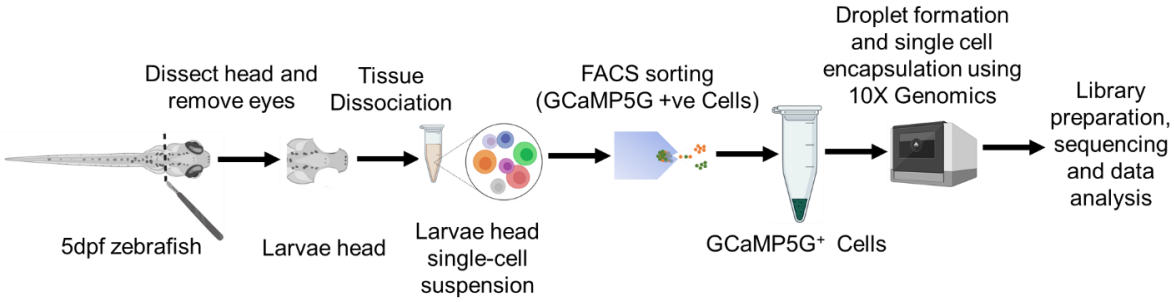

Figure 2.5. Schematic showing the cells preparation and processing of the 5dpf zebrafish brain, FACS sorting, library preparation and data analysis.

2.14.4 Single-cell RNA-seq data processing: Using 150 nt paired-end sequencing, single-cell libraries were sequenced on Illumina HiSeqXTen instruments. Using Cell Ranger 2.1.0 pipeline with default and recommended parameters, reads were processed. FASTQs generated from Illumina sequencing output were aligned to the zebrafish genome (GRCz10) as well as gene annotation (Ensembl 91) were downloaded from Ensembl, and the annotation was filtered with the 'mkgtf' command of Cell Ranger (options: '–attribute=gene_biotype:protein_coding –attribute=gene_biotype:lincRNA –attribute= gene_biotype-:antisense') using the STAR algorithm (Shi et al., 2020). Next, for each sample, by counting gene-Barcode matrices were generated unique molecular identifiers (UMIs) and filtering non-cell associated barcodes. Finally, we generated a gene-barcode matrix containing the barcoded cells and gene expression counts. The raw sequencing data was then processed with the 'count' command of the Cell Ranger software provided by 10X Genomics. Outputs from here were imported into the Seurat (v2.3.0) R toolkit for quality control and downstream analysis of our single-cell RNAseq data. All functions were used with default parameters. Low quality cells (<3 cells/gene and <200 genes/cell), including >5% mitochondrial genes were excluded.

2.14.5 Cell types identification and subtypes using t-SNE (nonlinear dimensional reduction): In R, the Seurat package was implemented to identify major cell types (Stuart et al., 2019). Highly variable genes were generated and used to perform principle component analysis (PCA). These groups were represented in t-SNE analysis run using previously computed principal components 1 to 20. The identities of cell types were characterized based on the expression of known markers.

2.14.6 Cell-cluster markers identification: Using the 'FindAllMarkers' function in the Seurat package, cluster-specific marker genes were identified on the normalized gene expression data. The 'find.markers' function was used to identify differentially expressed genes between two clusters.

2.15 Materials

2.15.1 Chemicals

Name	Source
Glutamate	Sigma-Aldrich
Pentylenetetrazol (PTZ)	Sigma-Aldrich
Pancuronium bromide	Sigma-Aldrich
Low melting agarose	Sigma-Aldrich
Qiazol	Qiagen
iScript cDNA Synthesis Kit	Bio-Rad
SuperScript IV First-Strand Synthesis System	Invitrogen
Precision Melt Supermix	Bio-Rad
TRI reagent	Invitrogen
RNA Clean and Concentrator Kit	ZYMO Research
Agarose	BioShop
Ethanol	VWR
Isopropanol	VWR
KH_2PO_4	Merck
NaOH	Merck
Na_2HPO_4	Sigma
PBS (pH 7.4)	Invitrogen
Triton-X-100	Sigma-Aldrich
$CaCl_2$	Sigma-Aldrich

EGTA	Sigma-Aldrich
Glucose	Sigma-Aldrich
KCl	Sigma-Aldrich
$MgCl_2$	Roth
NaCl	Sigma-Aldrich
Mbo II restriction enzymes	Thermo Scientific
QIAquick PCR Purification Kit	Qiagen
LightCycler 480 High-Resolution Melting Master	Roche
BioMix Red (RNA Polymerase)	Bioline
Proteinase K	Sigma-Aldrich

2.15.2 Cell culture media

1. DMEM supplemented with 10% FBS
2. Trypsin (0.25%) supplemented with 40 µL Collagenase (100 mg/mL concentration)

Ingredient	Source
DMEM	Gibco, Life technologies
Fetal Bovine Serum (FBS)	Sigma-Aldrich
Trypsin	Sigma-Aldrich
Collagenase	Sigma-Aldrich

2.15.3 Commonly used buffers

1. PBS (10X): 80 g NaCl, 2 g KCL, 14.4 g Na_2HPO_4, 2.4 g KH_2PO_4, ddH_2O (up to 1 Liter)

2. TE buffer (10X): 15.759 g Tris-Cl (pH 7.5), 2.92 g EDTA (pH 8.0), ddH_2O (up to 1 Liter)

3. E3 Water (50X): 0.63 g KCl, 14.6 g NaCl, 2.43 g $CaCl_2 \cdot 2H2O$, and 4.07 g $MgCl_2 \cdot 6H_2O$

2.17.4 Equipment

Equipment Name	Source
Argon Laser	LASOS
Lightsheet Microscope	Zeiss
Helium-Neon Laser	LASOS

Inverted microscope	Olympus
Cover glasses	VWR
Needles 27G/20G	VWR
Syringes 1, 2, 5, 10, 20 mL	VWR
Bio-Rad CFX Real-Time PCR Instruments	Bio-Rad
Electrophoresis gel run system	Bio-Rad
Agilent RNA 6000 Nano Chip	Agilent
LightCycler 96 System	Roche
ZebraBox high-throughput monitoring	ViewPoint Life Sciences
NGS NextSeq 500 (Illumina)	Agilent

2.15.5 Software

Software Name	Source	Website
ZEN2020 Black	Zeiss	http://www.zeiss.com/microscopy
Matlab	MathWorks	https://www.mathworks.com/products/matlab.html
R-Project	Bell Laboratories	https://www.r-project.org/
Bio-Rad CFX Maestro	Bio-Rad	https://www.bio-rad.com/
EndNote X8	Clarivate Analytics	https://endnote.com/
EthoVision XT	Noldus	https://www.noldus.com/ethovision-xt
FastQC (version0.11.4)	Babraham Bioinformatics	https://www.bioinformatics.babraham.ac.uk/projects/fastqc/
SeqMonk (Version 1.42.0)		https://www.bioinformatics.babraham.ac.uk/projects/seqmonk/

Chapter 3: Results

3.1 Genotyping of *stim2a*$^{-/-}$ mutant zebrafish line and phenotypic analysis

The *stim2a*$^{-/-}$ mutant zebrafish line was created using CRISP/Cas9 technology at ZeClinics, a leading CRISPR licensed Contract Research Organization in Barcelona. The embryos were imported and revived in Zebrafish Core Facility at the International Institute of Molecular and Cell Biology in Warsaw. The *stim2a* gene in zebrafish is located on chromosome-1 and has 12 exons (Ensembl ID: ENSDART00000114097.4) (**Figure 3.1A)**. Using CRISP/Cas9 technology, a deletion of 5 bp in the 7th exon (SOAR domain sequence) produced an early stop codon, resulting in truncation during the protein synthesis (**Figure 3.1A, B**). Adult fish with the mutation in *stim2a* were recognized by genotyping by PCR combined with enzyme restriction digestion (RD). This approach is inexpensive, sensitive, and fast, with a lower risk of cross-contamination or artifacts. Fin-clipping was done at two months old fish, and DNA was isolated using proteinase-K digestion overnight (Xing et al., 2014). Then PCR was done with specific genotyping primers, and 237 bp PCR product is clearly visible in the gel picture (**Figure 3.1C**). Restriction digestion was done using the Mbo II restriction enzyme on this PCR product. In *stim2a*$^{-/-}$ mutant zebrafish, the Mbo II restriction enzyme recognition site is absent, but it was present in WT. Based on that, samples from WT, heterozygous and homozygous fish could be clearly identified in the gel (**Figure 3.1C**). The *stim2a*$^{-/-}$ mutant zebrafish larvae did not exhibit any visible phenotype or developmental abnormalities compared to the WT (**Figure 3.2A**). Survival rate was also performed till 120 hpf for the *stim2a*$^{-/-}$ mutant zebrafish larvae and compared with WT, which exhibited no change (**Figure 3.2B**). Furthermore, adult *stim2a*$^{-/-}$ mutant zebrafish larvae were viable and fertile.

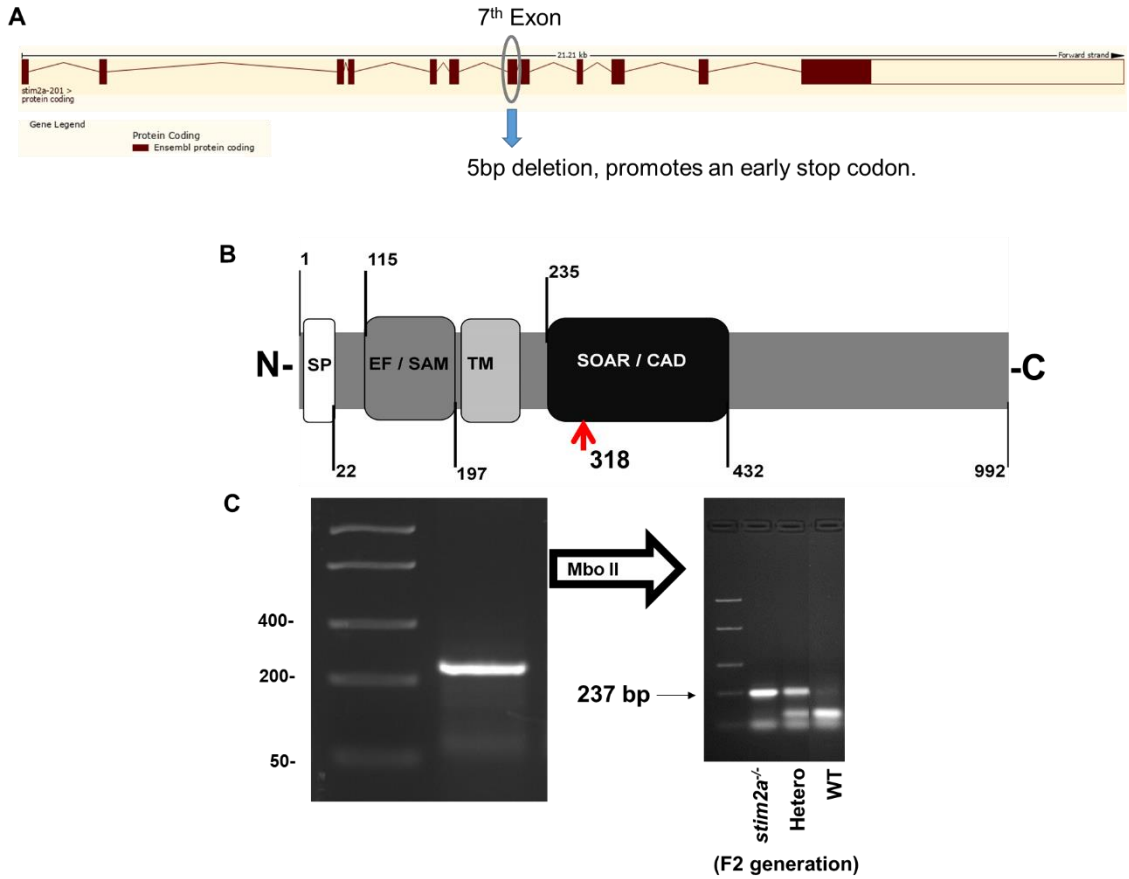

Figure 3.1. Generation of *stim2a*$^{-/-}$ mutant zebrafish line. (A) Schematics of *stim2a* in the zebrafish genome and Stim2a protein domains. EF/SAM, EF-hand/sterile α-motif (EF/SAM) Ca^{2+}-binding endoplasmic reticulum (ER)-luminal domain,; SP, signal peptide; TM, transmembrane domain; SOAR/CAD, STIM1 Orai1-activating region/CRAC-activating domain. Red arrow indicates the stop codon introduction site. (B) Representative gel electrophoresis of genotyping; WT, with two fragments of PCR product after restriction digestion with Mbo II restriction enzyme. The mutant is not cleaved and showed in one strong band of 237 bp. Sample heterozygous larvae showed three bands after restriction digestion with the Mbo II restriction enzyme.

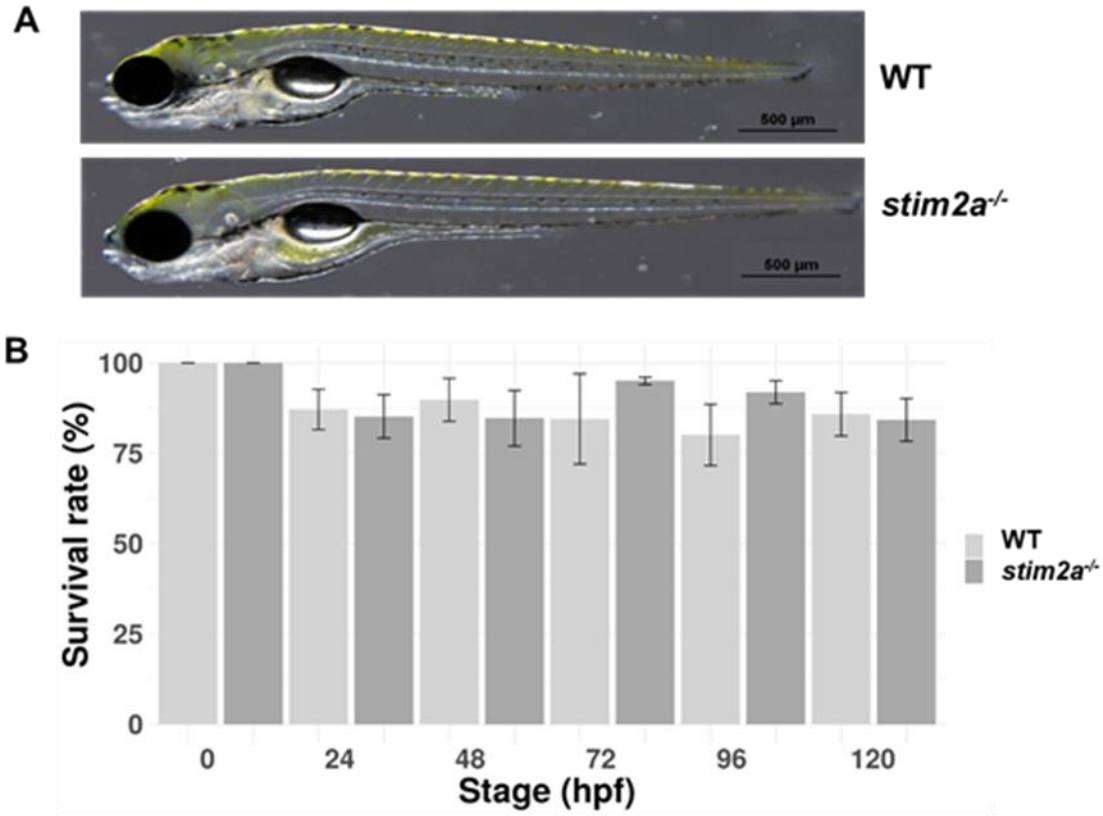

Figure 3.2. The survival and morphology of *stim2a*$^{-/-}$ mutants zebrafish larvae. (A) Side views of WT and *stim2a*$^{-/-}$ mutant zebrafish larvae at 5dpf. Scale bars = 500 µm. (B) Percentage of surviving WT and *stim2a*$^{-/-}$ mutant zebrafish larvae during the first 120 h of development. The data are expressed as mean ± SEM. Number of repetitions: 3. Number of larvae for each repetition: 200. (Zebrafish images were taken by Dr. Oksana Palchevska and figure opted from Gupta et al., 2020).

3.2 SOCE component transcripts analysis in *stim2a*$^{-/-}$ mutant zebrafish by real-time RT-PCR

The real-time RT-PCR was performed to check the expression level of the SOCE component genes in *stim2a*$^{-/-}$ mutant zebrafish. The *stim2a* gene was found to be significantly downregulated. However, the level of expression of other genes of the SOCE components did not show any significant change in expression (**Figure 3.3**).

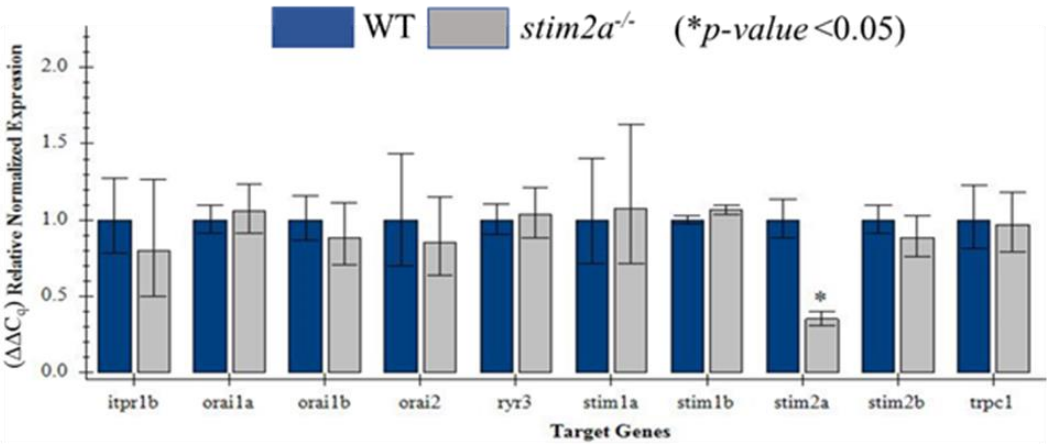

Figure 3.3. mRNA levels of SOCE components in 5-dpf zebrafish, quantified by real-time RT-PCR.

3.3 In the open field test *stim2a*$^{-/-}$ mutant zebrafish larvae showed increased thigmotaxis

Thigmotaxis reflects the preference of an organism's motion or orientation in response to a touch stimulus and tells the anxiolytic activity of the organism (Treit et al., 1988). Zebrafish reflect thigmotaxis behavior by showing the preference to stay at the border of the well compared to the central area (Blaser et al., 2010). To investigate the thigmotaxis behavior in *stim2a*$^{-/-}$ mutant zebrafish larvae, an open field test was done on 96-hpf larvae (**Figure 2.1**). Larvae were kept in a 12-well plate (1 larva/well), and the locomotor activity was recorded for 15 min. While analysis, data was divided into three phases, 5 min each. Also, the area of each well was divided into two equal parts in the border and center zone (**Figure 2.1**). In the first phase of the recording, it was assumed that the animals would be stressed as they were transferred from the dish to the experimental set-up. Both WT and *stim2a*$^{-/-}$ mutant zebrafish larvae spent more time in the well's border zone than the center, showing anxiety-like behavior (**Figure 3.4A**). However, when analyzed the distance moved in border and center zone, *stim2a*$^{-/-}$ mutant zebrafish larvae showed higher mobility than WT, indicating hyperactivity in both border and center zone. In the next phase (6-10 min interval), WT animals began to explore the entire well, as the data revealed WT were spending almost equal time in both the border and center zone of the well (**Figure 3.4A and 3.4B**). On the other hand, *stim2a*$^{-/-}$ mutant zebrafish larvae still preferred swimming at the border of the well and avoided the center (**Figure 3.4A and 3.4B**). Furthermore, in the third phase (11-15 min interval), WT and *stim2a*$^{-/-}$ mutant zebrafish larvae showed similar activity, i.e., spending the same amount of time in the border and center zone (**Figure 3.4A**). From these results, it was

concluded that *stim2a*$^{-/-}$ mutant zebrafish larvae required more time to habituate in the new environment, reflecting an increase in thigmotaxis.

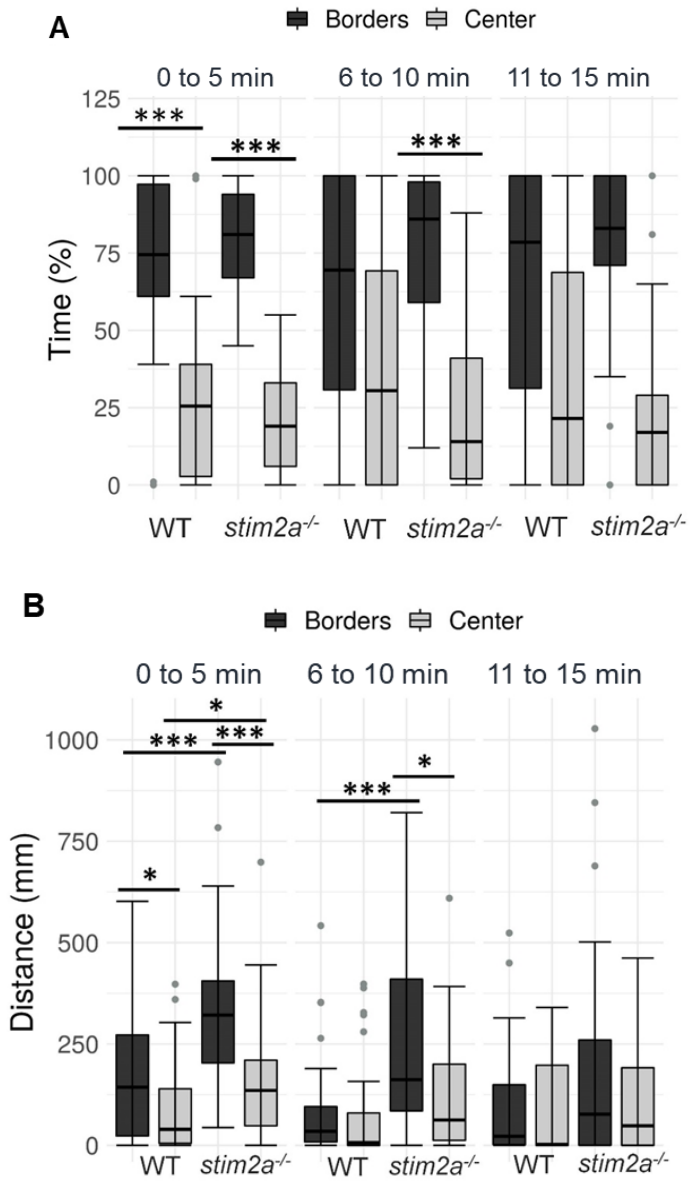

Figure 3.4. Higher thigmotaxis in *stim2a*$^{-/-}$ mutant zebrafish larvae in the open field test adopted for zebrafish larvae. Activity of larvae in a 12-well plate was recorded for 15 min. The analysis was divided into three phases, 5 min each (0-5 min, 6-10 min, and 11-15 min). (A) Box-plots of the time spent moving (duration of movement) while swimming either in the border zone or in the center of the well. (B) Box-plots show the distance traveled (in mm) in WT and *stim2a*$^{-/-}$ mutant zebrafish in either the border zone or in the center zone of the well. *$p < 0.05$, **$p < 0.01$, ***$p < 0.001$ (paired Wilcoxon rank-sum test for comparisons between border and center; unpaired Wilcoxon rank-sum test for comparisons between WT and *stim2a*$^{-/-}$ mutants). $n = 32$ for WT larvae. $n = 33$ *stim2a*$^{-/-}$ mutant larvae. Number of experiments: 3. (Figure opted from Gupta et al., 2020).

3.4 In light/dark preference test *stim2a*$^{-/-}$ mutant zebrafish larvae showed lower phototaxis

The light/dark preference test gives information about the phototaxis, when an organism moves in response to the light stimulus, a kind of locomotory action that occurs. We performed this test on WT and *stim2a*$^{-/-}$ mutant zebrafish larvae. We calculated three parameters, time fish spent in the light zone and dark zone of the Petri dish (**Figure 3.5A**), distance traveled in the light zone and dark zone of the Petri dish (**Figure 3.5B**), and total distance traveled by the fish in each group (**Figure 3.5C**). It was found that *stim2a*$^{-/-}$ mutant zebrafish larvae do not show any specific preference for the light or dark zone as it spent as much time in either zone of the Petri dish, in contrast to the WT, which stayed a significant amount of time in light zone (**Figure 3.5A**). This finding indicates that *stim2a*$^{-/-}$ mutant zebrafish larvae did not exhibit significant phototaxis. Furthermore, distance traveled in each zone showed that *stim2a*$^{-/-}$ mutant zebrafish larvae did not have any preference of light zone or dark zone as it swam almost a comparable distance in either zone of the Petri dish, in comparison to the WT, which traveled significant distance in the light zone (**Figure 3.5B**). In addition, overall mobility (total distance traveled in both zone combined) showed that *stim2a*$^{-/-}$ mutant zebrafish larvae traveled approximately four times higher than the WT fish (**Figure 3.5C**). Combining these three parameters, it was concluded that larvae with *stim2a* deletion had exhibited increased activity and significantly lower phototaxis.

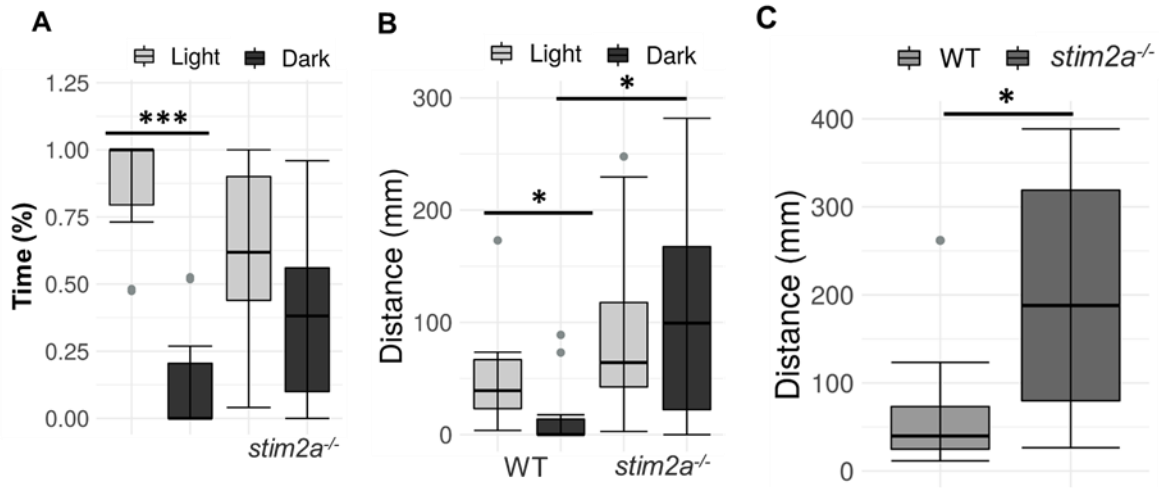

Figure 3.5. Hyperactivity and lower phototaxis in *stim2a*$^{-/-}$ mutant zebrafish larvae in the light/dark preference test. (A) Box-plots of the time spent moving (duration of movement) in the light and dark zones in WT and *stim2a*$^{-/-}$ mutant zebrafish larvae. (B) Box-plots of the distance traveled (in mm) in the light and dark zones of the Petri dish in WT and *stim2a*$^{-/-}$ mutant zebrafish larvae. (C) Box-plots of

the cumulative distance traveled (in mm) by WT and *stim2a*$^{-/-}$ mutant zebrafish larvae. *$p < 0.05$, **$p < 0.01$, ***$p < 0.001$ (unpaired Wilcoxon rank-sum test for comparisons between WT and *stim2a*$^{-/-}$ mutant zebrafish larvae; paired Wilcoxon rank-sum test for comparisons between the light and dark zones). n = 10 WT larvae. n = 11 *stim2a*$^{-/-}$ mutant zebrafish larvae. Number of experiments: 5. (Figure opted from Gupta et al., 2020).

3.5 The *stim2a*$^{-/-}$ mutant zebrafish larvae showed activity in the visual-motor response (VMR) test

Locomotor activity of WT and *stim2a*$^{-/-}$ mutant zebrafish larvae in response to a light stimulus, the visual-motor response (VMR) test was performed (**Figure 2.3**). In this test, zebrafish larvae react to light intensity modulations by exhibiting startle response, a very similar phenomenon in higher vertebrates. Changes in activity were measured due to switching in light/dark phases. Distance traveled was calculated during the three phases of the experiment: baseline (0% light illumination), low activity (70% light illumination), and high activity (0% light illumination) (**Figure 3.6**). No significant difference was detected in mobility between *stim2a*$^{-/-}$ mutant zebrafish larvae and WT in the baseline. However, with subsequent changes in light intensity, both groups showed a significant decrease in mobility. Though *stim2a*$^{-/-}$ mutant zebrafish larvae moved a significantly longer distance in this light phase, in the subsequent high activity phase (when the light was turned off), both WT and *stim2a*$^{-/-}$ mutant zebrafish larvae showed an increase in mobility and no significant difference was observed in the total distance traveled between both groups the dark phase, as it was in baseline phase (**Figure 3.6**). These findings of the VMR test were further supported the hyperactivity-phenotype of *stim2a*$^{-/-}$ mutant zebrafish larvae, which was shown in the open field test (**Figure 3.4**) and light preference test (**Figure 3.5**). Interestingly, the *stim2a*$^{-/-}$ mutant zebrafish larvae were able to differentiate the light and dark phases as proficiently as WT, which indicates that they were able to react to light.

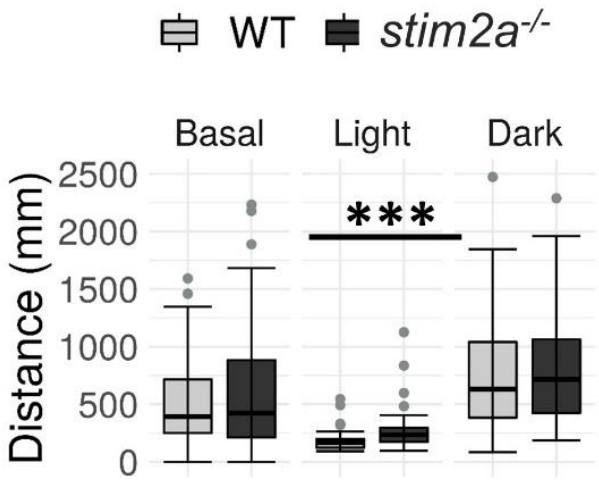

Figure 3.6. The *stim2a*$^{-/-}$ mutant zebrafish larvae reacted to changes in light and shoed hyperactivity during the low activity phase in the visual-motor response (VMR) test. Activity was recorded during a 30-min period that consisted of a baseline phase (Basal phase, 0% light illumination), low activity phase (Light phase; 70% light illumination), and high activity phase (Dark phase; 0% light illumination). Box-plots show the distance traveled (in mm) during the respective phase. ***$p <$ 0.001 (Wilcoxon rank-sum test). n = 53 WT larvae. n = 52 *stim2a*$^{-/-}$ mutant zebrafish larvae. Number of experiments: 6. (Figure opted from Gupta et al., 2020).

3.6 Visual-motor response (VMR) test after treatment with Pentylenetetrazol (PTZ) and glutamate

VMR test was performed after fish were treated with chemical agents to explore the alterations in behavioral reactions in response to the treatment. Two drugs, pentylenetetrazol (PTZ) and glutamate, known to stimulate neuronal activity, were administered, and VMR test (**Figure 2.3**) was performed. PTZ induces seizures, and glutamate increases locomotor activity by affecting the neuronal activity in zebrafish (Baraban et al., 2005, McCutcheon et al., 2016). More importantly, it was shown that glutamate was primarily attributable to an increase in brain activity as it can infiltrate the skin and reach the brain neurons.

15 mM concentration of PTZ treatment and 600 µM of glutamate were used. After treatment, distance traveled in baseline (0% light illumination), low activity (70% light illumination), and high activity (0% light illumination) were calculated (**Figure 3.7**). Both PTZ and glutamate affected the neuronal activity reflected by a significant increase in the distance traveled in each phase of the experiment. In exposure to the 15 mM PTZ, no significant difference was observed in the distance traveled by *stim2a*$^{-/-}$ mutant, compared to the WT (**Figure 3.7A**). However, a significant increase in the distance traveled was observed

after 15 mM PTZ exposure of WT, compared to the no exposure. Similarly, in *stim2a*$^{-/-}$ mutant, an increase in the distance traveled was observed after exposure to the 15 mM PTZ. This could be the result of seizure-like episodes. Furthermore, both WT and *stim2a*$^{-/-}$ mutant zebrafish larvae showed hyperactivity and no decrease in distance traveled with 15 mM PTZ treatment in the light (**Figure 3.7A**). Surprisingly, *stim2a*$^{-/-}$ zebrafish larvae reacted to 600 μM glutamate with a milder induction of locomotor behavior in the baseline phase (**Figure 3.7B**). Finally, no difference was observed in behavior between WT and *stim2a*$^{-/-}$ mutant zebrafish larvae during the high activity phase with either treatment (**Figure 3.7A, 3.7B**).

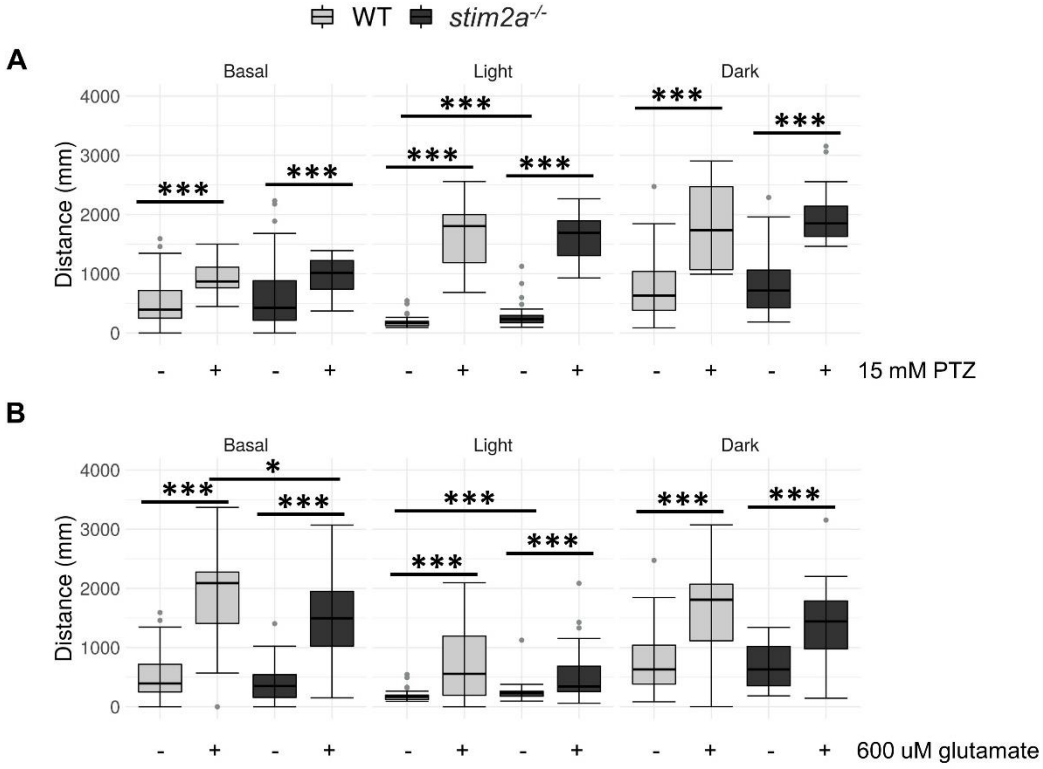

Figure 3.7. Exposure to PTZ and glutamate did not induce additional hyperactivity in *stim2a*$^{-/-}$ mutant zebrafish larvae. (A) Box-plots of the distance traveled (in millimeters) in WT and *stim2a*$^{-/-}$ mutant zebrafish larvae treated with PTZ. (B) Box-plots of the distance traveled (in mm) in WT and *stim2a*$^{-/-}$ mutant zebrafish larvae treated with glutamate. Activity was recorded during a 30-min period that consisted of a baseline phase (Basal phase, 0% light illumination), low activity phase (Light phase, 70% light illumination), and high activity phase (Dark phase, 0% light illumination). Half of the E3 medium was exchanged for either PTZ solution, just before the experiment, (15 mM final concentration) or glutamate solution (600 μM). –, untreated; +, treated. *$p < 0.05$, **$p < 0.01$, ***$p < 0.001$ (Wilcoxon rank-sum test). n = 18 larvae/group for PTZ treatment. n = 36 WT larvae and n = 35 for *stim2a*$^{-/-}$ mutant zebrafish larvae for glutamate treatment. Number of

experiments: 3. (Experiment was done in cooperation with Dr. Oksana Palchevska) (Figure opted from Gupta et al., 2020).

3.7 Increase in neuronal activity revealed *in vivo* by calcium imaging in the brain

In vivo Ca^{2+} imaging was performed to explore the changes in neuronal activity in *stim2a*$^{-/-}$ mutant zebrafish. Spontaneous Ca^{2+} activity in the brain neurons in WT and *stim2a*$^{-/-}$ mutant zebrafish larvae were monitored using the GCaMP5G Ca^{2+} sensor using lightsheet fluorescent microscope (LSFM)/selective plane illumination microscope (SPIM). The preview clearly showed that the brain somata were tightly packed (almost no extracellular space) in WT and *stim2a*$^{-/-}$ mutant zebrafish larvae (**Figure 2.4**). It was already shown from the other groups that optic tectum mediates the light response in behavior tests with light and dark (Suzuki et al., 2019). Considering that, neuronal cells from the sub-region in the periventricular gray zone of the optic tectum were chosen to analyze the spontaneous Ca^{2+} activity. Basal level average Ca^{2+} oscillation frequency was significantly higher in *stim2a*$^{-/-}$ mutant zebrafish larvae than WT (**Figure 3.8A**). This indicates an increase in neuronal activity in this brain region, so neurons were firing with higher frequency in *stim2a*$^{-/-}$ mutant zebrafish larvae. Nevertheless, the average Ca^{2+} oscillation amplitude was lower in *stim2a*$^{-/-}$ mutant zebrafish larvae than in the WT (**Figure 3.8B**).

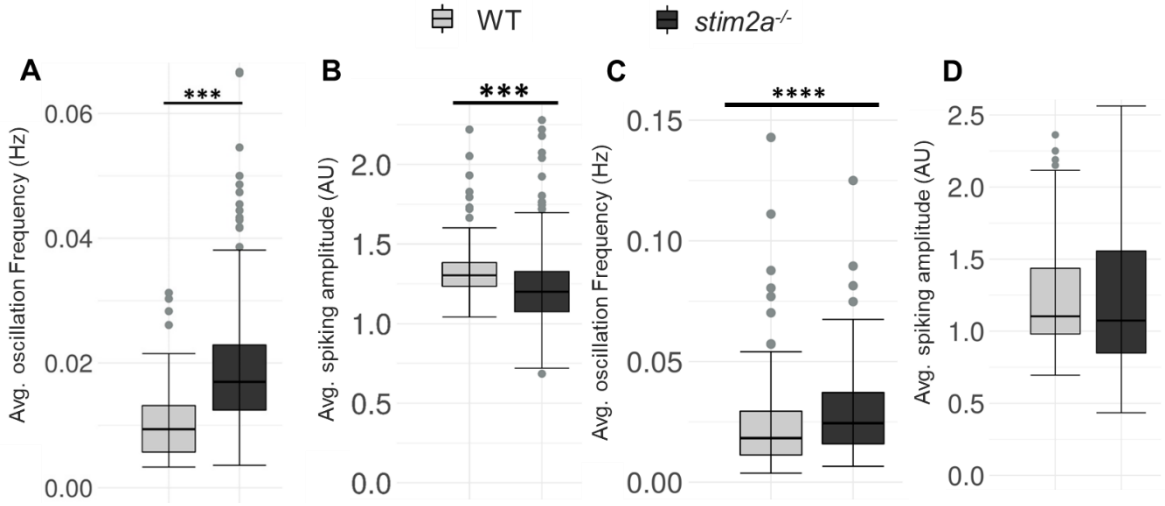

Figure 3.8. Increase in the Ca^{2+}spike frequency of neurons in *stim2a*$^{-/-}$ mutant zebrafish. *In vivo* Ca^{2+} imaging of WT and *stim2a*$^{-/-}$ mutant zebrafish larvae. (A) Box-plots show the basal level (in E3 water) of average Ca^{2+} oscillation frequency (in Hz). (B) Basal level (in E3 water) average Ca^{2+} oscillation amplitude (arbitrary unit). Number of cells: 168 WT, 392 *stim2a*$^{-/-}$ mutant zebrafish larvae. (C) Box-plots show the average Ca^{2+} oscillation frequency (in Hz) after treatment with 600 µM glutamate. (D) Average Ca^{2+} oscillation amplitude (arbitrary unit) after treatment

with 600 µM glutamate. Number of cells: 276 WT, 166 *stim2a*$^{-/-}$ mutant. Wilcoxon rank-sum test to compare *in vivo* Ca^{2+} responses of the brain between WT and *stim2a*$^{-/-}$ mutant zebrafish larvae. Number of animals: 3 WT, 7 *stim2a*$^{-/-}$ mutant. ***$p < 0.001$. (Figure opted from Gupta et al., 2020).

The same parameters were analyzed after 600 µM glutamate treatment. Interestingly, an increase in the average Ca^{2+} oscillation frequency was observed in the case of the *stim2a*$^{-/-}$ mutant zebrafish larvae in comparison to the WT (**Figure 3.8C**), though there was no significant difference in average Ca^{2+} oscillation amplitude between WT and *stim2a*$^{-/-}$ mutant zebrafish larvae (**Figure 3.8D**). This indicates that after glutamate treatment, the neuronal firing rate was increased. However, no change in oscillation amplitude occurred.

3.8 Differential gene expression analysis by next-generation RNA sequencing

To gain insights into molecular changes caused by *stim2a* deletion, we analyzed differentially expressed genes (DEGs) in WT and *stim2a*$^{-/-}$ mutant zebrafish larvae using next-generation RNA sequencing. Quality-checked of the raw reads were done with FastQC software. FastQC's plots of Phred scores by position (**Figure 3.9A and 3.9B**) for WT and *stim2a*$^{-/-}$ mutant zebrafish larvae showed typical profiles decreasing quality towards the ends of reads. 95% bases having Phred score 30 or better. The distribution of quality scores is presented (**Figure 3.9C and 3.9D**) for WT and *stim2a*$^{-/-}$ mutant zebrafish larvae. These analyses revealed that the raw sequence data were of high quality. FastQC analysis also detected duplicate reads, which was expected as the library construction involved a PCR amplification step. The RBowtie2 aligner (v 2-2.0.0-beta7) uniquely mapped the sequences with the reference genome.

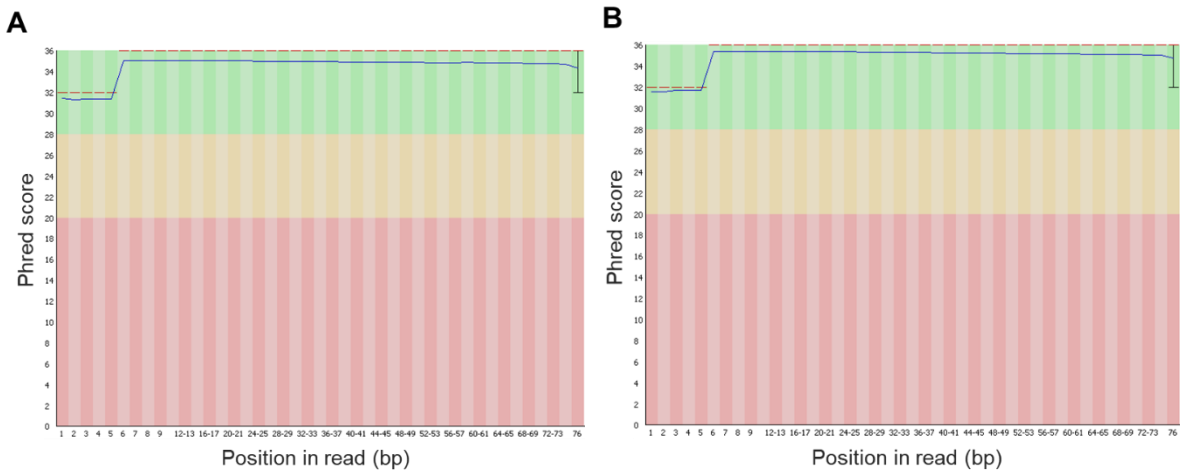

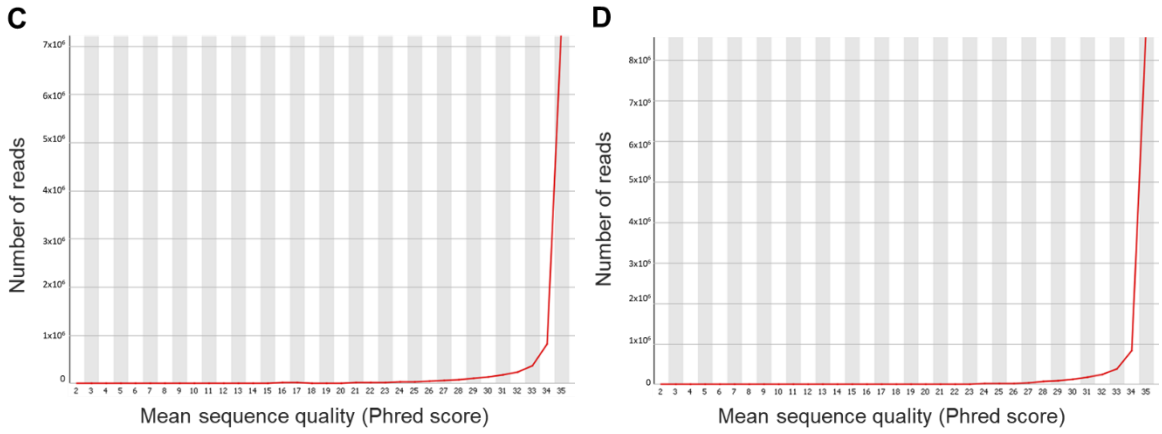

Figure 3.9. RNA sequencing data quality check. (A and B) Per base sequence quality expressed as Phred score by position, sample 1, first reads in WT and *stim2a*$^{-/-}$ mutant zebrafish larvae. (C and D) Quality score distribution over all reads of sample 1, in WT and *stim2a*$^{-/-}$ mutant zebrafish larvae.

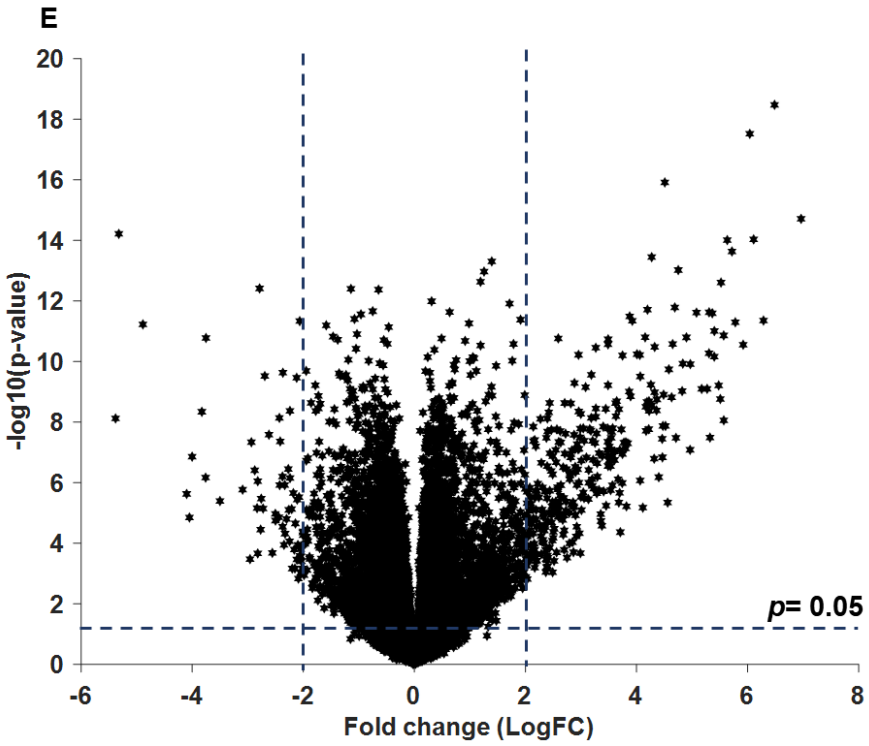

Figure 3.10. RNA sequencing analysis. Volcano plot of transcriptional differences between *stim2a*$^{-/-}$ zebrafish larvae and WT. The logarithms of fold changes in individual genes (x-axis) are plotted against negative logarithms of their *p*-value to base 10 (y-axis). Positive log2 (fold change) values represent upregulation in *stim2a*$^{-/-}$ mutant zebrafish larvae compared with WT, and negative log2 (fold change) values represent downregulation. Points those are above the dotted line parallel to the x-axis represent differentially expressed genes in *stim2a*$^{-/-}$ mutant zebrafish larvae with $p < 0.05$ after correction for multiple testing. (Figure opted from Gupta et al., 2020).

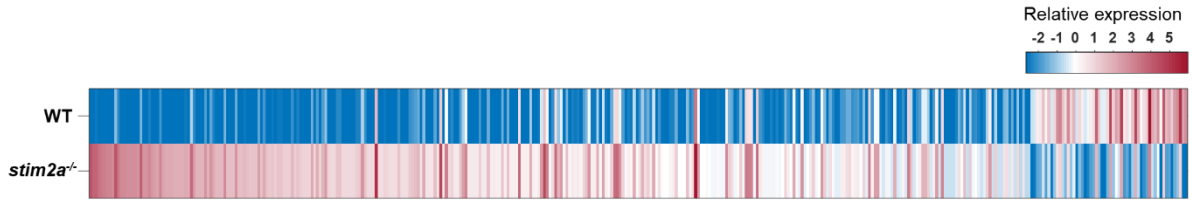

Figure 3.11. Heat map representing a total of 392 genes that were identified as being differentially expressed (log2 [fold change] ≥ 2) between WT and *stim2a*$^{-/-}$ mutant zebrafish larvae, including 336 upregulated genes and 56 downregulated genes.

A volcano plot was used to show all DEGs' overall distribution to give an overview of interesting genes (**Figure 3.10**). The fold-change in genes and *p*-value for the comparisons of WT versus *stim2a*$^{-/-}$ mutant zebrafish larvae were shown in the volcano plot. A total of 392 genes showed ≥ 2 fold change. A heatmap was plotted to compare the relative expression levels of these 392 genes (**Figure 3.11**). In that 392 genes, ~86% of genes were upregulated (336 genes), and ~14% were downregulated (56 genes). In the DEGs, those genes which were identified earlier in the CaTK genes (Wasilewska et al., 2019) were of special interest. It was found that some immediate early genes encoding proteins involved in the regulation of calcium signaling in the neurons (were upregulated) *egr4* and *fosl1a*, and some were downregulated like *fosab* and *npas4l*. Another gene, known as *smc1a*, encodes a cohesin complex protein involved in regulating nervous system development (Chinen et al., 2019), which was highly expressed in *stim2a*$^{-/-}$ mutant zebrafish larvae. Few other genes, which encode important proteins such as *kcnc1a*, *slc20a2*, *slc25a17*, *slc25a25b*, and *slc31a1*, are involved in transporter activity biomolecules, showed significant changes in expression in *stim2a*$^{-/-}$ mutant zebrafish larvae.

After that, gene ontology annotation (GO annotation) was done online using PANTHER (**Figure 3.12**) (Thomas et al., 2003). Mainly molecular pathway, cellular component molecular function GO terms were looked (**Figure 3.12A, 3.12B, and 3.12C**). The cellular component hits (538) indicated the locations of the genes mainly in the cell junctions, synapses, membranes. The molecular function hits (170) showed that these genes were involved in transcription and translation regulators. The molecular pathway hits (86) showed that these genes were involved in catalytic and transporter activity. Furthermore, genes also showed the involvement in many signaling pathways of neurodegenerative diseases like AD, HD, and PD (**Figure 3.12C**).

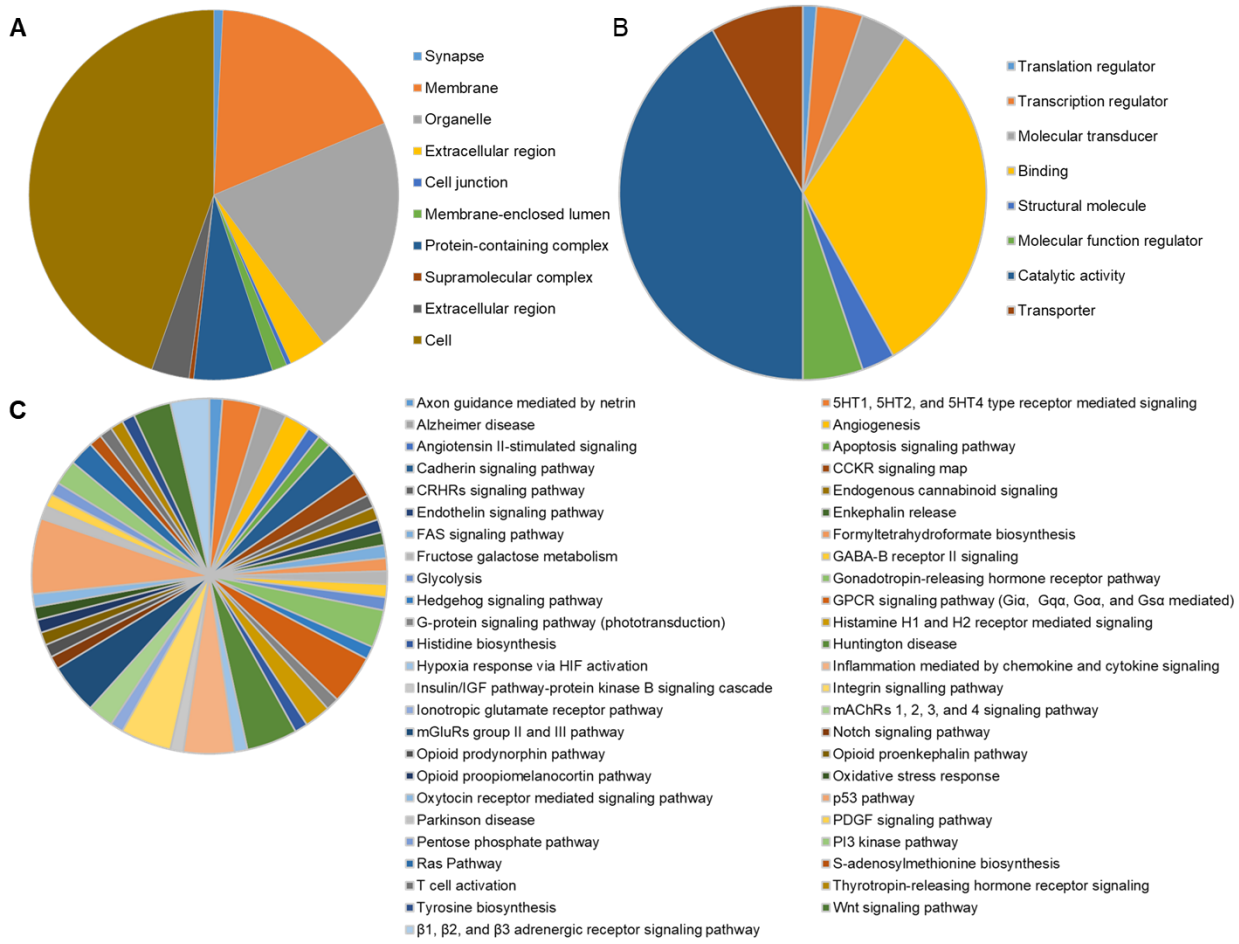

Figure 3.12. PANTHER Gene Ontology annotation analysis [58]. (A) Cellular Component GO terms (B) Molecular Function GO terms (C) Molecular Pathway GO terms.

As it was found that neuronal activity has been increased in *stim2a*$^{-/-}$ mutant, further analysis was performed to identify the CaTK genes encoding proteins involved in Ca^{2+} signaling and showed significant up- or downregulation. So, the genes that belonged to the zebrafish CaTK (published by our group (Wasilewska et al., 2019)) were looked for. Eight genes (*anxa3a*, *grinab*, *hp*, *hpca*, *mast2*, *pkn3*, *pvalb7*, *and slc25a25b*) which were significantly upregulated and were found common in the zebrafish CaTK genes and DEGs in the *stim2a*$^{-/-}$ mutant zebrafish larvae. Additionally, the *cdh13*, *scin*, *dgkaa*, *mmp13a*, *LOC101882496*, *LOC103908715*, and *vwa2* genes, which encode proteins involved in calcium signaling, showed significant differential expression in the *stim2a*$^{-/-}$ mutant, but they were not found in the zebrafish CaTK we described.

3.9 Identification of the distinct cell clusters and their CaTK genes in WT fish using single-cell RNA sequencing

Neuronal Ca^{2+} signaling primarily depends on gene expression in each cell. Using bulk RNA sequencing, genes involved in Ca^{2+} signaling (CaTK) were identified in WT (Wasilewska et al., 2019). These available bulk RNA seq data gave a significant understanding about proteins involved in the Ca^{2+} signaling. However, finding out the genes involved in the neuronal Ca^{2+} signaling in a specific cell type is more informative. Therefore, we aimed to identify the CaTK genes in cells of neuronal origin by single-cell RNA sequencing (scRNA-seq). It was performed on cell population from the brains of 5dpf *Tg(HuC:GCaMP5G)* transgenic zebrafish larvae. Single-cell suspensions of brain cells were obtained by enzymatic and mechanical digestion and sorted swiftly by fluorescence-activated cell sorting (FACS) to get the cells based on GCaMP5G activity, i.e., green fluorescence. This GCaMP5G is expressed only in cells in which the *Huc* promotor is active, so these cells represent a population of cells of the neuronal origin (Kim et al., 1996)). A scRNA-seq was performed using 10X Chromium chemistry (V3), with chromium controller 10x genomics equipment which is available at the Nencki Institute of Experimental Biology. Seurat R-package (V3) was used to analyze the data (Stuart et al., 2019). 13 different clusters were identified automatically based on cellular marker genes representing different cell types (**Figure 3.13A**). 11 of them were classified as a specific type of neurons (dopaminergic, GABAergic Type 1 and 2, glutamatergic neurons, Purkinje cells, thalamocortical) and neuronal progenitor cells Type1 and 2, progenitor cell (glia type), oligodendrocyte progenitor cells, and terminally differentiated oligodendrocytes. Two clusters were identified as not known (not known 1 and not known2).

Genes encoding proteins involved in Ca^{2+} signaling and homeostasis were identified in each cell cluster. Overall, a total of 88 unique genes were found. However, their number varied significantly between the clusters **(Figure 3.13B)**, (thalamocortical neurons (19 genes), GABAergic neurons Type1 (28 genes), dopaminergic neurons (29 genes), not known1 (24 genes), neuronal progenitor cells Type1 (14 genes), GABAergic neurons Type2 (8 genes), neuronal progenitor cells Type2 (11 genes), progenitor cells (glia type) (33 genes), Purkinje cells (18 genes), glutamatergic neurons (22 genes), oligodendrocyte progenitor cells (47 genes), terminally differentiated oligodendrocytes (30 genes), and not known2 (38 genes) (Appendix I: Table 1).

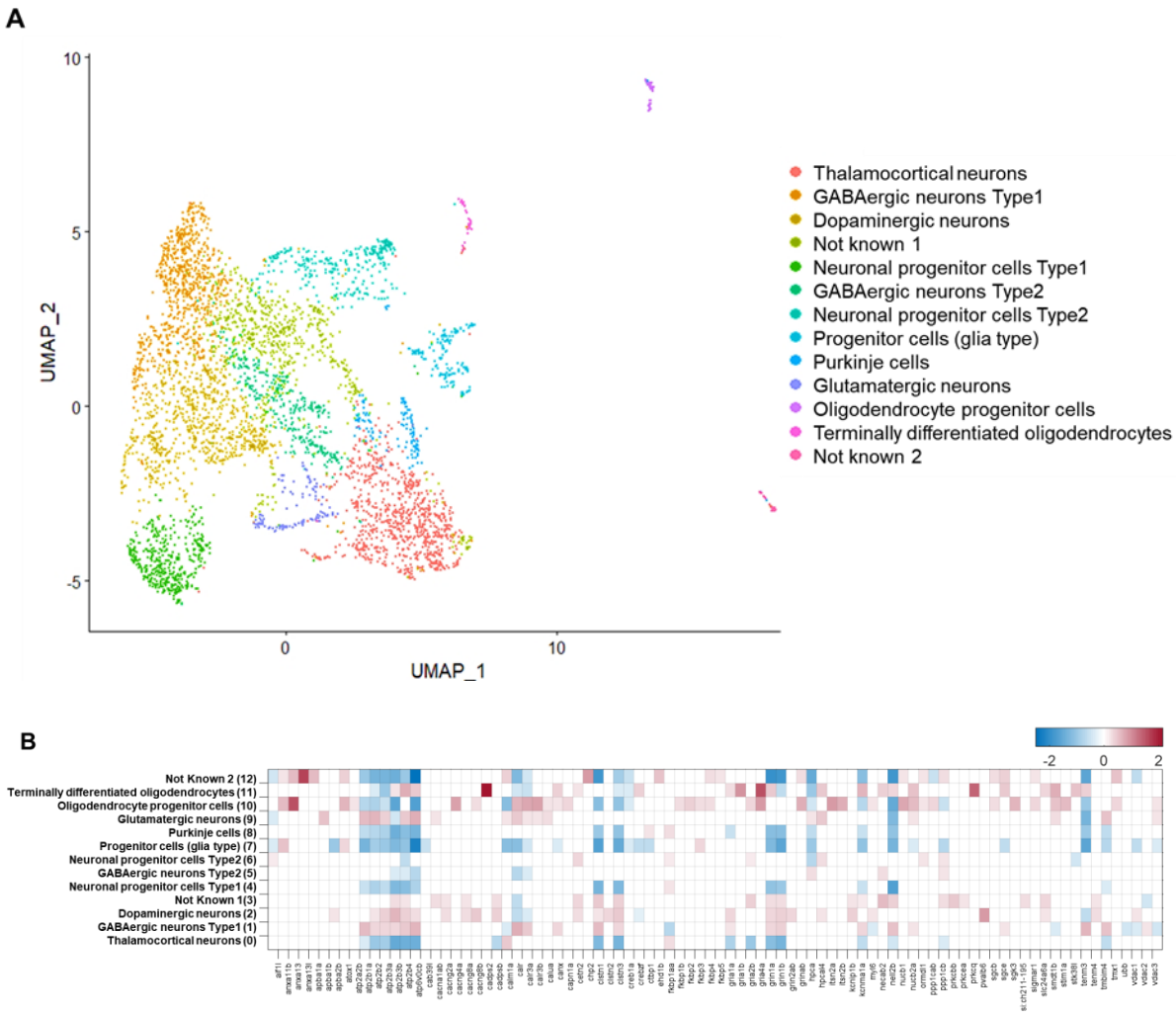

Figure 3.13. Single-cell RNA seq analysis from cells of neuronal origin in WT. (A) UMAP representation demonstrates the distribution of WT zebrafish brain cells from neuronal origin. A total of 13 clusters were identified. (B) Heatmap showing the expression level of genes of Ca^{2+} signaling proteins in each neuronal origin cell cluster in WT. The oligodendrocyte progenitor cell type has the highest number of these genes (47 genes), and the GABAergic neurons Type2 have the lowest (8 genes).

3.10 Identification of the distinct cell clusters and their CaTK genes in *(stim2a;stim2b)*$^{-/-}$ double mutant using single-cell RNA sequencing

Single-cell RNA sequencing was performed also using cell population from the brains of 5dpf *Tg(elavl3:GCaMP5G):(stim2a;stim2b)*$^{-/-}$ transgenic double mutant zebrafish larvae.

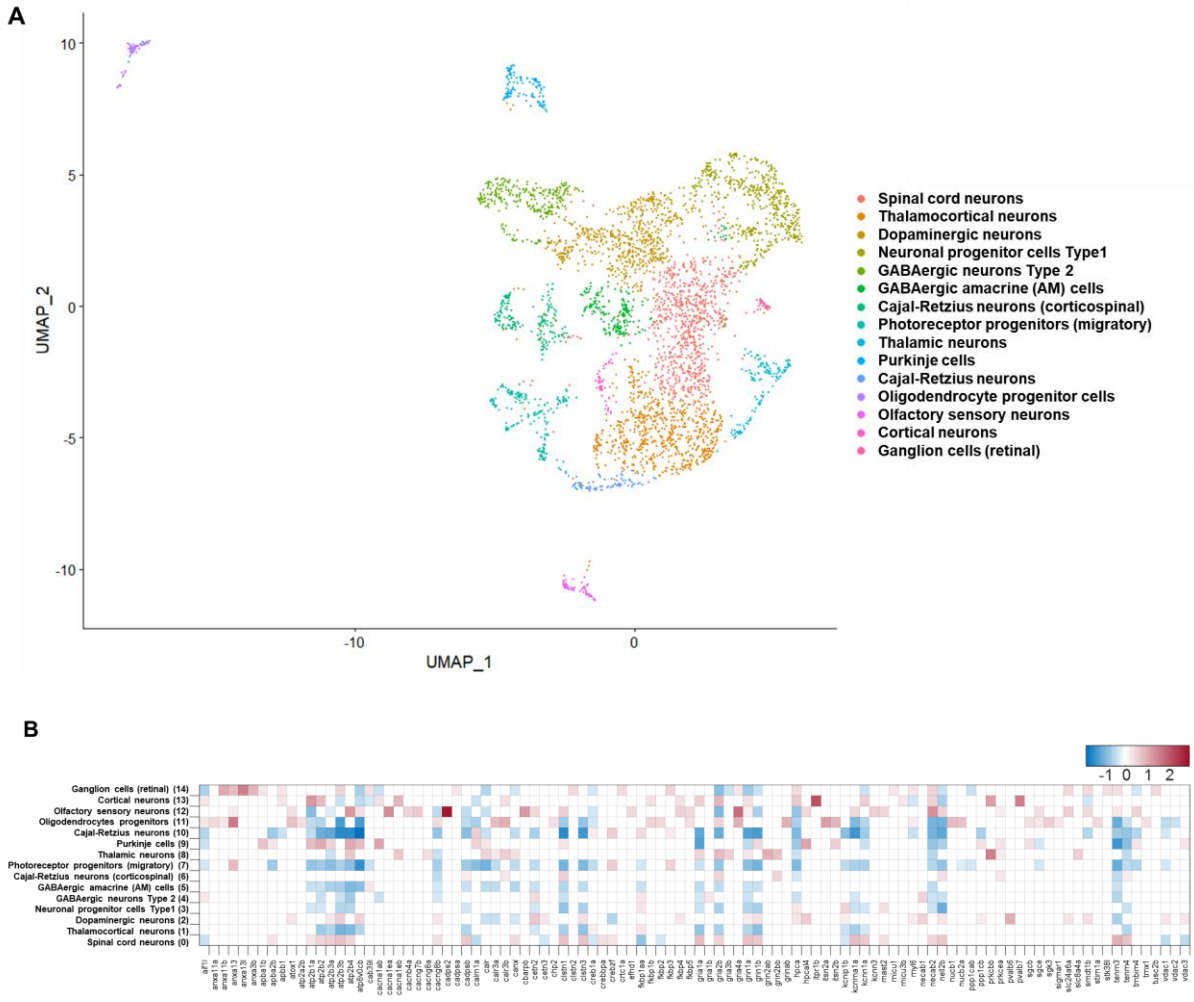

Figure 3.14. Single-cell RNA seq analysis in the cell from neuronal origin in *(stim2a;stim2b)*$^{-/-}$ double mutant. (A) UMAP representation demonstrates the distribution of *(stim2a;stim2b)*$^{-/-}$ double mutant zebrafish brain cells from the neuronal origin. A total of 15 clusters were identified. (B) Heatmap showing the expression level of genes of Ca^{2+} signaling proteins in each neuronal origin cell cluster in *(stim2a;stim2b)*$^{-/-}$ double mutant. Oligodendrocytes progenitors type has the highest number of these genes (45 genes), and Cajal-Retzius neurons (corticospinal origin) have the lowest (11 genes).

Cells were processed exactly as it was done in the case of WT. After FACS separation of GCaMP5G positive cells, scRNA-seq was performed using 10X Chromium chemistry (V3) at the Nencki Institute of Experimental Biology. Then Seurat R-package (V3) was used to analyze the data (Stuart et al., 2019). 15 different cell types clusters were identified based on cellular marker genes (**Figure 3.14A**). Cell clusters were classified as a specific type of neurons (spinal cord neurons, thalamocortical neurons, dopaminergic neurons, GABAergic neurons Type 2, GABAergic amacrine (AM) cells, Cajal-Retzius neurons (corticospinal),

thalamic neurons, Purkinje cells, Cajal-Retzius neurons, olfactory sensory neurons, cortical neurons, and ganglion cells (retinal), and neuronal progenitor cells Type1, photoreceptor progenitors (migratory), and oligodendrocyte progenitor cells (**Figure 3.14A**). CaTK genes were present in each cell cluster. Overall, a total of 102 unique genes were identified. However, in each cluster, their number varied **(Figure 3.14B)**, spinal cord neurons (33 genes), thalamocortical neurons (19 genes), dopaminergic neurons (28 genes), neuronal progenitor cells Type1 (21 genes), GABAergic neurons Type2 (18 genes), GABAergic amacrine (AM) cells (22 genes), Cajal-Retzius neurons (corticospinal) (11 genes), photoreceptor progenitors (migratory) (44 genes), thalamic neurons (21 genes), Purkinje cells (29 genes), Cajal-Retzius neurons (38 genes), oligodendrocyte progenitor cells (45 genes), olfactory sensory neurons (37 genes), cortical neurons (26 genes), ganglion cells (retinal) (36 genes) (Appendix I: Table 2).

3.11 Comparison of CaTK genes identified in WT and *(stim2a;stim2b)*$^{-/-}$ double mutant

After identifying the CaTK genes in each cell cluster from WT and *(stim2a;stim2b)*$^{-/-}$ double mutant fish comparison was performed as shown in Table 3.1. We took into account only 6 clusters, which were identified in both scRNASeq analyses. A total of 77 genes were common in both WT and *(stim2a;stim2b)*$^{-/-}$ double mutant, while in WT only 11 genes, and in *(stim2a;stim2b)*$^{-/-}$ mutant 25 genes were unique from overall cell types.

Table 3.1: CaTK genes common in WT and *(stim2a;stim2b)*$^{-/-}$ double mutant, only present in WT, and only present in *(stim2a;stim2b)*$^{-/-}$ double mutant in the scRNA seq data from all cell clusters. (Full description of each gene is given in Appendix I: Table 3). Genes labelled in yellow were identified as upregulated in *stim2a*$^{-/-}$ knockout line.

CaTK_common in WT and *(stim2a;stim2b)*$^{-/-}$	**CaTK-WT**	**CaTK-*(stim2a;stim2b)*$^{-/-}$**
aif1l, anxa11b, anxa13, anxa13l, apba1b, apba2b, atox1, atp2a2b, atp2b1a, atp2b2, atp2b3a, atp2b3b, atp2b4, atp6v0cb, cab39l, cacna1ab, cacng8a, cacng8b, cadps2, cadpsb, calm1a, calr, calr3a, calr3b, canx, cetn2, chp2, clstn1, clstn2, clstn3, creb1a, crebzf, fkbp1aa, fkbp1b, fkbp2, fkbp3, fkbp4, fkbp5, gria1a, gria1b, gria2b, gria4a, grin1a, grin1b, grin2ab, grinab, hpca, hpcal4, itsn2a, itsn2b, kcnip1b, kcnma1a, myl6, necab2, nell2b, nucb1, nucb2a, ppp1cab, ppp1cb, prkcbb, prkcea, pvalb6, sgcb, sgce, sgk3, sigmar1,	*apba1a, cacng2a, cacng4a, calua, capn1a, ctbp1, ehd1b, ormdl1, prkcq, si:ch211-195, ubb*	*anxa11a, anxa3b, apbb1, cacna1ea, cacna1eb, cacnb4a, cacng7b, cadpsa, cbarpb, cetn3, crebbpa, crtc1a, efhd1, gria3b, grin2bb, itpr1b, kcnn1a, kcnn3, mast2, micu1, micu3b, necab1, pvalb7, slc8a4a, tusc2b*

slc24a6a, smdt1b, stim1a, stk38l, tenm3, tenm4, tmbim4, tmx1, vdac1, vdac2, vdac3		

Table 3.2: Name of the cell clusters of the neuronal origin in WT and *(stim2a;stim2b)*$^{-/-}$. If a particular cell cluster is present, it is indicated by 'Yes' otherwise '-'. Clusters **in bold** were identified in both fish lines, and their CaTK genes are in Table 3.3. In the small bracket, the number of Ca^{2+} signaling was identified. (Top 5 gene is given in Appendix I: Table 4).

Name	WT	*(stim2a;stim2b)*$^{-/-}$
Thalamocortical neurons	Yes (19)	Yes (19)
GABAergic neurons Type1	Yes (28)	-
Dopaminergic neurons	Yes (29)	Yes (28)
Not known 1	Yes (24)	-
Neuronal progenitor cells Type1	Yes (14)	Yes (21)
GABAergic neurons Type2	Yes (8)	Yes (18)
Neuronal progenitor cells Type2	Yes (11)	-
Progenitor cells (glia type)	Yes (33)	-
Purkinje cells	Yes (18)	Yes (29)
Glutamatergic neurons	Yes (22)	-
Oligodendrocyte progenitor cells	Yes (47)	Yes (45)
Terminally differentiated oligodendrocytes	Yes (30)	-
Not known 2	Yes (38)	-
Spinal cord neurons	-	Yes (33)
GABAergic amacrine (AM) cells	-	Yes (22)
Cajal-Retzius neurons (corticospinal)	-	Yes (11)
Photoreceptor progenitors (migratory)	-	Yes (44)
Thalamic neurons	-	Yes (21)
Cajal-Retzius neurons	-	Yes (38)
Olfactory sensory neurons	-	Yes (37)
Cortical neurons	-	Yes (26), (*parvalb7*)

Ganglion cells (retinal)	-	Yes (36)

Table 3.3: Cell clusters identified in WT and *(stim2a;stim2b)*$^{-/-}$ and their CaTK genes (common in WT and *(stim2a;stim2b)*$^{-/-}$, only in WT and only in *(stim2a;stim2b)*$^{-/-}$). (Full description of each gene is given in Appendix I: Table 3).

Name	**CaTK - common (in WT and *(stim2a;stim2b)*$^{-/-}$**	**WT**	***(stim2a;stim2b)*$^{-/-}$**
Thalamocortical neurons	*atp2b2, atp2b3a, atp2b3b, atp2b4, atp6v0cb, cadpsb, clstn1, clstn3, fkbp1aa, gria1a, gria2b, grin1a, grin1b, kcnma1a* - **14**	*atp2b1a, calm1a nell2b, ppp1cb tmbim4* - **5**	*cetn2, creb1a, kcnip1b, kcnn1a tenm4* - **5**
Dopaminergic neurons	*atp2b3a, atp2b3b, atp6v0cb, cacng8b, calr, calr3a, cetn2, clstn3, crebzf, grin1a, grin1b, hpcal4, kcnip1b, myl6, pvalb6, slc24a6a, tenm3, vdac1*- **18**	*apba2b, atp2b2, atp2b4, cacng2a cacng8a, cadpsb clstn1, clstn2, gria1a, grin2ab, tenm4* - **11**	*atox1, canx, cetn3 fkbp4, hpca, necab1, nell2b, ppp1cb, smdt1b, vdac3,* - **10**
Neuronal progenitor cells Type1	*atp2b1a, atp2b2, atp2b3b, atp2b4, clstn1, clstn3, fkbp1aa, grin1a, grin1b, kcnma1a, nell2b* - **11**	*atp2b3a, atp6v0cb, tmbim4* - **3**	*Cadpsb, cetn2, gria1a, gria2b, hpca, kcnip1b, kcnn1a, mast2, necab2, tenm4* - **10**
GABAergic neurons Type2	*atp2b3b, atp2b4, hpca, necab2* - **4**	*atp6v0cb, calr, calr3a, ppp1cb* - **4**	*aif1l, atp2b2, cacna1ab, cacng8b, cetn2, clstn1, fkbp1aa, gria1a, gria1b, grin1a, kcnma1a, necab1, nell2b, tenm3* - **14**
Purkinje cells	*atp2b1a, atp2b2, atp2b3a, atp2b4, atp6v0cb, clstn1, gria1a, grin1a, grin1b, hpca, nell2b, tenm3, tmbim4* - **14**	*atp2b3b, clstn3, ctbp1, fkbp1aa, kcnma1a* - **5**	*aif1l, apba1b, apba2b, cacna1ab, calm1a, calr, hpcal4, itsn2b, kcnn1a, necab2, ppp1cb, prkcea, sgcb, sgce tenm4, vdac3* - **16**
Oligodendrocyte progenitor cells	*anxa13, anxa11b, atox1, atp2a2b, atp2b1a, atp2b2, atp2b3b, atp6v0cb, cacng8b, calm1a, calr3a, calr3b, clstn1, clstn3,*	*atp2b3a, cacng4a, calr, calua, canx, capn1a, fkbp3, fkbp4, ormdl1, ppp1cab, ppp1cb,*	*aif1l, anxa11a, cadpsb, chp2, fkbp5, kcnn1a, necab2, sgce, tenm4, vdac1*

	creb1a, fkbp1b, fkbp2, gria2b, gria4a, grinab, hpca, itsn2a, itsn2b, kcnma1a, myl6, nell2b, nucb1, nucb2a, sgcb, sgk3, sigmar1, stim1a, tenm3, tmx1- **35**	*smdt1b, vdac3*- **13**	*vdac2* - **11**

WT has seven unique cell clusters, and six cell clusters were common in both WT and *(stim2a;stim2b)*$^{-/-}$ double mutant, and in *(stim2a;stim2b)*$^{-/-}$ double mutant, nine cell types have become visible (**Table 3.2**). The thalamocortical neurons, dopaminergic neurons, neuronal progenitor cells Type1, GABAergic neurons Type2, Purkinje cells, and oligodendrocyte progenitor cells were common cell types in both WT and *(stim2a;stim2b)*$^{-/-}$ double mutant. It was interesting to compare genes in cell clusters that were common in the WT and *(stim2a;stim2b)*$^{-/-}$ double mutant (**Table 3.3**). WT and *(stim2a;stim2b)*$^{-/-}$ double mutant shared 14 common genes, and 5 genes were different in both genotypes in the thalamocortical neurons. In the case of dopaminergic neurons, both genotypes shared 18 common genes, WT had 11 different genes, and *(stim2a;stim2b)*$^{-/-}$ double mutant had 10 different genes. In the neuronal progenitor cells Type1, there were 11 common genes in both genotypes, although *(stim2a;stim2b)*$^{-/-}$ double mutant was having a greater number of different genes (10 genes) than the WT (3 genes). Furthermore, GABAergic neurons Type 2 shared only 4 CaTK genes in both WT and *(stim2a;stim2b)*$^{-/-}$ double mutant, and WT had 4 different genes then *(stim2a;stim2b)*$^{-/-}$ double mutant, where 14 different genes were present. In the case of Purkinje cells, both genotypes shared 14 common genes, WT had 5 different genes, and *(stim2a;stim2b)*$^{-/-}$ double mutant had 16 different genes. In the last common cell type, Oligodendrocyte progenitor cells, there were 35 common genes in both genotypes, although *(stim2a;stim2b)*$^{-/-}$ double mutant was having a lesser number of different genes (11 genes) than the WT (13 genes). This analysis indicates that there was much heterogeneity present at the level of the genes, even in similar cell types.

Eight CaTK genes (*anxa3a, grinab, hp, hpca, mast2, pkn3, pvalb7*, and *slc25a25b*) were found to be significantly upregulated in bulk RNA sequencing data of *stim2a*$^{-/-}$ mutant (**page 39**). Out of these eight CaTK genes, four (*grinab*, *hpca*, *mast2*, and *pvalb7*) were identified in the scRNA seq data in the cells of neuronal origin shown in Table 3.3. The *hpca* gene was found to be present in GABAergic neurons Type2 and in Purkinje cells of both WT and *(stim2a;stim2b)*$^{-/-}$ double mutant. However, the *hpca* gene was also found in

dopaminergic neurons and neuronal progenitor cells Type1, but only in *(stim2a;stim2b)*$^{-/-}$ double mutant. This suggests that the upregulation of *hpca* gene detected by bulk RNA sequencing occurred mostly in these two types of cells. Another CaTK gene, *mast2,* was found in neuronal progenitor cells Type1 only in the *(stim2a;stim2b)*$^{-/-}$ double mutant (Table 3.3). The *pvalb7* was not found in any cell populations shown in Table 3.3, while the *grinab* gene was present in oligodendrocyte progenitor cells of WT cells and *(stim2a;stim2b)*$^{-/-}$ double mutant. The other four genes (*anxa3a, hp, pkn3*, and *slc25a25b*), which were found to be upregulated by bulk RNA-Seq in *stim2a*$^{-/-}$ larvae brains, were not identified in GCAMP5G positive cells by scRNA seq. This indicates that they were expressed in other cells than cells of neuronal origin. This interpretation seems to be justified since it was found recently in our lab that the *anxa3a* gene was upregulated in the GCAMP5G negative cell population separated by FACS from the *(stim2a;stim2b)*$^{-/-}$ double mutant. The additional analysis pointed out its expression to occur likely in the microglial cells (Majewski, *unpublished*).

Chapter 4: Discussion

4.1 Zebrafish as an alternative model for the study of neuronal calcium homeostasis

Since the time STIM and Orai were discovered as the crucial components of SOCE, there has been remarkable progress in understanding the mechanistic events in the process of calcium entry through Orai/Trp channels (Park et al., 2009). It has been discovered that STIM and Orai proteins are ubiquitously expressed throughout the human and murine brains (Klejman et al., 2009, Skibinska-Kijek et al., 2009). Our group has also demonstrated that both STIM proteins interact and form complexes with Orai in neurons (Gruszczynska-Biegala et al., 2011) and provided evidence for the interaction between endogenous STIM1 and endogenous Orai (Gruszczynska-Biegala et al., 2013). In mice, primary neuronal culture or mammalian cell lines, either *Stim1* or *Stim2* or both *Stim* genes were inactivated, have been used to identify the role of these proteins in the nervous system. For instance, deletion of *Stim1* and *Stim2* genes in the forebrain of mice resulted in impairment of spatial learning and memory (Garcia-Alvarez et al., 2015). In *STIM2*$^{-/-}$ mice, subtle alterations in the shape and density of dendritic spines in CA1 neurons were observed, and STIM2 was found to be required for stable expression of both long-term potentiation (LTP) and long-term-depression (LTD) at CA3-CA1 hippocampal synapses (Yap et al., 2017). *STIM2* knockout mice survive only for a few weeks after birth (Oh-Hora et al., 2008) and show pronounced cognitive deficits (Berna-Erro et al., 2009). As investigating long-term effects of systemic knockout of *STIM2*, and changes in behavior in rodent models are impossible due to the lethality as mentioned earlier, using zebrafish that has two STIM2 isoforms represents a valid alternative.

Furthermore, zebrafish shows significant reproductive capacity, and the nervous system develops at an early stage of development and allows larvae to exhibit complex behavior (Colwill et al., 2011, Kedra et al., 2020). Another very useful feature of zebrafish is its almost complete transparency during the early developmental stages. This is particularly important for *in vivo* Ca^{2+} analysis imaging experiments combined with genetically encoded calcium probes, like GCaMP5, in brain neurons (Howe et al., 2013, Soman et al., 2019). We took advantage of these unique zebrafish features in the present study. We aimed to describe the behavioral phenotype, *in vivo* Ca^{2+} imaging in brain neurons, and gene expression analysis to better understand the regulation of neuronal Ca^{2+} signaling and the effects on

behavior in *stim2a*$^{-/-}$ knockout zebrafish line. The *stim2a*$^{-/-}$ knockout zebrafish yielded a viable animal, which was demonstrated in the present study.

4.2. SOCE proteins in zebrafish

Ca^{2+} signaling regulates numerous cellular processes by altering the Ca^{2+} flux speed, amplitude, and spatial patterning, with a broad range of Ca^{2+}-sensing, Ca^{2+}-buffering, and Ca^{2+}-transport proteins (Berridge et al., 2000). Ca^{2+} influx via SOCE is one of them. Many SOCE proteins genes were identified in CaTK genes. The qPCR of SCOE genes in this present study in *stim2a*$^{-/-}$ also showed the presence of SOCE components transcripts, where *stim2a* was downregulated significantly (Gupta et al., 2020). This findings provides a support that SOCE proteins are present in zebrafish and make this zebrafish as a new alternative model to study further the role of SOCE in *in vivo* conditions.

4.3 Genes expression changes in *stim2a*$^{-/-}$ mutant zebrafish

One of the upregulated genes in *stim2a*$^{-/-}$ fish was *smc1a*. This gene encodes the structural maintenance of chromosomes 1A (Smc1a) protein with DNA binding domain and is involved in developmental growth and central nervous system development. In humans, this gene is implicated in Cornelia de Lange syndrome 2 and early infantile epileptic encephalopathy (Fang et al., 2021, Naik et al., 2021). This indicates that Stim2a plays a vital role in developmental growth and the central nervous system in zebrafish. The absence of Stim2b, the other isoform of Stims, showed the susceptibility to seizures (Wasilewska et al., 2020), further indicating the possible role of Stim2a isoform in the neuronal function and provide neuroprotection in coordination with structural maintenance of chromosomes 1A (Smc1a) protein. Expression of the *anxa3a* gene was also found upregulated above 5 times in mutant larvae than in WT larvae. This *anxa3a* gene was also found upregulated significantly in *stim2b*$^{-/-}$ mutant (Wasilewska et al., 2020). Interestingly, annexins were found upregulated in epileptic brains and injured brains (Chong et al., 2010, Zub et al., 2019). It was also found recently that in schizophrenia patients, the Annexin A3 level was reduced (Joaquim et al., 2020). Preliminary data of our group indicate that annexin3 affects SOCE (Majewski, Dyrda, *unpublished*), showed the link that Stim2a is needed to facilitate normal SOCE function. Another gene, *rhocb*, was found to be upregulated in bulk RNA seq. The protein was found to be localized at neuron projection and have GTPase and protein kinase binding activity. The protein encoded by this gene was found to be involved in axon regeneration after spinal cord

injury in zebrafish (Li et al., 2020). A report on virus-mediated knockdown of STIM2 protein showed mushroom spine shrinkage and loss of nSOC in hippocampal dendritic spines (Sun et al., 2014). So, the overexpression of *rhocb* could be an indication that neurons were more vulnerable in the absence of Stim2a and triggered the overexpression of *rhocb*. Mushroom dendritic spines are essential for long-term memory storage, and the stability of mushroom spines depends on the STIM2-mediated nSOC pathway. Downregulation of STIM2 proteins was observed in cells from AD patients and in AD mouse models, which also explained the loss of mushroom postsynaptic spines and memory defects in aging and Alzheimer's disease (AD) (Bojarski et al., 2009, Sun et al., 2014, Chanaday et al., 2021). This could also be linked with the significant increase in the expression of *ndel1b* gene was due to the absence of Stim2a, which was found to be highly expressed in the brain, hindbrain neural plate, and notochord and implicated in psychiatric and neurodevelopmental disorders (Bradshaw et al., 2017). Another interesting gene, *igf1rb*, was found slightly upregulated in bulk RNA seq. This gene encodes insulin-like growth factor 1b receptor protein found on the surface of the cells. In humans, this gene is implicated in several neurological disorders, including dementia, nervous system cancer, and neurodegenerative diseases (Ratcliffe et al., 2018, Chi et al., 2019, Tanokashira et al., 2019). These reports suggest that the absence of Stim2a could perturb the insulin-like growth factor 1b receptor protein, which could make neurons more vulnerable and lead to several neurodegenerative diseases. A recent study on the rat model showed that IGF-1 favors the fear extinction memory (Maglio et al., 2021).

For the genes that were downregulated in *stim2a*$^{-/-}$ mutant, one gene is potentially interesting: *fosab*. It encodes a transcription factor, has DNA binding domain, and was shown to be crucial for the proper nervous system development in zebrafish. The *fosab* is an immediate early gene, regulates the neuronal calcium transients by overexpression (Brenet et al., 2020). Short-term exposure to N-Ethylpentylone (NEP) and gallic acid (GA) causes significant upregulation of gene *fosab* in immediate response to the stress and anxiety in zebrafish (Annona et al., 2021, Fan et al., 2021). However, in *stim2a*$^{-/-}$ mutant, *fosab* was slightly downregulated due to the absence of Stim2a and restricting the immediate response to the stress and anxiety, which might explain the observed hyperactive behavior.

4.4 Behavioral changes in *stim2a*$^{-/-}$ mutant

To study the function of Stim proteins *in vivo*, *Stim2* knockout mouse lines were created. However, these *Stim2* knockout mouse lines showed developmental delay at 4-5

weeks of the postnatal and did not survive afterward (Oh-Hora et al., 2008, Berna-Erro et al., 2009). Very limited studies have been done to correlate the role of Stim2 in behavior due to this early lethality in mice. Mice with a conditional double knockout of *Stim1*/*Stim2* in the forebrain showed a greater propensity to engage in exploration as it spent more time on the open arms of the elevated plus-maze, suggesting a decrease in anxiety-like behavior (Garcia-Alvarez et al., 2015). Furthermore, in mice overexpressing STIM2 and ORAI1, reductions in anxiety-like behavior, including increases in the exploration of the arena in the open field test and time spent on the elevated plus-maze open arms, were observed (Majewski et al., 2020). In this present study, we analyzed behavioral changes in zebrafish larvae in *stim2a*$^{-/-}$ mutant. Compared to the WT, hyperactivity and an increase in thigmotaxis were observed in *stim2a*$^{-/-}$ zebrafish larvae. Moreover, reduction of phototaxis in *stim2a*$^{-/-}$ zebrafish larvae was also observed compared to WT fish. The reason for such irregularity in phototaxis and thigmotaxis might be that the brain network connectivity controlling such behavior might have altered due to the absence of Stim2a isoform. The ability to make choices and carry out appropriate behavioral actions is critical for individual survival and well-being, though it is a critical process, which involved hard-wired synchronous neuronal response to the surrounding changes (Lau et al., 2011). Also, it has already been shown that different parts of the brain control different behavioral activity (Lau et al., 2011, Jimenez et al., 2018). It has been reported that STIM2 is a predominant isoform in the hippocampus (Gruszczynska-Biegala et al., 2011, Zhang et al., 2016). In hippocampal neurons, STIM2 stabilized the mushroom spines by STIM2-mediated nSOC in the normal condition, but was reported to be compromised in AD mouse models, aging neurons, and sporadic AD patients (Zhang et al., 2016). Here, in *stim2a*$^{-/-}$ zebrafish, neuronal synchronicity might be disturbed severely due to the deterioration of neural circuits and lack of coordination in the neuronal activity due to the absence of Stim2a. This could also be linked with the downregulation of the *fosab* gene in *stim2a*$^{-/-}$ zebrafish, which is an immediate-early gene for the immediate response to the stress and anxiety in zebrafish. The VMR test was performed to eliminate the possibility that *stim2a*$^{-/-}$ mutants had a problem in distinguishing dark and light. The *stim2a*$^{-/-}$ zebrafish larvae reacted to changes in light and showed higher activity in the low activity phase (light phase) in the VMR test. It has already been established that an increase in locomotor activity is associated with alterations of neurotransmission in the brain, including alterations by chemical agents such as pentylenetetrazole (PTZ) and glutamate (Baraban et al., 2005, Kundap et al., 2017). The PTZ-treated larvae showed an increase in swimming abnormalities

and circular trajectory motion (Baraban et al., 2007). The VMR test was performed after treatment with these two chemicals. The *stim2a*$^{-/-}$ zebrafish larvae reacted in the same way to both chemical treatments, the activity was increased during all phases of light, compared with the no-treatment condition. Previously, in *tsc*$^{-/-}$ mutant larvae, a similar type of phenotype (i.e., increase in thigmotaxis and decrease in phototaxis) was observed (Kedra et al., 2020).

4.5 Calcium oscillation increased in *stim2a*$^{-/-}$ larvae neurons

In order to establish the link between the change in behavior with cellular events, *in vivo* Ca^{2+} activity in neurons was measured. The optic tectum reason of the brain was chosen for the analysis because it is involved in visual stimuli processing and motor response activation (Suzuki et al., 2019). It was found that *stim2a*$^{-/-}$ larvae showed greater frequency and higher amplitude of Ca^{2+} oscillations in the neurons in the periventricular zone of the optic tectum as compared to the WT. Neurons possess many other Ca^{2+} permeable channels with high conductance, such as voltage-gated calcium channels, NMDA receptors, and AMPA receptors which help in sequester the Ca^{2+} flux (Yamakage et al., 2002, Wojda et al., 2013), which could be the alternate of STIM2-mediated nSOC in the normal condition. However, Ca^{2+} permeable channels with high conductance involved in the rapid action of the neurons (Wilson et al., 2005, Cens et al., 2006), and studies have shown that the increased levels of intracellular calcium ions could lead to neuronal loss (Raza et al., 2007). The higher Ca^{2+} oscillations frequency and higher amplitude were attributable to increased activity in the optic tectum, which could be the reason for disruption in the phototactic response in the absence of Stim2a. This could also have resulted from dysregulation of genes in the absence of Stim2a, which are important for neurodevelopment, such as *smc1a, igf1rb*, and *ndel1b*.

In the behavior test, zebrafish response was analyzed after the glutamate stimulation to further understand the possible behavioral alterations due to the absence of Stim2a, and *stim2a*$^{-/-}$ larvae showed an increase in mobility. Furthermore, it has been suggested that glutamate can diffuse through the zebrafish larvae's skin and reach into the neurons (McCutcheon et al., 2016). Ca^{2+} activity *in vivo* were measured in neurons after larvae were treated with glutamate, which showed a significant increase in the neuronal Ca^{2+} oscillation frequency in *stim2a*$^{-/-}$ larvae. Glutamate facilitates Ca^{2+} influx via NMDA receptor channels present on the neuronal surface and increases the Ca^{2+} oscillation frequency (Kovalchuk et al., 2000).

4.6 Single-cell RNA seq revealed the genes involved in Ca signaling in neuronal clusters

Among the differentially expressed genes in the bulk RNA seq, CaTK genes were also identified. Few particular CaTK genes, involved in Ca^{2+} signaling *anxa3a, grinab, hp, hpca, mast2, pkn3, pvalb7,* and *slc25a25b* showed significant change in expression in *stim2a*$^{-/-}$ zebrafish. That provided classical insights to look the gene expression. However, recent studies showed that the scRNAseq analysis application would enable the opportunity to look at the transcriptome at the single-cell resolution (Raj et al., 2018, Gupta et al., 2020). Here, scRNA seq was done on the cells from the neuronal origin, in the case of the WT and *(stim2a;stim2b)*$^{-/-}$ double mutant. The major challenge was to extract the cells from the neuronal origin. Such attempts have been made using the *gng8*-GFP transgenic line, which eventually labels most neurons selectively in the habenula in the zebrafish brain (Pandey et al., 2018). Although scRNAseq is now well established, using it for zebrafish neurons is technically challenging. In this present study, *Tg(HuC:GCaMP5G)* transgenic zebrafish line was used. This gives the opportunity to extract the cells from the neuronal origin (Kim et al., 1996).

Based on scRNA-seq in WT larvae, 13 distinct subsets of neuronal origin cells and *(stim2a;stim2b)*$^{-/-}$ double mutant, a total of 15 cell types were identified. When the genes that are involved in the Ca^{2+} signaling were identified across these cell types in both genotypes, there was a huge variation in the presence of these genes and their expression level. This implicate that cell-type identification is important because individual neurons may change in response to various stimuli or neurodegenerative diseases (Cascella et al., 2021, Hidalgo et al., 2021). Furthermore, several behaviors such as fear responses (Agetsuma et al., 2010) and anxiety (Dreosti et al., 2015) in zebrafish can be modulated by Ca^{2+} signaling in the brain cells. While cell-type identification and the presence of the CaTK genes in those cells are essential for understanding the function of neural circuits, an important future goal could be to relate the modulation of Ca^{2+} signaling in the defined neuronal types, would give a better functional understanding of the specific cell type (Zeng et al., 2017). Myelination of the neurons is one of the important processes for the proper functioning of neuronal cells. The maintenance of the myelin integrity is governed by the oligodendrocytes and oligodendrocyte precursor cells (Marisca et al., 2020). In WT scRNAseq data, the clusters, which are known as oligodendrocytes or oligodendrocytes precursor cells, were identified. Earlier report showed that these cell types help in neuronal myelination (Karadottir et al., 2008). In *(stim2a;stim2b)*$^{-/-}$ double mutant scRNAseq data, only one subpopulation was

oligodendrocyte precursor cells. This could be due to the knockout of both *stim2a* and *stim2b* genes, as it was shown the myelination-related genes were recurrently perturbed in the Alzheimer's disease pathology (Mathys et al., 2019).

In the *(stim2a;stim2b)*$^{-/-}$ double mutant, there were some very important new genes identified which are involved in the Ca^{2+} signaling. One of these genes is *apbb1*, which encodes amyloid beta (A4) precursor protein-binding, family B, member 1 protein. In humans, this gene is involved in the early-onset form of AD (Csiszar et al., 2013). This implicates the role of the Stim2a in neuroprotection because the emergence of this gene comes in correlation with the downregulation of STIM2 proteins was observed in cells from AD patients and in AD mouse models, which also explained the loss of mushroom postsynaptic spines and memory defects in aging and Alzheimer's disease (AD) (Bojarski et al., 2009, Sun et al., 2014). Another interesting gene that was identified only in *(stim2a;stim2b)*$^{-/-}$ double mutant was *gria3b*, which encodes glutamate receptor, ionotropic, AMPA3b, an alternative splicing product of the AMPA receptor (Okamoto et al., 2021), and associated with controlling the social conflict and learning behavior, hyperthermia-induced seizures and neurobehavioral abnormalities in zebrafish larvae (Hunt et al., 2012, Probst et al., 2020). Another gene that emerged in the *(stim2a;stim2b)*$^{-/-}$ double mutant was *grin2bb*, which encodes glutamate receptor, ionotropic, N-methyl D-aspartate 2B, genome duplicate b. It is localized to NMDA selective glutamate receptor complex and in the postsynaptic density membrane and is involved in excitatory postsynaptic potential and LTP. A recent report showed that this particular gene is associated with induced apoptotic hair-cell death in zebrafish (Sheets 2017), which correlates with altered behavior in zebrafish. Next important gene emerged in the *(stim2a;stim2b)*$^{-/-}$ double mutant, was *itpr1b*, which encodes inositol 1,4,5-trisphosphate receptor, type 1b protein. This gene was found to be present in Purkinje cells and granule cells in the zebrafish cerebellum and associated with the abnormal cerebellar development and ataxia in zebrafish (Aspatwar et al., 2013, Takeuchi et al., 2017). This protein is localized to the endoplasmic reticulum and is an integral component of the membrane. In humans, this gene is implicated in Gillespie syndrome and spinocerebellar ataxia type. Analysis *in vivo* of the mice model of spinocerebellar ataxia type 2 showed spontaneous firing of cerebellar Purkinje cells (Egorova et al., 2021), which could be correlated with increased Ca^{2+} oscillation frequency and amplitude in the *stim2a*$^{-/-}$ mutant. Another important gene that emerged in the *(stim2a;stim2b)*$^{-/-}$ double mutant was kcnn3,

which is basically a subfamily of potassium calcium-activated channels associated with cognitive performance schizophrenia (Grube et al., 2011).

Furthermore, four (*grinab*, *hpca*, *mast2*, and *pvalb7*) out of eight CaTK genes, which were found to be significantly upregulated in bulk RNA sequencing data of *stim2a*$^{-/-}$ mutant, were also found to be present in the scRNA seq data in the cells of neuronal origin. The *grinab* gene encodes glutamate receptor, ionotropic, N-methyl D-aspartate-associated protein 1b (glutamate binding) in zebrafish. In the zebrafish, this gene was found to be working in association with *tmbim3b* in the protection of developing embryos against cold stress (Chen et al., 2019). Another research study based on zebrafish and *D. melanogaster* revealed an essential role that, in association with *Tmbim3, grinab* controls the apoptosis during neuronal development by modulation of ER stress and ER Ca^{2+} homeostasis (Rojas-Rivera et al., 2012). The *hpca* encodes hippocalcin protein (a calcium-binding protein belonging to the neuronal calcium sensor (NCS) family proteins). This gene was found to be highly expressed in the nervous system and plays a vital role in spatial learning (O'Callaghan et al., 2002). In humans, the homozygous missense variant in the *HPCA* gene is implicated in torsion dystonia 2, neuronal excitability, and altered cognition (Osypenko et al., 2019, Siegert et al., 2021). Expression of the *pvalb7* gene, which encodes parvalbumin (PV) protein, was also found common in bulk RNA seq and scRNa seq. PV is a calcium-binding protein, present in some GABAergic interneurons (Cowan et al., 1990), in Purkinje cells in the cerebellum (Schwaller et al., 2002), and in hippocampal neurons (Klausberger et al., 2005). This elevated expression of the *pvalb7* gene could be a compensatory mechanism to normalize the Ca^{2+} homeostasis in the GABAergic interneurons, Purkinje cells, and hippocampal neurons in the absence of Stim2a, implicating an important neuroprotective role of Stim2a. Though, more investigation is needed in this direction to explain the contribution of PV in these neuronal cell types. The *mast2* gene, predominantly expressed in post-mitotic neurons, encode microtubule-associated serine-threonine kinase 2 protein, is present in both dendritic and axonal compartments (Tripathy et al., 2018). It was found that the microtubule-associated serine-threonine kinase 2 protein is a key negative regulator of the survival of the neurons (Delhommel et al., 2015). A study based on the human and mice model demonstrated that the mutations in MAST1 cause mega-corpus-callosum syndrome (Tripathy et al., 2018). In another mice model of high-fat diet induced-experimental autoimmune encephalomyelitis (HFD-EAE), *mast2* was found to be significantly upregulated (Hasan et al., 2017). The other four genes (*anxa3a*, *hp*, *pkn3*, and *slc25a25b*), which were found to be upregulated by bulk

RNA-Seq in *stim2a*$^{-/-}$ larvae but were not identified in GCAMP5G positive cells by scRNA seq, indicates that these genes might be expressed in other cells than cells of neuronal origin. It was found recently in our lab that the *anxa3a* gene was upregulated in the GCAMP5G negative cell population (likely in the microglial cells (Majewski, *unpublished*)) separated by FACS from the *(stim2a;stim2b)*$^{-/-}$ double mutant.

Chapter 5: Conclusions and future directions

In summary, the present study revealed that the absence of Stim2a in neurons changes the expression levels of numerous genes that encode proteins involved in Ca^{2+} signaling and homeostasis. This altered expression of genes has dysregulated the Ca^{2+} signaling. The changes in behavior, for example, hyperactivity, might be the effect of immediate changes of Ca^{2+} signaling or due to the dysregulation in gene expression. Thus, Stim2a could be considered to have affected Ca^{2+} signaling pathways leading to the gene expression involved in neuronal protection against selected insults in *stim2a*$^{-/-}$ zebrafish. This study provides some understanding; first, it provides a robust protocol for studying neurological disorders using zebrafish as an animal model. Second, it shows that deletion of *stim2a* leads to unprecedented behavior changes, implicating the neuroprotective role of Stim2a isoform. This was also supported by the Ca^{2+} imaging *in vivo*. It showed an increase in the basal level neuronal activity and the presence of glutamate, a neurotransmitter, and indicates the involvement of AMPA receptors, NMDA receptors, and metabotropic glutamate receptors. This indicates that the absence of *stim2a* genes could affect Ca^{2+} signaling and affect the behavior. Data from the scRNA seq showed the presence of four CaTK common genes from the bulk RNA seq. Those common genes were found to be encoding neuronal cell receptors, neuronal calcium sensors, and serine/threonine kinases and found to be involved in neuronal cell death by modulating the calcium homeostasis and ER stress. The scRNA seq also revealed that some genes were not expressed in the cells from the non-neuronal origin (*anxa3a* gene likely in the microglial cells (Majewski, *unpublished*)). Overall, the single-cell-resolution analysis highlights the complexity of Ca^{2+} signaling in response to the absence of *stim2a* and *stim2b* genes. There are many foresee and immediate applications of this analysis in zebrafish. For example, it is now feasible to identify dozens of cell types by profiling cells from brain tissues using scRNA-seq and then identify the genes involved in the Ca^{2+} signaling. This would help set up the relationships of the CaTK genes involved in neurodegenerative diseases. Based on the presented data in this work, future research could open a new scope to investigate the role of Stim2a in neuroprotection versus pathogenicity and the responsive versus the driving nature of Ca^{2+} signaling and transcriptional alterations.

References

Agetsuma, M., H. Aizawa, T. Aoki, et al., (2010). "The habenula is crucial for experience-dependent modification of fear responses in zebrafish." Nat Neurosci **13**(11): 1354-1356.

Ahrens, M. B., M. B. Orger, D. N. Robson, et al., (2013). "Whole-brain functional imaging at cellular resolution using light-sheet microscopy." Nat Methods **10**(5): 413-420.

Annona, G., A. Tarallo, V. Nittoli, et al., (2021). "Short-term exposure to the simple polyphenolic compound gallic acid induces neuronal hyperactivity in zebrafish larvae." Eur J Neurosci **53**(5): 1367-1377.

Aspatwar, A., M. E. Tolvanen, E. Jokitalo, et al., (2013). "Abnormal cerebellar development and ataxia in CARP VIII morphant zebrafish." Hum Mol Genet **22**(3): 417-432.

Baraban, S. C., M. T. Dinday, P. A. Castro, et al., (2007). "A large-scale mutagenesis screen to identify seizure-resistant zebrafish." Epilepsia **48**(6): 1151-1157.

Baraban, S. C., M. R. Taylor, P. A. Castro, et al., (2005). "Pentylenetetrazole induced changes in zebrafish behavior, neural activity and c-fos expression." Neuroscience **131**(3): 759-768.

Bergmeier, W., C. Weidinger, I. Zee, et al., (2013). "Emerging roles of store-operated Ca(2)(+) entry through STIM and ORAI proteins in immunity, hemostasis and cancer." Channels (Austin) **7**(5): 379-391.

Berna-Erro, A., A. Braun, R. Kraft, et al., (2009). "STIM2 regulates capacitive Ca2+ entry in neurons and plays a key role in hypoxic neuronal cell death." Sci Signal **2**(93): ra67.

Berridge, M. J. (2013). "Dysregulation of neural calcium signaling in Alzheimer disease, bipolar disorder and schizophrenia." Prion **7**(1): 2-13.

Berridge, M. J., P. Lipp and M. D. Bootman (2000). "The versatility and universality of calcium signalling." Nat Rev Mol Cell Biol **1**(1): 11-21.

Blaser, R. E., L. Chadwick and G. C. McGinnis (2010). "Behavioral measures of anxiety in zebrafish (Danio rerio)." Behav Brain Res **208**(1): 56-62.

Bojarski, L., J. Herms and J. Kuznicki (2008). "Calcium dysregulation in Alzheimer's disease." Neurochem Int **52**(4-5): 621-633.

Bojarski, L., P. Pomorski, A. Szybinska, et al., (2009). "Presenilin-dependent expression of STIM proteins and dysregulation of capacitative Ca2+ entry in familial Alzheimer's disease." Biochim Biophys Acta **1793**(6): 1050-1057.

Bradshaw, N. J. and M. A. Hayashi (2017). "NDE1 and NDEL1 from genes to (mal)functions: parallel but distinct roles impacting on neurodevelopmental disorders and psychiatric illness." Cell Mol Life Sci **74**(7): 1191-1210.

Brandman, O., J. Liou, W. S. Park, et al., (2007). "STIM2 is a feedback regulator that stabilizes basal cytosolic and endoplasmic reticulum Ca2+ levels." Cell **131**(7): 1327-1339.

Brenet, A., J. Somkhit, R. Hassan-Abdi, et al., (2020). "Organophosphorus diisopropylfluorophosphate (DFP) intoxication in zebrafish larvae causes behavioral defects, neuronal hyperexcitation and neuronal death." Sci Rep **10**(1): 19228.

Bresciani, E., E. Broadbridge and P. P. Liu (2018). "An efficient dissociation protocol for generation of single cell suspension from zebrafish embryos and larvae." MethodsX **5**: 1287-1290.

Brustein, E., S. Cote, J. Ghislain, et al., (2013). "Spontaneous glycine-induced calcium transients in spinal cord progenitors promote neurogenesis." Dev Neurobiol **73**(2): 168-175.

Cascella, R. and C. Cecchi (2021). "Calcium Dyshomeostasis in Alzheimer's Disease Pathogenesis." Int J Mol Sci **22**(9).

Cens, T., M. Rousset, J. P. Leyris, et al., (2006). "Voltage- and calcium-dependent inactivation in high voltage-gated Ca(2+) channels." Prog Biophys Mol Biol **90**(1-3): 104-117.

Champagne, D. L., C. C. Hoefnagels, R. E. de Kloet, et al., (2010). "Translating rodent behavioral repertoire to zebrafish (Danio rerio): relevance for stress research." Behav Brain Res **214**(2): 332-342.

Chanaday, N. L., E. Nosyreva, O. H. Shin, et al., (2021). "Presynaptic store-operated Ca(2+) entry drives excitatory spontaneous neurotransmission and augments endoplasmic reticulum stress." Neuron **109**(8): 1314-1332 e1315.

Chen, K., X. Li, G. Song, et al., (2019). "Deficiency in the membrane protein Tmbim3a/Grinaa initiates cold-induced ER stress and cell death by activating an intrinsic apoptotic pathway in zebrafish." J Biol Chem **294**(30): 11445-11457.

Chi, L. M., L. P. Wang and D. Jiao (2019). "Identification of Differentially Expressed Genes and Long Noncoding RNAs Associated with Parkinson's Disease." Parkinsons Dis **2019**: 6078251.

Chinen, Y., S. Nakamura, T. Kaneshi, et al., (2019). "A novel nonsense SMC1A mutation in a patient with intractable epilepsy and cardiac malformation." Hum Genome Var **6**: 23.

Chong, K. W., M. J. Chen, E. S. Koay, et al., (2010). "Annexin A3 is associated with cell death in lactacystin-mediated neuronal injury." Neurosci Lett **485**(2): 129-133.

Collymore, C., A. Tolwani, C. Lieggi, et al., (2014). "Efficacy and safety of 5 anesthetics in adult zebrafish (Danio rerio)." J Am Assoc Lab Anim Sci **53**(2): 198-203.

Colwill, R. M. and R. Creton (2011). "Locomotor behaviors in zebrafish (Danio rerio) larvae." Behav Processes **86**(2): 222-229.

Cowan, R. L., C. J. Wilson, P. C. Emson, et al., (1990). "Parvalbumin-containing GABAergic interneurons in the rat neostriatum." J Comp Neurol **302**(2): 197-205.

Csiszar, A., Z. Tucsek, P. Toth, et al., (2013). "Synergistic effects of hypertension and aging on cognitive function and hippocampal expression of genes involved in beta-amyloid generation and Alzheimer's disease." Am J Physiol Heart Circ Physiol **305**(8): H1120-1130.

Delhommel, F., A. Chaffotte, E. Terrien, et al., (2015). "Deciphering the unconventional peptide binding to the PDZ domain of MAST2." Biochem J **469**(1): 159-168.

Demaurex, N. and P. Nunes (2016). "The role of STIM and ORAI proteins in phagocytic immune cells." Am J Physiol Cell Physiol **310**(7): C496-508.

Dey, K., M. A. Bazala and J. Kuznicki (2020). "Targeting mitochondrial calcium pathways as a potential treatment against Parkinson's disease." Cell Calcium **89**: 102216.

Dreosti, E., G. Lopes, A. R. Kampff, et al., (2015). "Development of social behavior in young zebrafish." Front Neural Circuits **9**: 39.

Egorova, P. A., A. V. Gavrilova and I. B. Bezprozvanny (2021). "In vivo analysis of the spontaneous firing of cerebellar Purkinje cells in awake transgenic mice that model spinocerebellar ataxia type 2." Cell Calcium **93**: 102319.

Emrich, S. M., R. E. Yoast, P. Xin, et al., (2021). "Omnitemporal choreographies of all five STIM/Orai and IP3Rs underlie the complexity of mammalian Ca(2+) signaling." Cell Rep **34**(9): 108760.

Fan, E., Z. Xu, J. Yan, et al., (2021). "Acute exposure to N-Ethylpentylone induces developmental toxicity and dopaminergic receptor-regulated aberrances in zebrafish larvae." Toxicol Appl Pharmacol **417**: 115477.

Fang, H., X. Zhang, B. Xiao, et al., (2021). "A de novo mutation in SMC1A gene identified in a Chinese infant with nonclassical Cornelia de Lange syndrome and drug-resistant epilepsy." Neurol Sci **42**(1): 329-331.

Felizola, S. J., T. Maekawa, Y. Nakamura, et al., (2014). "Voltage-gated calcium channels in the human adrenal and primary aldosteronism." J Steroid Biochem Mol Biol **144 Pt B**: 410-416.

Feng, J., C. Zhang, J. E. Lischinsky, et al., (2019). "A Genetically Encoded Fluorescent Sensor for Rapid and Specific In Vivo Detection of Norepinephrine." Neuron **102**(4): 745-761 e748.

Froghi, S., C. R. Grant, R. Tandon, et al., (2021). "New Insights on the Role of TRP Channels in Calcium Signalling and Immunomodulation: Review of Pathways and Implications for Clinical Practice." Clin Rev Allergy Immunol **60**(2): 271-292.

Garcia-Alvarez, G., M. S. Shetty, B. Lu, et al., (2015). "Impaired spatial memory and enhanced long-term potentiation in mice with forebrain-specific ablation of the Stim genes." Front Behav Neurosci **9**: 180.

Gasanov, E. V., J. Jedrychowska, J. Kuznicki, et al., (2021). "Evolutionary context can clarify gene names: Teleosts as a case study." Bioessays **43**(6): e2000258.

Genovese, I., F. Giamogante, L. Barazzuol, et al., (2020). "Sorcin is an early marker of neurodegeneration, Ca(2+) dysregulation and endoplasmic reticulum stress associated to neurodegenerative diseases." Cell Death Dis **11**(10): 861.

Grossman, L., E. Utterback, A. Stewart, et al., (2010). "Characterization of behavioral and endocrine effects of LSD on zebrafish." Behav Brain Res **214**(2): 277-284.

Grube, S., M. F. Gerchen, B. Adamcio, et al., (2011). "A CAG repeat polymorphism of KCNN3 predicts SK3 channel function and cognitive performance in schizophrenia." EMBO Mol Med **3**(6): 309-319.

Gruszczynska-Biegala, J. and J. Kuznicki (2013). "Native STIM2 and ORAI1 proteins form a calcium-sensitive and thapsigargin-insensitive complex in cortical neurons." J Neurochem **126**(6): 727-738.

Gruszczynska-Biegala, J., P. Pomorski, M. B. Wisniewska, et al., (2011). "Differential roles for STIM1 and STIM2 in store-operated calcium entry in rat neurons." PLoS One **6**(4): e19285.

Gupta, R. K. and J. Kuznicki (2020). "Biological and Medical Importance of Cellular Heterogeneity Deciphered by Single-Cell RNA Sequencing." Cells **9**(8).

Gupta, R. K., I. Wasilewska, O. Palchevska, et al., (2020). "Knockout of stim2a Increases Calcium Oscillations in Neurons and Induces Hyperactive-Like Phenotype in Zebrafish Larvae." Int J Mol Sci **21**(17).

Guzel, M., M. Naziroglu, O. Akpinar, et al., (2021). "Interferon Gamma-Mediated Oxidative Stress Induces Apoptosis, Neuroinflammation, Zinc Ion Influx, and TRPM2 Channel Activation in Neuronal Cell Line: Modulator Role of Curcumin." Inflammation.

Halaidych, O. V., C. L. Mummery and V. V. Orlova (2019). "Quantifying Ca(2+) signaling and contraction in vascular pericytes and smooth muscle cells." Biochem Biophys Res Commun **513**(1): 112-118.

Hartmann, J., R. M. Karl, R. P. Alexander, et al., (2014). "STIM1 controls neuronal Ca(2)(+) signaling, mGluR1-dependent synaptic transmission, and cerebellar motor behavior." Neuron **82**(3): 635-644.

Hasan, M., J. E. Seo, K. A. Rahaman, et al., (2017). "Novel genes in brain tissues of EAE-induced normal and obese mice: Upregulation of metal ion-binding protein genes in obese-EAE mice." Neuroscience **343**: 322-336.

He, L., L. Wang, H. Zeng, et al., (2021). "Engineering of a bona fide light-operated calcium channel." Nat Commun **12**(1): 164.

Heyes, S., W. S. Pratt, E. Rees, et al., (2015). "Genetic disruption of voltage-gated calcium channels in psychiatric and neurological disorders." Prog Neurobiol **134**: 36-54.

Hidalgo, S., J. M. Campusano and J. J. L. Hodge (2021). "Assessing olfactory, memory, social and circadian phenotypes associated with schizophrenia in a genetic model based on Rim." Transl Psychiatry **11**(1): 292.

Howe, K., M. D. Clark, C. F. Torroja, et al., (2013). "The zebrafish reference genome sequence and its relationship to the human genome." Nature **496**(7446): 498-503.

Hunt, H., A. Tilunaite, G. Bass, et al., (2020). "Ca(2+) Release via IP3 Receptors Shapes the Cardiac Ca(2+) Transient for Hypertrophic Signaling." Biophys J **119**(6): 1178-1192.

Hunt, R. F., G. A. Hortopan, A. Gillespie, et al., (2012). "A novel zebrafish model of hyperthermia-induced seizures reveals a role for TRPV4 channels and NMDA-type glutamate receptors." Exp Neurol **237**(1): 199-206.

Jaworska, A., J. Dzbek, M. Styczynska, et al., (2013). "Analysis of calcium homeostasis in fresh lymphocytes from patients with sporadic Alzheimer's disease or mild cognitive impairment." Biochim Biophys Acta **1833**(7): 1692-1699.

Jimenez, J. C., K. Su, A. R. Goldberg, et al., (2018). "Anxiety Cells in a Hippocampal-Hypothalamic Circuit." Neuron **97**(3): 670-683 e676.

Joaquim, H. P. G., A. C. Costa, M. H. Serpa, et al., (2020). "Reduced Annexin A3 in schizophrenia." Eur Arch Psychiatry Clin Neurosci **270**(4): 489-494.

Karadottir, R., N. B. Hamilton, Y. Bakiri, et al., (2008). "Spiking and nonspiking classes of oligodendrocyte precursor glia in CNS white matter." Nat Neurosci **11**(4): 450-456.

Kedra, M., K. Banasiak, K. Kisielewska, et al., (2020). "TrkB hyperactivity contributes to brain dysconnectivity, epileptogenesis, and anxiety in zebrafish model of Tuberous Sclerosis Complex." Proc Natl Acad Sci U S A **117**(4): 2170-2179.

Khachaturian, Z. S. (1994). "Calcium hypothesis of Alzheimer's disease and brain aging." Ann N Y Acad Sci **747**: 1-11.

Kim, C. H., E. Ueshima, O. Muraoka, et al., (1996). "Zebrafish elav/HuC homologue as a very early neuronal marker." Neurosci Lett **216**(2): 109-112.

Kim, J. M., M. Lee, N. Kim, et al., (2016). "Optogenetic toolkit reveals the role of Ca2+ sparklets in coordinated cell migration." Proc Natl Acad Sci U S A **113**(21): 5952-5957.

Klausberger, T., L. F. Marton, J. O'Neill, et al., (2005). "Complementary roles of cholecystokinin- and parvalbumin-expressing GABAergic neurons in hippocampal network oscillations." J Neurosci **25**(42): 9782-9793.

Klejman, M. E., J. Gruszczynska-Biegala, A. Skibinska-Kijek, et al., (2009). "Expression of STIM1 in brain and puncta-like co-localization of STIM1 and ORAI1 upon depletion of Ca(2+) store in neurons." Neurochem Int **54**(1): 49-55.

Knafo, S., K. Fidelin, A. Prendergast, et al., (2017). "Mechanosensory neurons control the timing of spinal microcircuit selection during locomotion." Elife **6**.

Kovalchuk, Y., J. Eilers, J. Lisman, et al., (2000). "NMDA receptor-mediated subthreshold Ca(2+) signals in spines of hippocampal neurons." J Neurosci **20**(5): 1791-1799.

Kundap, U. P., Y. Kumari, I. Othman, et al., (2017). "Zebrafish as a Model for Epilepsy-Induced Cognitive Dysfunction: A Pharmacological, Biochemical and Behavioral Approach." Front Pharmacol **8**: 515.

Kyung, T., S. Lee, J. E. Kim, et al., (2015). "Optogenetic control of endogenous Ca(2+) channels in vivo." Nat Biotechnol **33**(10): 1092-1096.

Langmead, B. and S. L. Salzberg (2012). "Fast gapped-read alignment with Bowtie 2." Nat Methods **9**(4): 357-359.

Latoszek, E. and M. Czeredys (2021). "Molecular Components of Store-Operated Calcium Channels in the Regulation of Neural Stem Cell Physiology, Neurogenesis, and the Pathology of Huntington's Disease." Front Cell Dev Biol **9**: 657337.

Lau, B. Y., P. Mathur, G. G. Gould, et al., (2011). "Identification of a brain center whose activity discriminates a choice behavior in zebrafish." Proc Natl Acad Sci U S A **108**(6): 2581-2586.

Lefkimmiatis, K., M. Srikanthan, I. Maiellaro, et al., (2009). "Store-operated cyclic AMP signalling mediated by STIM1." Nat Cell Biol **11**(4): 433-442.

Li, F. and J. Z. Tsien (2009). "Memory and the NMDA receptors." N Engl J Med **361**(3): 302-303.

Li, J. H., Z. J. Shi, Y. Li, et al., (2020). "Bioinformatic identification of key candidate genes and pathways in axon regeneration after spinal cord injury in zebrafish." Neural Regen Res **15**(1): 103-111.

Liou, J., M. L. Kim, W. D. Heo, et al., (2005). "STIM is a Ca2+ sensor essential for Ca2+-store-depletion-triggered Ca2+ influx." Curr Biol **15**(13): 1235-1241.

Liu, Y., R. Carmer, G. Zhang, et al., (2015). "Statistical Analysis of Zebrafish Locomotor Response." PLoS One **10**(10): e0139521.

Love, M. I., W. Huber and S. Anders (2014). "Moderated estimation of fold change and dispersion for RNA-seq data with DESeq2." Genome Biol **15**(12): 550.

Ma, G., M. Wei, L. He, et al., (2015). "Inside-out Ca(2+) signalling prompted by STIM1 conformational switch." Nat Commun **6**: 7826.

Maglio, L. E., J. A. Noriega-Prieto, I. B. Maroto, et al., (2021). "IGF-1 facilitates extinction of conditioned fear." Elife **10**.

Majewski, L. and J. Kuznicki (2015). "SOCE in neurons: Signaling or just refilling?" Biochim Biophys Acta **1853**(9): 1940-1952.

Majewski, L., F. Maciag, P. M. Boguszewski, et al., (2020). "Transgenic Mice Overexpressing Human STIM2 and ORAI1 in Neurons Exhibit Changes in Behavior and Calcium Homeostasis but Show No Signs of Neurodegeneration." Int J Mol Sci **21**(3).

Marisca, R., T. Hoche, E. Agirre, et al., (2020). "Functionally distinct subgroups of oligodendrocyte precursor cells integrate neural activity and execute myelin formation." Nat Neurosci **23**(3): 363-374.

Mathys, H., J. Davila-Velderrain, Z. Peng, et al., (2019). "Single-cell transcriptomic analysis of Alzheimer's disease." Nature **570**(7761): 332-337.

Matthews, M., B. Trevarrow and J. Matthews (2002). "A virtual tour of the Guide for zebrafish users." Lab Anim (NY) **31**(3): 34-40.

Maximino, C., T. M. de Brito, R. Colmanetti, et al., (2010). "Parametric analyses of anxiety in zebrafish scototaxis." Behav Brain Res **210**(1): 1-7.

McCutcheon, V., E. Park, E. Liu, et al., (2016). "A Model of Excitotoxic Brain Injury in Larval Zebrafish: Potential Application for High-Throughput Drug Evaluation to Treat Traumatic Brain Injury." Zebrafish **13**(3): 161-169.

McDaid, J., C. A. Briggs, N. M. Barrington, et al., (2021). "Sustained Hippocampal Synaptic Pathophysiology Following Single and Repeated Closed-Head Concussive Impacts." Front Cell Neurosci **15**: 652721.

Moccia, F., E. Zuccolo, T. Soda, et al., (2015). "Stim and Orai proteins in neuronal Ca(2+) signaling and excitability." Front Cell Neurosci **9**: 153.

Muller, I., P. Lipp and G. Thiel (2012). "Ca2+ signaling and gene transcription in glucose-stimulated insulinoma cells." Cell Calcium **52**(2): 137-151.

Naik, N. A. and A. R. Shah (2021). "X linked Infantile Epileptic Encephalopathy due to SMC1A Truncating Mutation." Ann Indian Acad Neurol **24**(1): 98-101.

Nimmrich, V. and G. Gross (2012). "P/Q-type calcium channel modulators." Br J Pharmacol **167**(4): 741-759.

Niu, L. J., R. X. Xu, P. Zhang, et al., (2012). "Suppression of Frizzled-2-mediated Wnt/Ca(2)(+) signaling significantly attenuates intracellular calcium accumulation in vitro and in a rat model of traumatic brain injury." Neuroscience **213**: 19-28.

O'Callaghan, D. W., L. Ivings, J. L. Weiss, et al., (2002). "Differential use of myristoyl groups on neuronal calcium sensor proteins as a determinant of spatio-temporal aspects of Ca2+ signal transduction." J Biol Chem **277**(16): 14227-14237.

Oh-Hora, M., M. Yamashita, P. G. Hogan, et al., (2008). "Dual functions for the endoplasmic reticulum calcium sensors STIM1 and STIM2 in T cell activation and tolerance." Nat Immunol **9**(4): 432-443.

Oh, J., C. Lee and B. K. Kaang (2019). "Imaging and analysis of genetically encoded calcium indicators linking neural circuits and behaviors." Korean J Physiol Pharmacol **23**(4): 237-249.

Okamoto, H., B. W. Cherng, H. Nakajo, et al., (2021). "Habenula as the experience-dependent controlling switchboard of behavior and attention in social conflict and learning." Curr Opin Neurobiol **68**: 36-43.

Osypenko, D. S., A. V. Dovgan, N. I. Kononenko, et al., (2019). "Perturbed Ca(2+)-dependent signaling of DYT2 hippocalcin mutant as mechanism of autosomal recessive dystonia." Neurobiol Dis **132**: 104529.

Pandey, S., K. Shekhar, A. Regev, et al., (2018). "Comprehensive Identification and Spatial Mapping of Habenular Neuronal Types Using Single-Cell RNA-Seq." Curr Biol **28**(7): 1052-1065 e1057.

Panier, T., S. A. Romano, R. Olive, et al., (2013). "Fast functional imaging of multiple brain regions in intact zebrafish larvae using selective plane illumination microscopy." Front Neural Circuits **7**: 65.

Panula, P., Y. C. Chen, M. Priyadarshini, et al., (2010). "The comparative neuroanatomy and neurochemistry of zebrafish CNS systems of relevance to human neuropsychiatric diseases." Neurobiol Dis **40**(1): 46-57.

Park, C. Y., P. J. Hoover, F. M. Mullins, et al., (2009). "STIM1 clusters and activates CRAC channels via direct binding of a cytosolic domain to Orai1." Cell **136**(5): 876-890.

Peng, I. F., B. A. Berke, Y. Zhu, et al., (2007). "Temperature-dependent developmental plasticity of Drosophila neurons: cell-autonomous roles of membrane excitability, Ca2+ influx, and cAMP signaling." J Neurosci **27**(46): 12611-12622.

Peterson, S. M. and J. L. Freeman (2009). "RNA isolation from embryonic zebrafish and cDNA synthesis for gene expression analysis." J Vis Exp(30).

Poloz, Y. and D. H. O'Day (2012). "Ca2+ signaling regulates ecmB expression, cell differentiation and slug regeneration in Dictyostelium." Differentiation **84**(2): 163-175.

Probst, J., S. Kolker, J. G. Okun, et al., (2020). "Chronic hyperammonemia causes a hypoglutamatergic and hyperGABAergic metabolic state associated with neurobehavioral abnormalities in zebrafish larvae." Exp Neurol **331**: 113330.

Putney, J. W., Jr. (1986). "A model for receptor-regulated calcium entry." Cell Calcium **7**(1): 1-12.

Putney, J. W., Jr. (2003). "Capacitative calcium entry in the nervous system." Cell Calcium **34**(4-5): 339-344.

Raj, B., D. E. Wagner, A. McKenna, et al., (2018). "Simultaneous single-cell profiling of lineages and cell types in the vertebrate brain." Nat Biotechnol **36**(5): 442-450.

Ramirez, O. A., A. Cordova, M. Cerda, et al., (2021). "Ryanodine receptor-mediated Ca(2+) release and atlastin-2 GTPase activity contribute to IP3-induced dendritic Ca(2+) signals in primary hippocampal neurons." Cell Calcium **96**: 102399.

Rao, W., L. Zhang, C. Peng, et al., (2015). "Downregulation of STIM2 improves neuronal survival after traumatic brain injury by alleviating calcium overload and mitochondrial dysfunction." Biochim Biophys Acta **1852**(11): 2402-2413.

Ratcliffe, L. E., I. Vazquez Villasenor, L. Jennings, et al., (2018). "Loss of IGF1R in Human Astrocytes Alters Complex I Activity and Support for Neurons." Neuroscience **390**: 46-59.

Raza, M., L. S. Deshpande, R. E. Blair, et al., (2007). "Aging is associated with elevated intracellular calcium levels and altered calcium homeostatic mechanisms in hippocampal neurons." Neurosci Lett **418**(1): 77-81.

Richendrfer, H., S. D. Pelkowski, R. M. Colwill, et al., (2012). "On the edge: pharmacological evidence for anxiety-related behavior in zebrafish larvae." Behav Brain Res **228**(1): 99-106.

Rojas-Rivera, D., R. Armisen, A. Colombo, et al., (2012). "TMBIM3/GRINA is a novel unfolded protein response (UPR) target gene that controls apoptosis through the modulation of ER calcium homeostasis." Cell Death Differ **19**(6): 1013-1026.

Rossier, M. F. (2016). "T-Type Calcium Channel: A Privileged Gate for Calcium Entry and Control of Adrenal Steroidogenesis." Front Endocrinol (Lausanne) **7**: 43.

Salido, G. M., I. Jardin and J. A. Rosado (2011). "The TRPC ion channels: association with Orai1 and STIM1 proteins and participation in capacitative and non-capacitative calcium entry." Adv Exp Med Biol **704**: 413-433.

Santulli, G., R. Nakashima, Q. Yuan, et al., (2017). "Intracellular calcium release channels: an update." J Physiol **595**(10): 3041-3051.

Schnorr, S. J., P. J. Steenbergen, M. K. Richardson, et al., (2012). "Measuring thigmotaxis in larval zebrafish." Behav Brain Res **228**(2): 367-374.

Schwaller, B., M. Meyer and S. Schiffmann (2002). "'New' functions for 'old' proteins: the role of the calcium-binding proteins calbindin D-28k, calretinin and parvalbumin, in cerebellar physiology. Studies with knockout mice." Cerebellum **1**(4): 241-258.

Secondo, A. (2009). Ryanodine Receptors. xPharm: The Comprehensive Pharmacology Reference. S. J. Enna and D. B. Bylund. New York, Elsevier**:** 1-20.

Shanmughapriya, S., S. Rajan, N. E. Hoffman, et al., (2015). "Ca2+ signals regulate mitochondrial metabolism by stimulating CREB-mediated expression of the mitochondrial Ca2+ uniporter gene MCU." Sci Signal **8**(366): ra23.

Sheets, L. (2017). "Excessive activation of ionotropic glutamate receptors induces apoptotic hair-cell death independent of afferent and efferent innervation." Sci Rep **7**: 41102.

Shi, H., H. Shi and S. Xu (2020). "Efficient Multiple Sequences Alignment Algorithm Generation via Components Assembly Under PAR Framework." Front Genet **11**: 628175.

Shin, D. M., A. Son, S. Park, et al., (2016). "The TRPCs, Orais and STIMs in ER/PM Junctions." Adv Exp Med Biol **898**: 47-66.

Siegert, S., W. M. Schmidt, T. Pletschko, et al., (2021). "Specific Cognitive Changes due to Hippocalcin Alterations? A Novel Familial Homozygous Hippocalcin Variant Associated with Inherited Dystonia and Altered Cognition." Neuropediatrics.

Skibinska-Kijek, A., M. B. Wisniewska, J. Gruszczynska-Biegala, et al., (2009). "Immunolocalization of STIM1 in the mouse brain." Acta Neurobiol Exp (Wars) **69**(4): 413-428.

Skopin, A. Y., A. D. Grigoryev, L. N. Glushankova, et al., (2021). "A Novel Modulator of STIM2-Dependent Store-Operated Ca2+ Channel Activity." Acta Naturae **13**(1): 140-146.

Soman, S. K., M. Bazala, M. Keatinge, et al., (2019). "Restriction of mitochondrial calcium overload by mcu inactivation renders a neuroprotective effect in zebrafish models of Parkinson's disease." Biol Open **8**(10).

Soong, T. W., A. Stea, C. D. Hodson, et al., (1993). "Structure and functional expression of a member of the low voltage-activated calcium channel family." Science **260**(5111): 1133-1136.

Stewart, A. M., O. Braubach, J. Spitsbergen, et al., (2014). "Zebrafish models for translational neuroscience research: from tank to bedside." Trends Neurosci **37**(5): 264-278.

Stewart, A. M., J. F. Ullmann, W. H. Norton, et al., (2015). "Molecular psychiatry of zebrafish." Mol Psychiatry **20**(1): 2-17.

Striggow, F. and B. E. Ehrlich (1996). "Ligand-gated calcium channels inside and out." Current Opinion in Cell Biology **8**(4): 490-495.

Stuart, T., A. Butler, P. Hoffman, et al., (2019). "Comprehensive Integration of Single-Cell Data." Cell **177**(7): 1888-1902 e1821.

Sun, S., H. Zhang, J. Liu, et al., (2014). "Reduced synaptic STIM2 expression and impaired store-operated calcium entry cause destabilization of mature spines in mutant presenilin mice." Neuron **82**(1): 79-93.

Suzuki, D. G., J. Perez-Fernandez, T. Wibble, et al., (2019). "The role of the optic tectum for visually evoked orienting and evasive movements." Proc Natl Acad Sci U S A **116**(30): 15272-15281.

Takeuchi, M., S. Yamaguchi, Y. Sakakibara, et al., (2017). "Gene expression profiling of granule cells and Purkinje cells in the zebrafish cerebellum." J Comp Neurol **525**(7): 1558-1585.

Tang, T. S., E. Slow, V. Lupu, et al., (2005). "Disturbed Ca2+ signaling and apoptosis of medium spiny neurons in Huntington's disease." Proc Natl Acad Sci U S A **102**(7): 2602-2607.

Tanokashira, D., W. Fukuokaya and A. Taguchi (2019). "Involvement of insulin receptor substrates in cognitive impairment and Alzheimer's disease." Neural Regen Res **14**(8): 1330-1334.

Taylor, C. W. and S. C. Tovey (2010). "IP(3) receptors: toward understanding their activation." Cold Spring Harb Perspect Biol **2**(12): a004010.

Thomas, P. D., A. Kejariwal, M. J. Campbell, et al., (2003). "PANTHER: a browsable database of gene products organized by biological function, using curated protein family and subfamily classification." Nucleic Acids Res **31**(1): 334-341.

Treit, D. and M. Fundytus (1988). "Thigmotaxis as a test for anxiolytic activity in rats." Pharmacol Biochem Behav **31**(4): 959-962.

Tripathy, R., I. Leca, T. van Dijk, et al., (2018). "Mutations in MAST1 Cause Mega-Corpus-Callosum Syndrome with Cerebellar Hypoplasia and Cortical Malformations." Neuron **100**(6): 1354-1368 e1355.

Wasilewska, I., R. K. Gupta, O. Palchevska, et al., (2019). "Identification of Zebrafish Calcium Toolkit Genes and their Expression in the Brain." Genes (Basel) **10**(3).

Wasilewska, I., R. K. Gupta, B. Wojtas, et al., (2020). "stim2b Knockout Induces Hyperactivity and Susceptibility to Seizures in Zebrafish Larvae." Cells **9**(5).

Weber, D. K., U. V. Reddy, S. Wang, et al., (2021). "Structural basis for allosteric control of the SERCA-Phospholamban membrane complex by Ca(2+) and phosphorylation." Elife **10**.

Wegierski, T. and J. Kuznicki (2018). "Neuronal calcium signaling via store-operated channels in health and disease." Cell Calcium **74**: 102-111.

Williams, R. T., S. S. Manji, N. J. Parker, et al., (2001). "Identification and characterization of the STIM (stromal interaction molecule) gene family: coding for a novel class of transmembrane proteins." Biochem J **357**(Pt 3): 673-685.

Wilson, D. P., M. Susnjar, E. Kiss, et al., (2005). "Thromboxane A2-induced contraction of rat caudal arterial smooth muscle involves activation of Ca2+ entry and Ca2+ sensitization: Rho-associated kinase-mediated phosphorylation of MYPT1 at Thr-855, but not Thr-697." Biochem J **389**(Pt 3): 763-774.

Wojda, U. and J. Kuznicki (2013). "Alzheimer's disease modeling: ups, downs, and perspectives for human induced pluripotent stem cells." J Alzheimers Dis **34**(3): 563-588.

Wojda, U., E. Salinska and J. Kuznicki (2008). "Calcium ions in neuronal degeneration." IUBMB Life **60**(9): 575-590.

Xing, L., T. S. Quist, T. J. Stevenson, et al., (2014). "Rapid and efficient zebrafish genotyping using PCR with high-resolution melt analysis." J Vis Exp(84): e51138.

Yamakage, M. and A. Namiki (2002). "Calcium channels--basic aspects of their structure, function and gene encoding; anesthetic action on the channels--a review." Can J Anaesth **49**(2): 151-164.

Yap, K. A., M. S. Shetty, G. Garcia-Alvarez, et al., (2017). "STIM2 regulates AMPA receptor trafficking and plasticity at hippocampal synapses." Neurobiol Learn Mem **138**: 54-61.

You, J., S. M. Corley, L. Wen, et al., (2018). "RNA-Seq analysis and comparison of corneal epithelium in keratoconus and myopia patients." Sci Rep **8**(1): 389.

Zeng, H. and J. R. Sanes (2017). "Neuronal cell-type classification: challenges, opportunities and the path forward." Nat Rev Neurosci **18**(9): 530-546.

Zhang, H., J. Liu, S. Sun, et al., (2015). "Calcium signaling, excitability, and synaptic plasticity defects in a mouse model of Alzheimer's disease." J Alzheimers Dis **45**(2): 561-580.

Zhang, H., S. Sun, L. Wu, et al., (2016). "Store-Operated Calcium Channel Complex in Postsynaptic Spines: A New Therapeutic Target for Alzheimer's Disease Treatment." J Neurosci **36**(47): 11837-11850.

Zhang, H., L. Wu, E. Pchitskaya, et al., (2015). "Neuronal Store-Operated Calcium Entry and Mushroom Spine Loss in Amyloid Precursor Protein Knock-In Mouse Model of Alzheimer's Disease." J Neurosci **35**(39): 13275-13286.

Zheng, F., M. Zhang, Q. Ding, et al., (2016). "Voluntary running depreciates the requirement of Ca2+-stimulated cAMP signaling in synaptic potentiation and memory formation." Learn Mem **23**(8): 442-449.

Zheng, G. X., B. T. Lau, M. Schnall-Levin, et al., (2016). "Haplotyping germline and cancer genomes with high-throughput linked-read sequencing." Nat Biotechnol **34**(3): 303-311.

Zub, E., G. Canet, R. Garbelli, et al., (2019). "The GR-ANXA1 pathway is a pathological player and a candidate target in epilepsy." FASEB J **33**(12): 13998-14009.

Publications and conferences covering the results of this dissertation

Publications

1. **Gupta RK**, Misztal K, Wasilewska I, Pawel Segit, Kuźnicki J. New oligodendrocyte sub-types identified by single-cell RNA-seq in double knockout of (*stim2a;stim2b*) in zebrafish brain involved in myelin metabolism (*in preperation*).
2. **Gupta RK**, Wasilewska I, Palchevska O, Kuźnicki J. Knockout of *stim2a* increases calcium oscillations in neurons and induces hyperactive-like phenotype in zebrafish larvae. *Int. J. Mol. Sci*.**2020**.
3. **Gupta RK**, Kuznicki J. Biological and medical importance of cellular heterogeneity deciphered by single-cell RNA sequencing. *Cells*. **2020**. PubMed ID: 32707839.
4. Wasilewska I, **Gupta RK**, Wojtaś B, Palchevska O, Kuźnicki J. *stim2b* knockout induces hyperactivity and susceptibility to seizures in zebrafish larvae. *Cells*. **2020**.
5. Maciąg F, Majewski Ł, Boguszewski PM, **Gupta RK**, Wasilewska I, Wojtaś B, Kuznicki J. Behavioral and electrophysiological changes in female mice overexpressing ORAI1 in neurons. *Biochim Biophys Acta Mol Cell Res*. **2019**.
6. Wasilewska I, **Gupta RK**, Palchevska O, Kuźnicki J. Identification of zebrafish calcium toolkit genes and their expression in the brain. *Genes*. **2019**.

Conference Presentations

1. **Gupta RK**, Wasilewska I, Palchevska OP, Kuznicki J, Decoding the spontaneous *in vivo* Ca^{2+} oscillations in zebrafish brain neurons. 14th International Congress of the Polish Neuroscience Society (ICPNS), Katowice, Poland, Aug-2019.
2. **Gupta RK**, Wasilewska I, Palchevska OP, Kuznicki J, Encoding and decoding of Ca^{2+} oscillations in zebrafish brain neurons by in vivo Ca^{2+} imaging. FEBS Congress, Krakow, Poland, July-2019.
3. **Gupta RK**, Wasilewska I, Palchevska OP, Kuznicki J, Encoding and decoding of Ca^{2+} oscillations in zebrafish brain neurons by in vivo Ca^{2+} imaging. What do we know about Orai:STIM signaling?- Medical University of Graz, Austria, Feb-2019 (Oral presentation).
4. Palchevska OP, Wasilewska I, **Gupta RK**, Palchevskyy SS, Kuznicki J, The role of Stim2 isoforms in the brain of zebrafish. The 15^{th} International Meeting of the European Calcium Society (ECS)- Hamburg, Germany, Sep-2018.
5. Bazala M, Soman S, **Gupta RK,** Bandmann O, Kuznicki J, Calcium uptake in mitochondria of zebrafish measured in vitro. Zebrafish Disease Models-11 (ZDM11)- Leiden University, The Netherlands, July-2018.

Appendix: Table 1: CaTK genes in different neuronal cell types (in WT)

Cell cluster	Highly expressed genes		Low expressed genes	
Thalamocortical neurons	*calm1a*	0.581	*ppp1cb*	-0.303
	fkbp1aa	0.338	*atp2b1a*	-0.325
			nell2b	-0.385
			tmbim4	-0.539
			kcnma1a	-0.549
			cadpsb	-0.581
			gria1a	-0.677
			atp2b3a	-0.738
			gria2b	-0.814
			atp2b2	-0.838
			grin1a	-0.922
			clstn1	-1.026
			grin1b	-1.099
			clstn3	-1.133
			atp6v0cb	-1.175
			atp2b4	-1.182
			atp2b3b	-1.264
GABAergic neurons Type1	*calr*	0.882	*myl6*	-0.281
	tenm3	0.834	*smdt1b*	-0.295
	atp6v0cb	0.820	*vdac1*	-0.295
	atp2b1a	0.719	*calm1a*	-0.303
	clstn1	0.712	*vdac3*	-0.331
	nell2b	0.674	*ubb*	-0.400
	tmbim4	0.634	*fkbp1aa*	-0.603
	calr3a	0.612		
	atp2b4	0.606		
	grin1b	0.514		
	canx	0.482		
	atp2b2	0.481		
	atp2b3b	0.463		
	grin1a	0.462		
	atp2b3a	0.438		
	kcnma1a	0.434		
	clstn3	0.428		
	gria1a	0.331		
	nucb2a	0.330		
	sgce	0.279		
	vdac2	0.271		

Dopaminergic neurons	*pvalb6*	1.097	*crebzf*	-0.251
	atp2b3b	0.784	*calr3a*	-0.267
	clstn3	0.593	*tenm3*	-0.478
	cacng8b	0.574	*calr*	-0.529
	atp2b3a	0.523		
	grin1b	0.506		
	atp2b4	0.504		
	kcnip1b	0.499		
	cadpsb	0.495		
	grin2ab	0.477		
	gria1a	0.452		
	clstn2	0.426		
	grin1a	0.415		
	cacng8a	0.378		
	tenm4	0.349		
	atp6v0cb	0.348		
	cacng2a	0.347		
	cetn2	0.337		
	atp2b2	0.332		
	hpcal4	0.308		
	slc24a6a	0.305		
	vdac1	0.293		
	clstn1	0.290		
	myl6	0.276		
	apba2b	0.269		
Not Known type 1	*necab2*	0.708	*vdac2*	-0.359
	prkcbb	0.598	*calr*	-0.536
	clstn1	0.556		
	gria2b	0.555		
	clstn3	0.554		
	nell2b	0.534		
	cetn2	0.450		
	slc24a6a	0.415		
	atp2b3b	0.387		
	grin1b	0.370		
	grin1a	0.364		
	cadpsb	0.349		
	si:ch211-195	0.347		
	ppp1cb	0.341		
	cacna1ab	0.340		
	cacng8a	0.325		
	atp2b4	0.313		
	kcnip1b	0.312		
	cacng2a	0.284		

	prkcea 0.283 *tenm4* 0.272 *kcnma1a* 0.256	
Neuronal progenitor cells Type1	*fkbp1aa* 0.317	*tmbim4* -0.283 *kcnma1a* -0.447 *atp2b1a* -0.469 *atp2b3a* -0.487 *atp2b2* -0.658 *atp6v0cb* -0.660 *grin1b* -0.790 *grin1a* -0.885 *atp2b4* -0.929 *clstn3* -1.013 *atp2b3b* -1.034 *clstn1* -1.126 *nell2b* -1.380
GABAergic neurons Type2	*hpca* 0.360 *necab2* 0.343 *ppp1cb* 0.262	*atp2b3b* -0.281 *atp2b4* -0.289 *calr3a* -0.322 *atp6v0cb* -0.578 *calr* -0.587
Neuronal progenitor cells Type2	*cetn2* 0.442 *hpcal4* 0.364 *prkcbb* 0.298 *ppp1cab* 0.269 *aif1l* 0.260 *gria2b* 0.253 *fkbp1aa* 0.250	*tenm3* -0.365 *atp2b4* -0.501 *hpca* -0.559
Progenitor cell (glia type)	*anxa11b* 0.661 *fkbp3* 0.459 *atox1* 0.431	*nucb2a* -0.279 *vdac3* -0.285 *creb1a* -0.306 *aif1l* -0.316 *canx* -0.322 *calr3a* -0.346 *cab39l* -0.435 *crebzf* -0.477 *ctbp1* -0.478 *vdac1* -0.510 *sgce* -0.524 *ppp1cb* -0.602 *tmbim4* -0.615 *atp2b2* -0.767 *apba2b* -0.798 *hpca* -0.839 *atp2b3a* -0.840

			kcnma1a	-0.862
			atp2b4	-0.891
			calm1a	-0.926
			calr	-0.979
			grin1a	-1.004
			atp2b3b	-1.038
			nell2b	-1.068
			atp2b1a	-1.085
			clstn3	-1.269
			tenm3	-1.313
			grin1b	-1.359
			clstn1	-1.366
			atp6v0cb	-1.823
Purkinje cells	*fkbp1aa*	0.339	*gria1a*	-0.424
	ctbp1	0.295	*kcnma1a*	-0.431
			tmbim4	-0.482
			atp2b1a	-0.485
			hpca	-0.544
			atp2b2	-0.568
			atp2b3a	-0.688
			clstn1	-0.825
			tenm3	-0.825
			nell2b	-0.852
			clstn3	-0.898
			grin1a	-0.923
			atp2b4	-0.926
			grin1b	-0.955
			atp6v0cb	-1.070
			atp2b3b	-1.174
Glutamatergic neurons	*atp6v0cb*	0.902	*aif1l*	-0.325
	atp2b2	0.794	*atp2b3b*	-0.388
	atp2b1a	0.763	*nell2b*	-0.997
	apba1b	0.642	*tenm3*	-1.122
	tmbim4	0.632		
	hpcal4	0.613		
	atp2b4	0.599		
	calr	0.564		
	atp2b3a	0.492		
	calua	0.389		
	smdt1b	0.352		
	nucb2a	0.323		
	hpca	0.299		
	calr3b	0.297		
	calm1a	0.295		
	vdac3	0.294		

	cacna1ab	0.277		
	calr3a	0.275		
Oligodendrocyte progenitor cells	*anxa13*	1.947	*creb1a*	-0.286
	gria4a	1.118	*hpca*	-0.364
	itsn2a	1.075	*atp2b3a*	-0.418
	calr3b	1.037	*ppp1cb*	-0.446
	cacng4a	1.022	*kcnma1a*	-0.586
	calr3a	0.963	*atp2b1a*	-0.599
	nucb1	0.950	*atp2b2*	-0.650
	itsn2b	0.866	*tenm3*	-0.807
	grinab	0.858	*clstn3*	-0.864
	sgk3	0.817	*calm1a*	-0.928
	atox1	0.790	*clstn1*	-0.987
	calr	0.787	*nell2b*	-1.226
	nucb2a	0.768	*atp2b3b*	-1.345
	stim1a	0.756	*atp6v0cb*	-1.384
	anxa11b	0.754		
	smdt1b	0.696		
	fkbp2	0.533		
	sigmar1	0.464		
	ppp1cab	0.462		
	capn1a	0.462		
	gria2b	0.425		
	tmx1	0.419		
	sgcb	0.371		
	cacng8b	0.355		
	fkbp3	0.348		
	fkbp1b	0.339		
	fkbp4	0.338		
	ormdl1	0.330		
	canx	0.328		
	calua	0.315		
	atp2a2b	0.313		
	myl6	0.293		
	vdac3	0.269		
Terminally differentiated oligodendrocytes	*cadps2*	2.621	*atp2b2*	-0.285
	gria4a	1.886	*clstn3*	-0.323
	prkcq	1.703	*creb1a*	-0.327
	gria1b	1.216	*calr*	-0.346
	atp2b4	0.891	*calr3a*	-0.439
	smdt1b	0.888	*grin1b*	-0.492
	kcnma1a	0.823	*atp2b3a*	-0.795
	stk38l	0.702	*hpca*	-0.834
	nucb2a	0.636		
	grin1a	0.611		

	atp6v0cb	0.593		
	hpcal4	0.574		
	sgce	0.563		
	tenm3	0.524		
	canx	0.517		
	crebzf	0.516		
	necab2	0.512		
	nell2b	0.469		
	slc24a6a	0.455		
	gria1a	0.336		
	cetn2	0.328		
	atp2b3b	0.299		
Not Known 2	*anxa13l*	2.078	*calr3a*	-0.339
	chp2	1.139	*aif1l*	-0.376
	anxa13	0.766	*ppp1cab*	-0.426
	apba1a	0.718	*creb1a*	-0.461
	tmx1	0.642	*vdac1*	-0.527
	ehd1b	0.630	*clstn3*	-0.767
	atox1	0.551	*atp2b1a*	-0.778
	calm1a	0.501	*atp2b4*	-0.817
	sgce	0.501	*kcnma1a*	-0.955
	ppp1cb	0.397	*calr*	-0.999
	fkbp4	0.388	*atp2b2*	-1.102
	grinab	0.357	*atp2b3a*	-1.103
	sgcb	0.347	*atp2b3b*	-1.191
	anxa11b	0.324	*hpca*	-1.237
	fkbp5	0.293	*tenm3*	-1.312
	sigmar1	0.287	*clstn1*	-1.509
	ormdl1	0.273	*grin1b*	-1.533
	nucb1	0.266	*nell2b*	-1.535
			grin1a	-1.586
			atp6v0cb	-2.099

Appendix: Table 2: CaTK genes in different neuronal cell types (in *(stim2a; stim2b)* $^{-/-}$ double mutant)

Cell cluster	Highly expressed genes		Low expressed genes	
Spinal cord neurons	*tenm3*	0.966	*fkbp2*	-0.253
	gria1a	0.866	*creb1a*	-0.270
	kcnma1a	0.858	*cetn3*	-0.271
	tenm4	0.756	*kcnip1b*	-0.282
	atp2b3b	0.751	*aif1l*	-0.388
	grin1a	0.734	*vdac1*	-0.414
	clstn3	0.733	*calm1a*	-0.414
	clstn1	0.728	*vdac3*	-0.448
	grin1b	0.696	*fkbp1aa*	-0.729
	nell2b	0.691		
	cadpsb	0.675		
	kcnn1a	0.651		
	atp2b3a	0.590		
	gria2b	0.550		
	atp2b4	0.532		
	atp2b2	0.530		
	necab2	0.513		
	canx	0.489		
	crebbpa	0.392		
	mast2	0.380		
	cacng8b	0.345		
	crebzf	0.329		
	apba2b	0.297		
	atp2b1a	0.280		
Thalamocortical neurons	*fkbp1aa*	0.274	*cetn2*	-0.279
	creb1a	0.255	*kcnn1a*	-0.293
			kcnip1b	-0.399
			tenm4	-0.476
			cadpsb	-0.500
			grin1a	-0.520
			atp6v0cb	-0.531
			atp2b3a	-0.539
			kcnma1a	-0.558
			clstn1	-0.566
			gria2b	-0.615
			atp2b2	-0.627
			clstn3	-0.709
			gria1a	-0.766
			grin1b	-0.814
			atp2b4	-0.898

			atp2b3b	-0.944
Dopaminergic neurons	*pvalb6*	0.970	*canx*	-0.322
	cetn2	0.656	*calr*	-0.337
	hpcal4	0.636	*calr3a*	-0.351
	atp2b3b	0.581	*crebzf*	-0.494
	atp6v0cb	0.515	*tenm3*	-0.553
	necab1	0.506		
	grin1b	0.419		
	clstn3	0.391		
	smdt1b	0.359		
	cetn3	0.331		
	cacng8b	0.327		
	fkbp4	0.323		
	hpca	0.309		
	vdac1	0.290		
	slc24a6a	0.289		
	atox1	0.286		
	atp2b3a	0.285		
	nell2b	0.279		
	vdac3	0.271		
	grin1a	0.263		
	myl6	0.262		
	ppp1cb	0.258		
	kcnip1b	0.254		
Neuronal progenitor cells Type1	*kcnip1b*	0.544	*atp2b2*	-0.253
	mast2	0.401	*cetn2*	-0.273
	fkbp1aa	0.323	*cadpsb*	-0.279
	hpca	0.276	*kcnn1a*	-0.284
			atp2b1a	-0.312
			gria1a	-0.327
			tenm4	-0.369
			necab2	-0.396
			kcnma1a	-0.397
			atp2b3b	-0.480
			atp2b4	-0.505
			grin1a	-0.534
			gria2b	-0.559
			grin1b	-0.573
			clstn3	-0.594
			clstn1	-0.731
			nell2b	-0.998
GABAergic neurons Type2	*necab1*	0.524	*cacng8b*	-0.277
	cetn2	0.423	*kcnma1a*	-0.278
	aif1l	0.302	*gria1a*	-0.312
	fkbp1aa	0.293	*atp2b3b*	-0.338

	gria1b	0.277	*grin1a*	-0.338
			cacna1ab	-0.338
			necab2	-0.357
			atp2b2	-0.362
			nell2b	-0.370
			clstn1	-0.370
			hpca	-0.395
			tenm3	-0.481
			atp2b4	-0.654
GABAergic amacrine (AM) cells	*cab39l*	0.288	*cacng8b*	-0.310
			atp2b1a	-0.349
			cadpsb	-0.358
			fkbp1aa	-0.359
			atp2b2	-0.372
			grin1b	-0.383
			tenm3	-0.384
			grin1a	-0.385
			cetn2	-0.395
			calr3a	-0.403
			necab2	-0.419
			clstn3	-0.422
			gria2b	-0.428
			gria1a	-0.452
			calr	-0.457
			canx	-0.483
			clstn1	-0.499
			atp2b3a	-0.581
			atp2b3b	-0.585
			atp6v0cb	-0.847
			atp2b4	-0.878
Cajal-Retzius neurons (corticospinal)	*clstn1*	0.627	*hpca*	-0.311
	gria2b	0.534	*cacng8b*	-0.430
	grin2bb	0.517	*tenm3*	-0.456
	nell2b	0.352		
	prkcea	0.329		
	calr3b	0.305		
	tenm4	0.263		
	cadpsb	0.259		
Photoreceptor progenitors (migratory)	*anxa13*	0.856	*nucb2a*	-0.251
	crebzf	0.605	*vdac1*	-0.261
	fkbp3	0.528	*fkbp1aa*	-0.266
			ppp1cab	-0.274
			aif1l	-0.290
			sgce	-0.298
			cab39l	-0.327

			gria1a	-0.397
			kcnip1b	-0.418
			cetn2	-0.445
			tenm4	-0.445
			creb1a	-0.456
			canx	-0.466
			calr3a	-0.469
			tmbim4	-0.542
			necab2	-0.545
			kcnn1a	-0.607
			atp2b3b	-0.607
			kcnma1a	-0.611
			cacng8b	-0.618
			apba2b	-0.636
			cadpsb	-0.664
			atp2b2	-0.677
			gria2b	-0.718
			atp2b1a	-0.729
			nell2b	-0.731
			calm1a	-0.774
			atp2b4	-0.789
			atp2b3a	-0.796
			grin1a	-0.810
			hpca	-0.868
			clstn3	-0.869
			clstn1	-0.936
			calr	-0.966
			grin1b	-0.995
			tenm3	-1.067
			atp6v0cb	-1.381
Thalamic neurons	*calr*	0.549	*atp2b3a*	-0.337
	gria1a	0.507	*hpca*	-0.341
	canx	0.403	*cacng8b*	-0.372
	cacng8a	0.399	*tenm4*	-0.429
	grin1a	0.327	*necab2*	-0.506
	calr3a	0.297		
	prkcea	0.253		
Purkinje cells	*calm1a*	0.560	*sgce*	-0.296
	grin1b	0.436	*aif1l*	-0.346
	ppp1cb	0.355	*kcnn1a*	-0.346
	sgcb	0.347	*grin1a*	-0.425
	prkcea	0.324	*nell2b*	-0.610
	tmbim4	0.310	*hpca*	-0.662
	clstn1	0.290	*necab2*	-0.723
	apba2b	0.289	*tenm4*	-0.842

	calr	0.280	*gria1a*	-1.180
	vdac3	0.272	*tenm3*	-1.362
Cajal-Retzius neurons			*canx*	-0.411
			atp2b1a	-0.461
			smdt1b	-0.476
			aif1l	-0.480
			tmbim4	-0.523
			ppp1cb	-0.567
			cetn2	-0.608
			apba2b	-0.626
			tenm3	-0.629
			kcnn1a	-0.686
			cacng8b	-0.716
			tenm4	-0.755
			cadpsb	-0.796
			kcnip1b	-0.842
			hpca	-0.897
			necab2	-0.972
			atp2b2	-1.012
			gria2b	-1.036
			gria1a	-1.124
			atp2b3a	-1.125
			nell2b	-1.146
			grin1a	-1.189
			grin1b	-1.267
			kcnma1a	-1.311
			clstn3	-1.339
			atp2b4	-1.466
			atp2b3b	-1.475
			clstn1	-1.509
			atp6v0cb	-1.818
Oligodendrocyte progenitor cells	*atox1*	0.723	*creb1a*	-0.326
	sgk3	0.572	*tenm4*	-0.344
	gria2b	0.557	*vdac2*	-0.395
	fkbp1b	0.496	*atp2b1a*	-0.401
	anxa11a	0.484	*vdac1*	-0.450
	cacng8b	0.481	*cadpsb*	-0.451
	fkbp2	0.474	*atp2b2*	-0.526
	stim1a	0.462	*kcnn1a*	-0.543
	atp2a2b	0.407	*hpca*	-0.555
	sgcb	0.399	*calm1a*	-0.556
	chp2	0.382	*clstn1*	-0.626
	tmx1	0.362	*clstn3*	-0.773
	fkbp5	0.352	*kcnma1a*	-0.894
	sigmar1	0.327	*necab2*	-0.937

	anxa11b	0.323	*nell2b*	-0.947
	sgce	0.309	*tenm3*	-1.007
	aif1l	0.271	*atp6v0cb*	-1.251
	myl6	0.255	*atp2b3b*	-1.267
Olfactory sensory neurons	*clstn1*	0.582	*atp2b3a*	-0.251
	nell2b	0.565	*creb1a*	-0.301
	mast2	0.553	*calr*	-0.329
	tmbim4	0.530	*cadpsb*	-0.407
	cacnb4a	0.523	*cacng8b*	-0.458
	fkbp4	0.496	*grin1b*	-0.598
	smdt1b	0.484	*hpca*	-0.720
	hpcal4	0.483	*atp2b1a*	-0.794
	efhd1	0.477	*gria2b*	-0.915
	fkbp5	0.453		
	cetn2	0.449		
	kcnma1a	0.444		
	atp6v0cb	0.410		
	sgce	0.380		
	atox1	0.370		
	tenm3	0.272		
	prkcea	0.267		
	grin1a	0.267		
	anxa13	0.263		
Cortical neurons	*gria1a*	0.587	*myl6*	-0.278
	necab2	0.511	*smdt1b*	-0.300
	grin1a	0.413	*cab39l*	-0.300
	fkbp1b	0.396	*atp2b3b*	-0.369
	calr3b	0.388	*calm1a*	-0.382
	cacna1ab	0.384	*atp6v0cb*	-0.444
	fkbp4	0.359	*nell2b*	-0.619
	micu3b	0.339		
	apbb1	0.298		
	aif1l	0.296		
Ganglion cells (retinal)	*slc24a6a*	0.445	*canx*	-0.256
	clstn2	0.445	*tmbim4*	-0.260
	hpca	0.433	*creb1a*	-0.263
	smdt1b	0.424	*kcnn1a*	-0.327
	tenm3	0.408	*ppp1cab*	-0.331
	cab39l	0.370	*gria3b*	-0.350
	stk38l	0.352	*grin1b*	-0.374
	apbb1	0.337	*nell2b*	-0.379
	gria4a	0.311	*cacna1ab*	-0.398
	cadpsa	0.309	*calr*	-0.549
	apba1b	0.305	*aif1l*	-0.591
	myl6	0.296	*atp6v0cb*	-0.595

	micu1	0.296	*grin1a* *gria2b*	-0.640 -0.813

Appendix I: Table 3: CaTK genes identified in WT and in *(stim2a; stim2b)*$^{-/-}$ double mutant cells from the neuronal origin

CaTK-common in WT and *(stim2a; stim2b)*$^{-/-}$

Name of the genes	Full name of the gene	Descriptions (collected from www.zfin.org)
aif1l	Allograft inflammatory factor 1-like	Have actin filament binding activity and calcium ion binding activity. Colocalize with actin filament and ruffle membrane, and involved in actin filament bundle assembly and ruffle assembly. Expressed in several structures, including alar plate midbrain region; fin; immature eye; nervous system; and periderm. Orthologous to human AIF1L (allograft inflammatory factor 1 like).
anxa11b	Annexin a11b	Have calcium ion binding activity. Localize to cytoplasm, and involved in cytokinetic process and phagocytosis. Expressed in several structures, including cardiovascular system; digestive system; immature eye; integument; and sensory system. Human ortholog(s) of this gene implicated in amyotrophic lateral sclerosis type 23. Orthologous to human ANXA11 (annexin A11).
anxa13	Annexin A13	Have calcium ion binding activity. Localize to cytoplasm. Orthologous to human ANXA13 (annexin A13).
anxa13l	Annexin A13, like	Have calcium ion binding activity. Localize to cytoplasm. Expressed in basal plate midbrain region and nervous system.
apba1b	Amyloid beta (A4) precursor protein-binding, family A, member 1b	Have amyloid-beta binding activity. Localize to cytoplasm; dendritic spine; and plasma membrane, and involved in chemical synaptic transmission. Orthologous to human APBA1 (amyloid beta precursor protein binding family A member 1).
apba2b	Amyloid beta (A4) precursor protein-binding, family A, member 2b	Have amyloid-beta binding activity. Localize to cytoplasm; dendritic spine; and plasma membrane, and involved in chemical synaptic transmission. Orthologous to human APBA2 (amyloid beta precursor protein binding family A member 2).
atox1	Antioxidant 1 copper chaperone	Have copper chaperone activity. Localize to cytosol, and involved in cellular copper ion homeostasis and response to oxidative stress. Orthologous to human ATOX1 (antioxidant 1 copper chaperone).

atp2a2b	Atpase sarcoplasmic/ endoplasmic reticulum Ca2+ transporting 2b	Have atpase activity; calcium transmembrane transporter activity, phosphorylative mechanism; and proton-exporting atpase activity, phosphorylative mechanism. Localize to sarcoplasmic reticulum membrane, and involved in determination of heart left/right asymmetry. Expressed in axis; myotome; pectoral fin; and pectoral fin musculature. Human ortholog(s) of this gene implicated in acrokeratosis verruciformis; essential hypertension; keratosis follicularis; and pulmonary hypertension. Orthologous to human ATP2A2 (atpase sarcoplasmic/endoplasmic reticulum Ca2+ transporting 2).
atp2b1a	Atpase plasma membrane Ca2+ transporting 1a	Have PDZ domain binding activity and calcium transmembrane transporter activity, phosphorylative mechanism. Localize to integral component of plasma membrane and intracellular membrane-bounded organelleand involved in animal organ development and sensory perception of sound. Expressed in several structures, including digestive system; hematopoietic system; midbrain neural tube; nervous system; and pleuroperitoneal region. Orthologous to human ATP2B1 (atpase plasma membrane Ca2+ transporting 1).
atp2b2	Atpase plasma membrane Ca2+ transporting 2	Have PDZ domain binding activity and calcium transmembrane transporter activity, phosphorylative mechanism. Localize to several cellular components, including integral component of plasma membrane; intracellular membrane-bounded organelle; and postsynaptic density membrane, and involved in neuron differentiation and regulation of cytosolic calcium ion concentration. Expressed in several structures, including blood; eye; heart; liver; and pleuroperitoneal region. Human ortholog(s) of this gene implicated in autosomal recessive nonsyndromic deafness 12. Orthologous to human ATP2B2 (atpase plasma membrane Ca2+ transporting 2).
atp2b3a	Atpase plasma membrane Ca2+ transporting 3a	Have PDZ domain binding activity and calcium transmembrane transporter activity, phosphorylative mechanism. Localize to integral component of plasma membrane and intracellular membrane-bounded organelle, and involved in regulation of cytosolic calcium ion concentration. Expressed in blood; liver; muscle; nervous system; and pleuroperitoneal region. Human ortholog(s) of this gene implicated in X-linked spinocerebellar ataxia 1. Orthologous to human ATP2B3 (atpase plasma membrane Ca2+ transporting 3).
atp2b3b	Atpase plasma membrane Ca2+ transporting 3b	Have PDZ domain binding activity and calcium transmembrane transporter activity, phosphorylative mechanism. Localize to integral component of plasma membrane and intracellular membrane-bounded organelle, and involved in regulation of cytosolic calcium ion concentration. Expressed in brain and eye. Human ortholog(s) of this gene implicated in X-linked spinocerebellar ataxia 1 and autosomal

		recessive nonsyndromic deafness 12. Orthologous to several human genes including ATP2B3 (atpase plasma membrane Ca2+ transporting 3).
atp2b4	Atpase plasma membrane Ca2+ transporting 4	Have PDZ domain binding activity and calcium transmembrane transporter activity, phosphorylative mechanism. Localize to integral component of plasma membrane and intracellular membrane-bounded organelle, and involved in regulation of cytosolic calcium ion concentration. Expressed in several structures, including blood; eye; gill; liver; and pleuroperitoneal region. Orthologous to human ATP2B4 (atpase plasma membrane Ca2+ transporting 4).
atp6v0cb	Atpase H+ transporting V0 subunit cb	Exhibits voltage-gated calcium channel activity. Localizes to presynaptic active zone and synaptic vesicle, and involved in proton transmembrane transport. Expressed in head; nervous system; and neural tube. Human ortholog(s) of this gene implicated in thyroid gland carcinoma. Orthologous to human ATP6V0C (atpase H+ transporting V0 subunit c).
cab39l	Calcium binding protein 39-like	Have protein serine/threonine kinase activator activity. Involved in intracellular signal transduction. Orthologous to human CAB39L (calcium binding protein 39 like).
cacna1ab	P/Q type Calcium channel, voltage-dependent, , alpha 1A subunit, b	Have high voltage-gated calcium channel activity. Involved in swimming behavior, neuromuscular synaptic transmission; thigmotaxis.
cacng8a	voltage-dependent Calcium channel, , gamma subunit 8a	Possess voltage-gated calcium channel activity and channel regulator activity.
cacng8b	voltage-dependent Calcium channel, gamma subunit 8b	Possess voltage-gated calcium channel activity and channel regulator activity.

cadps2	Ca++-dependent secretion activator 2	Have metal ion binding activity. Localize to glutamatergic synapse. Is expressed in hatching gland; nervous system; otic vesicle; pronephric duct; and trigeminal placode, and involved in exocytosis and positive regulation of exocytosis. Orthologous to human CADPS2 (calcium dependent secretion activator 2).
cadpsb	Ca2+-dependent activator protein for secretion b	Have metal ion binding activity. Localize to glutamatergic synapse, and involved in exocytosis and positive regulation of exocytosis. Orthologous to human CADPS (calcium dependent secretion activator).
calm1a	Calmodulin 1a	Involved in midbrain-hindbrain boundary morphogenesis. Expressed in several structures, including mesoderm; midbrain neural keel; nervous system; neural tube; and trigeminal placode. Human ortholog(s) of this gene implicated in catecholaminergic polymorphic ventricular tachycardia 4 and long QT syndrome 14. Orthologous to human CALM1 (calmodulin 1).
calr	Calreticulin	Have calcium ion binding activity. Localize to endoplasmic reticulum membrane. Is expressed in several structures, including hatching gland; nervous system; notochord; polster; and trigeminal placode, and involved in endoplasmic reticulum unfolded protein response and protein folding. Human ortholog(s) of this gene implicated in essential thrombocythemia; myelofibrosis; sideroblastic anemia; and thrombocytosis. Orthologous to human CALR (calreticulin).
calr3a	Calreticulin 3a	Have calcium ion binding activity. Localize to endoplasmic reticulum membrane. Is expressed in several structures, including axis; cardiovascular system; hatching gland; periderm; and polster, and involved in endoplasmic reticulum unfolded protein response and protein folding. Orthologous to human CALR3 (calreticulin 3).
calr3b	Calreticulin 3b	Have calcium ion binding activity. Localize to endoplasmic reticulum membrane, and involved in endoplasmic reticulum unfolded protein response and protein folding. Expressed in several structures, including anterior axial hypoblast; axis; digestive system; ectoderm; and hatching gland. Orthologous to human CALR3 (calreticulin 3).
canx	Calnexin	Have calcium ion binding activity. Localize to endoplasmic reticulum membrane, and involved in posterior lateral line development. Expressed in several structures, including blood; fin; hatching gland; nervous system; and pleuroperitoneal region. Orthologous to human CANX (calnexin).
cetn2	Centrin, EF-hand protein, 2	Have calcium ion binding activity. Localize to centriole and centrosome, and involved in centriole replication; mitotic cell cycle; and nucleotide-excision repair. Predicted to . Expressed in pronephros. Orthologous to human CETN2 (centrin 2).

chp2	Calcineurin-like EF-hand protein 2	Have calcium ion binding activity. Orthologous to human CHP2 (calcineurin like EF-hand protein 2).
clstn1	Calsyntenin 1	Have calcium ion binding activity. Localize to cell surface and postsynaptic membrane. Is expressed in several structures, including axis; musculature system; nervous system; neural tube; and tail bud, and involved in several processes, including axon arborization; homophilic cell adhesion via plasma membrane adhesion molecules; and retrograde transport, endosome to plasma membrane. Orthologous to human CLSTN1 (calsyntenin 1).
clstn2	Calsyntenin 2	Have calcium ion binding activity. Localize to cell surface and postsynaptic membrane, and involved in homophilic cell adhesion via plasma membrane adhesion molecules. Expressed in nervous system. Orthologous to human CLSTN2 (calsyntenin 2).
clstn3	Calsyntenin 3	Have calcium ion binding activity. Localize to cell surface and postsynaptic membrane. Is expressed in forebrain; hindbrain; midbrain; spinal cord; and telencephalon, and involved in homophilic cell adhesion via plasma membrane adhesion molecules. Orthologous to human CLSTN3 (calsyntenin 3).
creb1a	Camp responsive element binding protein 1a	Have DNA-binding transcription factor activity, RNA polymerase II-specific and camp response element binding activity. Localize to ATF4-CREB1 transcription factor complex. Is expressed in nervous system; presumptive neural retina; and proliferative region, and involved in convergent extension involved in axis elongation; midbrain-hindbrain boundary development; and somitogenesis. Orthologous to human CREB1 (camp responsive element binding protein 1).
crebzf	CREB/ATF bzip transcription factor	Have transcription regulatory region sequence-specific DNA binding activity. Localize to nucleus, and involved in regulation of transcription by RNA polymerase II. Orthologous to human CREBZF (CREB/ATF bzip transcription factor).
fkbp1aa	FKBP prolyl isomerase 1Aa	Predicted to have peptidyl-prolyl cis-trans isomerase activity. Localize to cytoplasm and involved in chaperone-mediated protein folding and protein peptidyl-prolyl isomerization. Human ortholog(s) of this gene implicated in Graves' disease. Orthologous to human FKBP1A (FKBP prolyl isomerase 1A) and FKBP1B (FKBP prolyl isomerase 1B).
fkbp1b	FKBP prolyl isomerase 1B	Have peptidyl-prolyl cis-trans isomerase activity. Localize to cytoplasm, and involved in chaperone-mediated protein folding and protein peptidyl-prolyl isomerization. Expressed in basal plate midbrain region; brain; cranial ganglion; and myotome. Human ortholog(s) of this gene implicated in Graves' disease. Orthologous to several human genes including FKBP1B (FKBP prolyl isomerase 1B).
fkbp2	FKBP prolyl isomerase 2	Have peptidyl-prolyl cis-trans isomerase activity. Orthologous to human FKBP2 (FKBP prolyl isomerase 2).

fkbp3	FKBP prolyl isomerase 3	Have peptidyl-prolyl cis-trans isomerase activity. Expressed in alar plate midbrain region; immature eye; nervous system; pectoral fin musculature; and pharyngeal arch 3-7 skeleton. Orthologous to human FKBP3 (FKBP prolyl isomerase 3).
fkbp4	FKBP prolyl isomerase 4	Have peptidyl-prolyl cis-trans isomerase activity. Localize to cytoplasm, and involved in chaperone-mediated protein folding and protein peptidyl-prolyl isomerization. Orthologous to human FKBP4 (FKBP prolyl isomerase 4).
fkbp5	FKBP prolyl isomerase 5	Predicted to have peptidyl-prolyl cis-trans isomerase activity. Localize to cytoplasm and involved in chaperone-mediated protein folding and protein peptidyl-prolyl isomerization. Expressed in gut; head; and regenerating fin. Human ortholog(s) of this gene implicated in major depressive disorder. Orthologous to human FKBP5 (FKBP prolyl isomerase 5).
gria1a	ionotropic Glutamate receptor,(AMPA 1a)	Possess neurotransmitter receptor (AMPA receptor). Involved in calcium ion regulation in postsynaptic.
gria1b	ionotropic Glutamate receptor,(AMPA 1b)	Possess neurotransmitter receptor (AMPA receptor). Involved in calcium ion regulation in postsynaptic.
gria2b	ionotropic Glutamate receptor,(AMPA 2b)	Possess neurotransmitter receptor (AMPA receptor). Involved in calcium ion regulation in postsynaptic.
gria4a	ionotropic Glutamate receptor,(AMPA 4a)	Possess neurotransmitter receptor (AMPA receptor). Involved in calcium ion regulation in postsynaptic.
grin1a	Ionotropic, Glutamate receptor, (NMDA 1a)	NMDA receptor activity.

grin1b	Ionotropic, Glutamate receptor, (NMDA 1b)	NMDA receptor activity.
grin2ab	Ionotropic, Glutamate receptor, (NMDA 2ab)	NMDA receptor activity.
grinab	Ionotropic, Glutamate receptor, (NMDA ab)	NMDA receptor activity.
hpca	Hippocalcin	Have calcium ion binding activity. Expressed in hatching gland; nervous system; neural rod; and neural tube. Human ortholog(s) of this gene implicated in torsion dystonia 2. Orthologous to human HPCA (hippocalcin).
hpcal4	Hippocalcin like 4	Have calcium channel regulator activity and calcium ion binding activity. Involved in signal transduction. Orthologous to human HPCAL4 (hippocalcin like 4).
itsn2a	Intersectin 2a	Have molecular adaptor activity. Localize to several cellular components, including clathrin-coated pit; intracellular vesicle; and presynaptic membrane, and involved in clathrin-dependent synaptic vesicle endocytosis. Orthologous to human ITSN2 (intersectin 2).
itsn2b	Intersectin 2b	Have molecular adaptor activity. Localize to several cellular components, including clathrin-coated pit; intracellular vesicle; and presynaptic membrane, and involved in clathrin-dependent synaptic vesicle endocytosis. Orthologous to human ITSN2 (intersectin 2).
kcnip1b	Kv channel interacting protein 1 b	Have calcium ion binding activity. Expressed in heart and nervous system. Orthologous to human KCNIP1 (potassium voltage-gated channel interacting protein 1).

kcnma1a	calcium-activated Potassium channel, subfamily M, alpha member 1a	Have calcium-activated potassium channel activity. In human this gene implicated in alzheimer's disease.
myl6	Myosin, light chain 6, alkali, smooth muscle and non-muscle	Have calcium ion binding activity. Orthologous to several human genes including MYL6 (myosin light chain 6).
necab2	N-terminal EF-hand calcium binding protein 2	Have calcium ion binding activity. Localize to cytoplasm, and involved in regulation of amyloid precursor protein biosynthetic process. Expressed in brain; central nervous system; cranial ganglion; and neurons. Orthologous to human NECAB2 (N-terminal EF-hand calcium binding protein 2).
nell2b	Neural EGFL like 2b	Have heparin binding activity and protein kinase C binding activity. Localize to cytoplasm. Orthologous to human NELL2 (neural EGFL like 2).
nucb1	Nucleobindin 1	Have calcium ion binding activity. Localize to endoplasmic reticulum-Golgi intermediate compartment. Orthologous to human NUCB1 (nucleobindin 1).
nucb2a	Nucleobindin 2a	Have calcium ion binding activity. Localize to endoplasmic reticulum-Golgi intermediate compartment. Is expressed in several structures, including axial mesoderm; cardiovascular system; digestive system; gonad; and pectoral fin, and involved in response to food. Orthologous to human NUCB2 (nucleobindin 2).
ppp1cab	Protein phosphatase 1, catalytic subunit, alpha isozyme b	Have protein serine/threonine phosphatase activity. Localize to cytoplasm and nucleus, and involved in angiogenesis. Expressed in female organism. Orthologous to human PPP1CA (protein phosphatase 1 catalytic subunit alpha).
ppp1cb	Protein phosphatase 1, catalytic subunit, beta isozyme	Exhibits protein heterodimerization activity. Localize to cytoplasm and nucleus, and Involved in convergent extension involved in axis elongation and liver development. Expressed in intestine and liver. Human ortholog(s) of this gene implicated in Noonan syndrome-like disorder with loose anagen hair 2. Orthologous to human PPP1CB (protein phosphatase 1 catalytic subunit beta).

prkcbb	Protein kinase C, beta b	Have several functions, including androgen receptor binding activity; histone kinase activity (H3-T6 specific); and nuclear receptor coactivator activity. Localize to nucleus. Is expressed in brain; retinal neural layer; and somite border, and involved in blood coagulation and embryonic hemopoiesis. Human ortholog(s) of this gene implicated in dilated cardiomyopathy and lung non-small cell carcinoma. Orthologous to human PRKCB (protein kinase C beta).
prkcea	Protein kinase C, epsilon a	Have protein serine/threonine kinase activity. Localize to cytoplasm, and involved in intracellular signal transduction and peptidyl-serine phosphorylation. Expressed in brain; peripheral neurons; and spinal cord. Orthologous to human PRKCE (protein kinase C epsilon).
pvalb6	Parvalbumin 6	Have calcium ion binding activity. Localize to cytoplasm and nucleus. Expressed in nervous system and otic vesicle. Orthologous to human PVALB (parvalbumin).
sgcb	Sarcoglycan, beta (dystrophin-associated glycoprotein)	Localizes to sarcolemma. Expressed in somite and trunk musculature. Human ortholog(s) of this gene implicated in autosomal recessive limb-girdle muscular dystrophy type 2E and muscular dystrophy. Orthologous to human SGCB (sarcoglycan beta).
sgce	Sarcoglycan, epsilon	Have calcium ion binding activity. Localize to sarcoglycan complex. Expressed in central nervous system; retina; retinal ganglion cell layer; and retinal inner nuclear layer. Human ortholog(s) of this gene implicated in myoclonic dystonia. Orthologous to human SGCE (sarcoglycan epsilon).
sgk3	Serum/glucocorticoid regulated kinase family member 3	Have potassium channel regulator activity and protein serine/threonine kinase activity. Involved in intracellular signal transduction and peptidyl-serine phosphorylation. Orthologous to several human genes including c8orf44-SGK3 (c8orf44-SGK3 readthrough).
sigmar1	Sigma non-opioid intracellular receptor 1	Localize to endoplasmic reticulum and integral component of membrane, and involved in response to wounding. Expressed in gut; head; muscle; and retina. Human ortholog(s) of this gene implicated in amyotrophic lateral sclerosis type 16 and distal spinal muscular atrophy 2. Orthologous to human SIGMAR1 (sigma non-opioid intracellular receptor 1).
slc24a6a	Solute carrier family 24 member 6a	Have calcium channel activity and calcium, potassium:sodium antiporter activity. Localize to integral component of plasma membrane, and involved in calcium ion transmembrane transport and cellular calcium ion homeostasis. Orthologous to human SLC24A3 (solute carrier family 24 member 3).
smdt1b	Single-pass membrane protein with aspartate-rich tail 1b	Localize to integral component of mitochondrial inner membrane and uniplex complex, and involved in calcium import into the mitochondrion and mitochondrial calcium ion homeostasis. Orthologous to human SMDT1 (single-pass membrane protein with aspartate rich tail 1).

stim1a	Stromal interaction molecule 1a	Have calcium channel regulator activity and calcium ion binding activity. Localize to endoplasmic reticulum and plasma membrane, and involved in axon extension involved in axon guidance. Expressed in several structures, including brain; head; liver; pleuroperitoneal region; and skeletal muscle. Human ortholog(s) of this gene implicated in Stormorken syndrome; immunodeficiency 10; and tubular aggregate myopathy 1. Orthologous to human STIM1 (stromal interaction molecule 1).
stk38l	Serine/threonine kinase 38 like	possess serine/threonine kinase activity.
tenm3	Teneurin transmembrane protein 3	Have cell adhesion molecule binding activity; protein heterodimerization activity; and protein homodimerization activity. Localize to integral component of plasma membrane and neuron projection, and involved in dendrite guidance; retinal ganglion cell axon guidance; and visual perception. Expressed in several structures, including fin bud; immature eye; mesoderm; nervous system; and neural tube. Orthologous to human TENM3 (teneurin transmembrane protein 3).
tenm4	Teneurin transmembrane protein 4	Have cell adhesion molecule binding activity; protein heterodimerization activity; and protein homodimerization activity. Localize to several cellular components, including neuron projection; nucleus; and plasma membrane, and Involved in axon guidance. Expressed in several structures, including brain; midbrain hindbrain boundary neural rod; neural tube; optic vesicle; and retina. Human ortholog(s) of this gene implicated in essential tremor 5. Orthologous to human TENM4 (teneurin transmembrane protein 4).
tmbim4	Transmembrane BAX inhibitor motif containing 4	Localize to integral component of membrane. Orthologous to human TMBIM4 (transmembrane BAX inhibitor motif containing 4).
tmx1	Thioredoxin-related transmembrane protein 1	Localize to integral component of membrane. Orthologous to human TMX1 (thioredoxin related transmembrane protein 1).
vdac1	Voltage-dependent -ve ion channel 1	Possess voltage-gated anion channel activity.

vdac2	Voltage-dependent -ve ion channel 2	Possess voltage-gated anion channel activity.
vdac3	Voltage-dependent -ve ion channel 3	Possess voltage-gated anion channel activity.

CaTK_WT (present only in WT)

apba1a	A4 precursor protein-binding, family A, member 1a	Possess amyloid-beta binding activity
cacng2a	voltage-dependent calcium channel, γ2a	Possess voltage-gated calcium channel activity.
cacng4a	voltage-dependent calcium channel, γ4a	Possess voltage-gated calcium channel activity.
calua	calumenin a	Have calcium ion binding activity. Localize to endoplasmic reticulum. Is expressed in chordo neural hinge; floor plate; hypochord; notochord; and skeletal system. Orthologous to human calu (calumenin).
capn1a	calpain 1, (mu/I) large subunit a	Have calcium-dependent cysteine-type endopeptidase activity. Localize to cytoplasm and involved in brain development and branchiomotor neuron axon guidance. Expressed in brain. Human ortholog(s) of this gene implicated in hereditary spastic paraplegia 76. Human orthologous genes capn11 (calpain 11)

ctbp1	C-terminal binding protein 1	Have NAD binding activity; oxidoreductase activity, acting on the CH-OH group of donors, NAD or NADP as acceptor; and transcription corepressor activity. Localize to nucleus and Involved in retinoic acid receptor signaling pathway. Orthologous to human CTBP1 (C-terminal binding protein 1).
ehd1b	EH-domain containing 1b	Have ATP binding activity; GTP binding activity; and calcium ion binding activity. Localize to cytoplasmic vesicle; perinuclear region of cytoplasm; and plasma membrane. Involved in cilium assembly. Is expressed in several structures, including cardiovascular system; mesoderm; musculature system; pronephric duct; and sensory system. Orthologous to human EHD1 (EH domain containing 1).
ormdl1	ORMDL sphingolipid biosynthesis regulator 1	Involved in cellular sphingolipid homeostasis; ceramide metabolic process; and negative regulation of ceramide biosynthetic process. Localize to spots complex. Orthologous to human ormdl1 (ormdl sphingolipid biosynthesis regulator 1).
prkcq	protein kinase C, theta	Have protein serine/threonine kinase activity. Involved in intracellular signal transduction and peptidyl-serine phosphorylation. Localizes to immunological synapse. Expressed in mauthner neurons; brain; somite border; and spinal cord. Orthologous to human prkcq (protein kinase c theta).
si:ch211-195		
ubb	ubiquitin B	Have protein tag and ubiquitin protein ligase binding activity. Involved in modification-dependent protein catabolic process and protein ubiquitination. Localize to cytosolic small ribosomal subunit and nucleus. Orthologous to human genes ubc (ubiquitin c).

CaTK_*(stim2a;stim2b)*$^{-/-}$ (present only in *(stim2a;stim2b)*$^{-/-}$ double mutant)

anxa11a	annexin A11a	Have calcium ion binding activity. Localize to cytoplasm and involved in cytokinetic process and phagocytosis. Expressed in cardiovascular system; ectoderm; integument; mesoderm; and musculature system. Human ortholog(s) of this gene implicated in amyotrophic lateral sclerosis type 23. Orthologous to human anxa11 (annexin a11).
anxa3b	annexin A3b	Have calcium ion binding activity. Localize to cytoplasm. Expressed in dorsal aorta. Orthologous to human anxa3 (annexin a3).
apbb1	amyloid beta (A4) precursor protein-binding, family B,	Have amyloid-beta binding activity and transcription factor binding activity. Localize to cytoplasm and nucleus and involved in regulation of transcription, dna-templated. Human ortholog(s) of this gene implicated in alzheimer's disease. Orthologous to human apbb1 (amyloid beta precursor protein binding family b member 1).

	member 1 (Fe65)	
cacna1ea	R type voltage-dependent calcium channel, α1E subunit a	Possess voltage-gated calcium channel activity.
cacna1eb	R type voltage-dependent calcium channel, α1E subunit b	Possess voltage-gated calcium channel activity.
cacnb4a	voltage-dependent calcium channel, β4a subunit	Possess voltage-gated calcium channel activity.
cacng7b	voltage-dependent calcium channel, γ7b	Possess voltage-gated calcium channel activity.
cadpsa	Ca2+-dependent activator protein for secretion a	Have metal ion binding activity. Localize to glutamatergic synapse and involved in exocytosis and positive regulation of exocytosis. Expressed in olfactory placode and peripheral olfactory organ. Orthologous to human cadps (calcium dependent secretion activator).
cbarpb	CACN subunit beta associated regulatory protein b	Have ion channel binding activity. Colocalize with secretory granule and involved in negative regulation of calcium ion-dependent exocytosis and negative regulation of voltage-gated calcium channel activity. Orthologous to human cbarp (cacn subunit beta associated regulatory protein).
cetn3	centrin 3	Have calcium ion binding activity and microtubule binding activity. Localize to microtubule organizing center. Orthologous to human cetn3 (centrin 3).

crebbpa	CREB binding protein a	Localizes to cytoplasm and nucleus and have several functions, including RNA polymerase II transcription factor binding activity; chromatin DNA binding activity; and transcription coactivator activity. Involved in hematopoietic progenitor cell differentiation. Expressed in blastoderm; blastodisc; digestive system; segmental plate; and solid lens vesicle. Human ortholog(s) of this gene implicated in Rubinstein-Taybi syndrome; acute lymphoblastic leukemia; and acute myeloid leukemia. Orthologous to human CREBBP (CREB binding protein).
crtc1a	CREB regulated transcription coactivator 1a	Have camp response element binding protein binding activity. Localize to cytoplasm and nucleus and involved in positive regulation of CREB transcription factor activity and positive regulation of transcription by RNA polymerase II. Orthologous to human CRTC1 (CREB regulated transcription coactivator 1).
efhd1	EF-hand domain family, member D1	Have calcium ion binding activity. Orthologous to human efhd1 (ef-hand domain family member d1).
gria3b	AMPA receptor, ionotropic, 3b	Possess AMPA receptor activity.
grin2bb	glutamate receptor, ionotropic, NMDA 2B	Possess NMAD receptor activity.
itpr1b	IP3R, type 1b	Possess IP3 binding activity and calcium-release channel activity.
kcnn1a	potassium intermediate/ small conductance calcium-activated channel, subfamily N, member 1a	Have calmodulin binding activity and small conductance calcium-activated potassium channel activity. Localize to neuron projection; neuronal cell body; and plasma membrane and involved in potassium ion transmembrane transport. Orthologous to human kcnn1 (potassium calcium-activated channel subfamily n member 1).
kcnn3	potassium intermediate/ small conductance calcium-activated channel,	Have calmodulin binding activity and small conductance calcium-activated potassium channel activity. Localize to neuron projection; neuronal cell body; and plasma membrane and involved in potassium ion transmembrane transport. Expressed in atrium and cardiac ventricle. Human ortholog(s) of this gene implicated in paranoid schizophrenia and schizophrenia. Orthologous to human kcnn3 (potassium

	subfamily N, member 3	calcium-activated channel subfamily n member 3).
mast2	serine/threonine kinase 2 (microtubule associated)	Possess serine/threonine kinase activity.
micu1	mitochondrial calcium uptake 1	Have calcium ion binding activity. Localize to integral component of mitochondrial membrane; mitochondrial intermembrane space; and uniplex complex and involved in calcium import into the mitochondrion and positive regulation of mitochondrial calcium ion concentration. Human ortholog(s) of this gene implicated in myopathy with extrapyramidal signs. Orthologous to human micu1 (mitochondrial calcium uptake 1).
micu3b	mitochondrial calcium uptake family, member 3b	Have calcium ion binding activity. Localize to integral component of membrane and involved in mitochondrial calcium ion transmembrane transport. Orthologous to human micu3 (mitochondrial calcium uptake family member 3).
necab1	N-terminal EF-hand calcium binding protein 1	Have calcium ion binding activity. Localize to cytoplasm and involved in regulation of amyloid precursor protein biosynthetic process. Is expressed in nervous system. Orthologous to human necab1 (n-terminal ef-hand calcium binding protein 1).
pvalb7	parvalbumin 7	Have calcium ion binding activity. Localize to cytoplasm and nucleus. Expressed in central nervous system; midbrain interneuron; musculature system; and somite. Orthologous to human pvalb (parvalbumin).
slc8a4a	solute carrier family 8 member 4a	Exhibits calcium:sodium antiporter activity. Localize to several cellular components, including axon; postsynapse; and sarcolemma and Involved in several processes, including heart contraction; heart looping; and skeletal muscle tissue development. Expressed in several structures, including Kupffer's vesicle; blood; digestive system; muscle; and pleuroperitoneal region. Human ortholog(s) of this gene implicated in hypertension. Orthologous to human SLC8A1 (solute carrier family 8 member A1).
tusc2b	tumor suppressor 2, mitochondrial calcium regulator b	Involved in inflammatory response and regulation of mitochondrial membrane potential. Localize to mitochondrion. Orthologous to human tusc2 (tumor suppressor 2, mitochondrial calcium regulator).

Appendix I: Table 4: Top 5 marker in WT and in *(stim2a; stim2b)*$^{-/-}$ double mutant

Top 5 markers in the clusters in WT cells

cluster0	**cluster1**	**cluster2**	**cluster3**	**cluster4**
barhl2	mt-co3	gad1b	slc17a6b	pax7b
rpl19	mt-co2	gad2	npas4a	tal1
lef1	zgc:171772	slc32a1	adcyap1b	emx2
lhx9	rpl39	slc6a1b	bdnf	sox14
rplp0	mt-atp6	aldocb	fosab	pax7a
cluster5	**cluster6**	**cluster7**	**cluster8**	**cluster9**
hoxb3a	dlx5a	tuba8l	alcamb	fat2
phox2bb	dlx2a	nutf2l	her6	nebl
meis2a	dlx1a	selenop	shox2	zic5
hoxa4a	dlx6a	gsta.1	tbr1b	zic4
hoxd3a	isl1	gstp1	eomesa	zic2a
cluster10	**cluster11**	**cluster12**		
aplnra	si:ch1073-90m23.1	cldnk		
kcnj11l.1	si:dkey-117i10.1	mpz		
olig2	GPR151	si:dkey-200l5.4		
olig1	gng8	si:ch211-156j16.1		
aplnrb	CABZ01084564.1	elovl1b		

Top 5 markers in the clusters in *(stim2a; stim2b)*$^{-/-}$ double mutant cells

cluster0	**cluster1**	**cluster2**	**cluster3**	**cluster4**
zgc:158463	lhx9	atp1b1b	tal1	dlx5a
rpl19	barhl2	sncgb	sox14	dlx1a
rpl39	lef1	eno1a	emx2	dlx2a
h3f3d	ctnnbip1	si:dkey-7j14.5	pax7b	dlx6a

rpl22	pou4f1	snap25a	pax7a	dlx2b
cluster5	**cluster6**	**cluster7**	**cluster8**	**cluster9**
hoxb3a	eomesa	selenop	her6	fat2
meis2a	tbr1b	sparc	bnc2	nebl
hunk	tbr1a	mdka	slc1a6	slc17a7a
meis1b	emx3	si:ch211-286b5.5	raver2	zgc:92107
pik3r3b	foxg1a	fabp7a	shox2	cbln12
cluster10	**cluster11**	**cluster12**	**cluster13**	**cluster14**
ebf2	aplnra	gng8	ppp1r9alb	tbx20
dlb	kcnj11l.1	GPR151	itpr1b	si:dkey-43k4.5
dla	cd82a	si:ch1073-90m23.1	rorb	six1b
gadd45gb.1	olig2	cpne4b	plxdc1	isl2a
neurod4	aplnrb	synpr	lmo7a	CABZ01072077.1